May 2020

Intracellular Zinc Trafficking: An Interplay of Proteome, Metallothioneine and Glutathione

Afsana Mahim
University of Wisconsin-Milwaukee

INTRACELLULAR ZINC TRAFFICKING: AN INTERPLAY OF PROTEOME, METALLOTHIONEIN AND GLUTATHIONE

by

Afsana Alam Mahim

A Dissertation Submitted in

Partial Fulfillment of the

Requirements for the Degree of

Doctor of Philosophy

in Chemistry

at

The University of Wisconsin – Milwaukee

May 2020

ABSTRACT

INTRACELLULAR ZINC TRAFFICKING: AN INTERPLAY OF PROTEOME, METALLOTHIONEIN AND GLUTATHIONE

by

Afsana Alam Mahim

The University of Wisconsin-Milwaukee, 2020
Under the supervision of Professor David H. Petering

Zinc is the second most abundant transition metal in living organisms. Typically, a eukaryotic cell contains approximately 3000 zinc binding proteins, in which zinc plays structural or catalytic roles. Recently, zinc has been reported to have signaling functions as a secondary messenger. Considering the diverse cellular functions of zinc, the trafficking pathways that help zinc, following its uptake into cytosol, find the target proteins and generate native Zn-Proteins are not well-understood. For past few decades, metallothionein, a zinc binding protein with large stability constants for Zn^{2+}, has been thought of as a mediator in transferring zinc to apo-Proteins. However, gene knock-outs of metallothionein isoforms, reportedly, do not affect the birth and survival of metallothionein-null mice, implying that metallothionein is not absolutely required for zinc trafficking, but may have a supporting role in the process. Beyond metallothionein, zinc encounters numerous potential zinc binding ligands with varying stability constants, including the Proteome's adventitious zinc binding sites and glutathione. In this research, we characterized the non-specific zinc binding sites of Proteome using a colorimetric zinc sensor and then investigated if Proteome, metallothionein and glutathione, alone or with the presence of others, can mediate the transfer of zinc to apo-Proteins to generate native Zn-

Proteins. For this, we have used Zn-carbonic anhydrase as a model Zn-Protein, and dansyl amide as a Zn-carbonic anhydrase sensor. The experimental results indicate that the mechanism of cellular zinc trafficking leading to the formation of native Zn-Proteins does not involve the straight-forward transfer of zinc from one particular cellular component or chaperone to apo-Proteins. Instead, trafficking occurs through a complex interconnected pathway that primarily includes proteomic non-specific zinc binding sites, metallothionein and glutathione.

TABLE OF CONTENTS

LIST OF FIGURES

LIST OF TABLES

ACKNOWLEDGEMENTS

I am greatly thankful to my mentor and supervisor Dr. David H Petering for his outstanding cooperation and constant support throughout my graduate research. Aside from research, Dr. Petering also helped me to build up my mental strength at difficult times of my research.

I would also like thank my PhD committee members, Dr. Mahmun Hossain, Dr. Andrew Pacheco, Dr. Guilherme Indig and Dr. Nicholas Silvaggi, for their valuable suggestions and advice in the milestone meetings that helped improve my thesis.

I am very grateful to Professor David N. Frick for his help and support in my admission into graduate program, and also for giving me the opportunity to work in his research group at the beginning of my graduate program.

I would also like to take the opportunity of thanking my parents (Mohammad Badiul Alam and Monowara Begum), my husband, daughter and my friends for their active support throughout my PhD program.

Last but not least, I am thankful to National Institute of Health and University of Wisconsin-Milwaukee for funding my graduate research.

1. INTRODUCTION

Metal ions play important roles in a plethora of biochemical processes in both prokaryotes and eukaryotes [1, 2]. In fact, thousands of cellular proteins, named metalloproteins, bind various metal ions via amino acid side chains containing carboxylate, thiol, and imidazole ligands to maintain their tertiary or quaternary structures and to perform catalytic functions [3]. Besides proteins, nucleic acids, such as RNA, require metal ions as well for their structure and function [4]. The deficiency of these metal ions often results in various biological and pathological disorders, whereas an excess may turn out to be toxic [1, 2]. Therefore, a proper balance of intracellular metal ion concentrations and their distribution among organelles and metal binding sites is very critical and thus tightly regulated by cells [5-7]. Among the biological metal ions, divalent iron, zinc, copper, calcium, magnesium and manganese ions are present in detectable amounts (micromolar concentrations) [1, 2].

Zinc is the second most abundant transition metal ion present in living organisms after iron [8]. Under steady state conditions, the intracellular zinc concentration of a eukaryotic cell is in the range of 100 – 500 µM, mostly bound tightly to thousands of native Zn-proteins, collectively known as the Zn-Proteome [9, 10]. At physiological pH, conditional stability constants of a few Zn-proteins have been calculated as between 10^9 and 10^{12} M^{-1} [11, 12]. The steady state intracellular free zinc concentration is thought to be in the range of pM – nM [8-10, 13]. According to bioinformatic analysis, mammalian cells have approximately 3000 Zn-proteins, meaning that about 10% of the mammalian proteins require zinc for a wide range of cellular functions [4, 14]. Since divalent zinc ion has a fully occupied set of d orbitals, it does not

participate in cellular redox chemistry and, thus, mostly acts either as a structural component or a catalytical cofactor in Zn-proteins [4, 14-16]. For example, zinc is essential for the three-dimensional structures of zinc finger transcription factors, which bind the promoter regions of DNA and eventually initiate the transcription of many genes [4, 17]. As a catalytic cofactor in the active sites of enzymes, Zn^{2+} acts both as a Lewis acid and a binding site to help stabilize the enzyme-substrate complex [18, 19]. A few of the enzymes that require zinc at their active site for catalyzing biochemical reactions include carbonic anhydrase, alcohol dehydrogenase, and alkaline phosphatase.

In the extracellular medium, zinc remains bound mostly to albumin (stability constant 10^7 at pH 7.4), which acts a conduit for zinc into cells [20]. Zinc from extracellular medium is transported into cell cytosol across plasma membrane by ZIP (Zrt and Irtlike, SLC39A proteins) transporters, a family of 14 proteins, whereas ZnT transporters, a family of 10 proteins, transport zinc out of cells and internal organelles (**Figure 1**) [10, 21-23]. In **Figure 1**, L represents any zinc-binding ligand, e.g., albumin, in the case of extracellular medium. The existence of so many zinc transporter proteins emphasizes the importance of tight regulation of cellular and organelle zinc levels. The structure of ZIP transporters consists of eight transmembrane helices, whereas ZnT proteins have six transmembrane helices [22, 24]. Although the transport mechanism of zinc across plasma membrane at a molecular level is poorly understood, some studies have reported that transmembrane zinc binding site in a transporter is composed of three aspartate carboxylates and a histidine imidazole at interface of two helices [25-27].

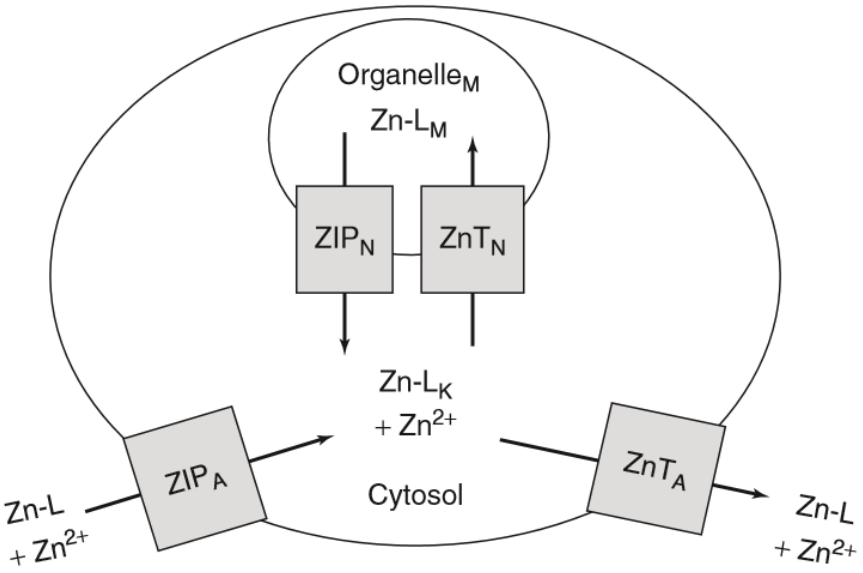

Figure 1. Transportation of zinc into and out of cells and internal organelles. [29]

Following the cellular uptake into cytosol by ZIP transporter proteins, zinc eventually binds the precursor apo-proteins to generate native Zn-proteins. However, the trafficking mechanism that helps zinc to find its target apo-proteins remains unclear. It has been hypothesized that zinc follows the similar trafficking mechanism as the well-established copper trafficking mechanism to find its target proteins [28]. Following the entry into cytosol, copper binds to specific chaperone proteins that assists in delivering Cu to the specific target protein and copper is then transferred to the apo-protein via ligand substitution. However, one of the key differences between cellular copper and zinc is that there are only a small number of copper proteins, as opposed to about 3000 Zn-proteins. Therefore, it is implausible to assume that cells have thousands of individual ligand substitution pathways involving chaperone proteins for the synthesis of 3000 Zn-proteins and thus a chaperone-mediated trafficking mechanism of zinc

seems unreasonable. Indeed, the fact that inside cells, zinc can potentially bind both specifically and adventitiously to a plethora of large and small ligands makes the zinc trafficking mechanism leading to find target proteins complicated [9, 29]. Figure 2 shows the hypothetical zinc trafficking pathways for the formation of native, specific Zn-proteins.

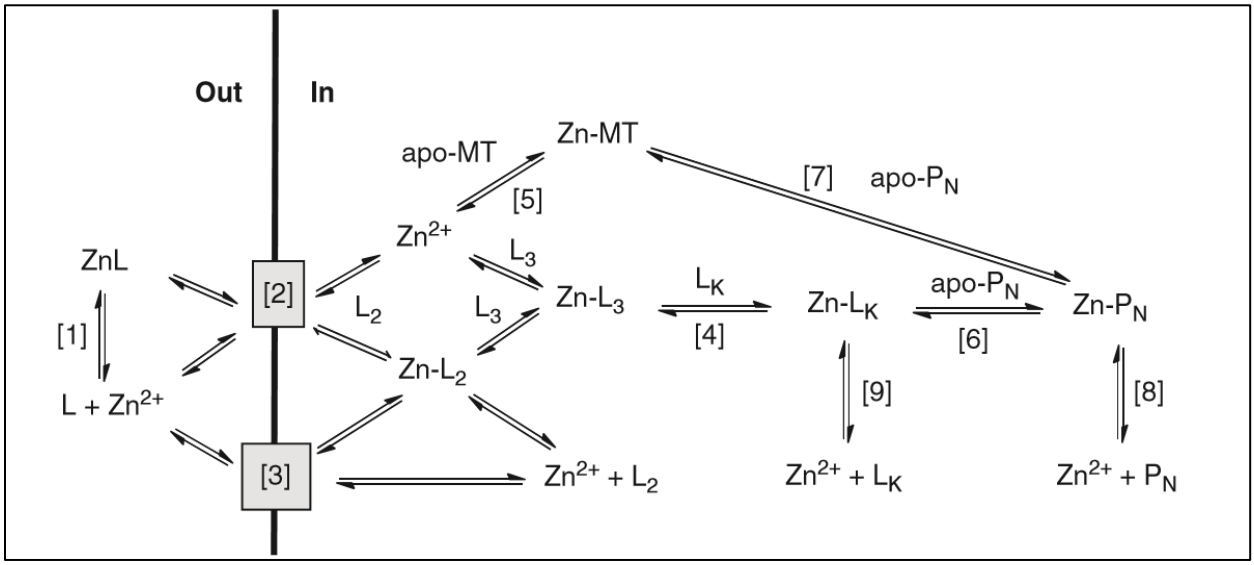

Figure 2. Hypothetical pathways for zinc trafficking to generate native Zn-proteins. L represents potential zinc binding ligands, including proteins and small molecules, such as glutathione. [29]

Once inside the cell, zinc can bind to numerous cellular components, including non-specific binding via amino acid side chains of non-specific proteins [29-31]. The side chains containing carboxylate, thiolate, and imidazole groups exhibit zinc binding affinity to varying extents [32]. Earlier studies reported that the Proteome is capable of binding excess zinc beyond that needed for the constitution of native Zn-proteins [29-31, 33]. This characteristic of Proteome has been termed as *zinc buffering capacity* by Maret and Krezel [9]. Because of zinc binding

affinity of Proteome's adventitious sites and their abundance in cells, Proteome is a potential intermediate in zinc trafficking pathways to form native Zn-proteins [29, 31]. According to this view, after entry into cytosol, zinc binds to adventitious sites of Proteome (L) and eventually finds target proteins (P_N) via ligand substitution (Reaction sequence 1).

$$Zn^{2+} + L_2 \leftrightarrows Zn\text{-}L_2;\ Zn\text{-}L_2 + L_3 \leftrightarrows Zn\text{-}L_3 + L_2;\ Zn\text{-}L_3 + L_K \leftrightarrows Zn\text{-}L_K + L_3;\ Zn\text{-}L_K + P_N \leftrightarrows Zn\text{-}P_N + L_K \quad (1)$$

Moreover, the dissociation of zinc from adventitious sites of Proteome may create a pool of free zinc that can directly bind apo-Proteins (P_N) to make native Zn-Proteins ($Zn\text{-}P_N$) [29].

$$Zn\text{-}L_K \leftrightarrows Zn^{2+} + L_K;\ P_N + Zn^{2+} \leftrightarrows Zn\text{-}P_N \quad (2)$$

Metallothionein (MT), a high affinity zinc binding protein, is considered another potential intermediate in intracellular zinc trafficking [29, 31]. It is a sulfhydryl-rich small protein containing 20 cysteine residues [34, 35]. In its fully saturated form, metallothionein can bind seven zinc ions in two thiolate clusters - α domain (Zn_4S_{11}) and β domain (Zn_3S_9) (**Figure 3**) [34, 36]. The stability constants of MT for zinc ion have been reported in the range of $10^{11\text{-}12}$ per zinc ion [37, 38]. Apart from zinc, it can bind other physiological and toxic metals, including copper, cadmium, mercury, etc [34, 35, 39, 40]. An elevated uptake of cellular zinc induces the synthesis of metallothionein [41-44]. Since some of the native Zn-Proteins have comparable zinc binding constants, e.g. zinc carbonic anhydrase ($10^{11\text{-}12}$) as metallothionein, some studies have reported metallothionein Is a key player in intracellular zinc trafficking (Reaction 3) [15, 31, 37, 38, 45]. Moreover, cellular electrophiles can react with thiolate ligands of metallothionein, and, thus, make free zinc available to participate in zinc trafficking [46-51]. Nevertheless, it has been reported that gene knock-outs of metallothionein do not affect the

birth and survival of metallothionein-null mice, implying that MT is not absolutely necessary for cellular zinc trafficking, but may have a supporting role in the process [52].

$$Zn_7\text{-MT} + n\ \text{apo-CA} \leftrightarrows n\ \text{Zn-CA} + Zn_{7-n}\text{-MT} \quad (3)$$

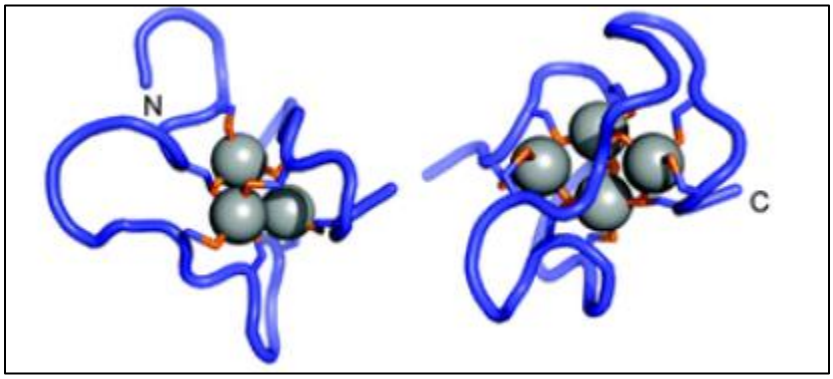

Figure 3. Two metal-thiolate clusters of metallothionein - β domain (left) and α domain (right).

Besides its roles as a structural component and catalytic cofactor in the Zn-Proteome, according to recent studies, zinc can act as a secondary messenger and, thus, as a signaling agent (). For example, zinc has been reported to participate in dynamic cellular signaling processes, such as synaptic chemical transmission and endocrine signaling [53, 54]. It is released from synaptic vesicles of glutamatergic neurons into the synaptic cleft in response to neuronal stimulation [55-57]. One of the prominent examples of zinc signaling is the upregulation of metallothionein, when intracellular free zinc concentration is elevated [58, 59]. At increased intracellular zinc concentration, it binds to and activates the metal response element (MRE)-binding transcription factor 1 (MTF-1), which in turn binds to MRE sequences of various gene promoters

and upregulates the synthesis of the corresponding proteins, including metallothionein (MT) and ZnT1 (Reaction 4 and 5) [60-63]. MT then binds extra intracellular zinc and ZnT1 effluxes zinc out of the cell, and in the process, cellular zinc homeostasis is maintained [64].

$$\text{MTF-1 (inactive)} + n\ Zn^{2+}\text{(high)} \leftrightarrows Zn_n\text{-MTF-1 (active)} \quad (4)$$

$$Zn_n\text{-MTF-1} + \text{MRE} \leftrightarrows Zn_n\text{-MTF-1}\bullet\text{MRE} \quad (5)$$

The role of zinc as an intracellular signaling agent suggests that besides the large pool of static zinc that is bound to zinc metallo-proteins, cells have a pool of labile, reactive zinc as well. It has been suggested that this mobile pool of zinc can be generated from dissociation of zinc from proteomic ligands (Reaction 6) or can be released from storage vesicles, as some articles have reported [29, 53-57]. In reaction 6, L represents any zinc binding ligand, including proteins and other small molecules, such as glutathione.

$$Zn\text{-L} \leftrightarrows Zn^{2+} + L \quad (6)$$

Our view is that the labile pool is not free zinc, Zn^{2+}, but, instead, Proteome-bound zinc as portrayed in reaction sequence 1.

To understand the dynamics and functions of the intracellular mobile zinc pool, the use of fluorescent/colorimetric sensors as analytical tools has been increasingly popular over the past couple of decades (**Figure 4**). These sensors exhibit varying binding affinity for zinc with apparent dissociation constants at pH 7.4 ranging from micromolar to nanomolar [1, 2, 65-67]. Typically, upon binding zinc, the sensor molecules show an enhancement of fluorescence/absorbance and/or a shift of wavelength maximum. To study intracellular, mobile

zinc, cells are usually loaded with a cell-permeable form of the sensor, and the subsequent change of optical properties of the sensor is interpreted as the response to intracellular zinc [68-74]. However, the chemistry of these sensors with cellular components remains understudied. Some are characterized by high zinc binding affinity. It would not be surprising if these molecules show reactivity with native Zn-proteins or other zinc binding ligands (reaction 7), along with free or labile zinc. Furthermore, some of these probes may form ternary adducts with zinc bound to Zn-proteins or adventurous sites (Reaction 8).

$$\text{Zn-Protein + Sensor} \leftrightarrows \text{apo-Protein + Zn-Sensor} \quad (7)$$

$$\text{Zn-Protein + Sensor} \leftrightarrows \text{Sensor-Zn-Protein} \quad (8)$$

As shown in **Figure 4**, 6-methoxy-8-p-toluenesulfonamido-quinoline (TSQ) and its derivative Zinquin (ZQ) are two of the widely used fluorescent sensors to image intracellular mobile zinc. They show fluorescence at 490 nm upon forming a 2:1 complex with zinc (Reaction 9) [67, 68, 72-75]. However, it has been reported that under steady state cellular conditions, these two sensors image predominantly intracellular native Zn-Proteins through ternary complex formation, not free zinc, as evident from the signature emission maximum of 470 nm (Reaction 10) [76-78].

$$2\ \text{TSQ/ZQ} + Zn^{2+} \leftrightarrows \text{Zn(TSQ/ZQ)}_2 \quad (9)$$

$$\text{TSQ/ZQ + Zn-Protein} \leftrightarrows \text{TSQ/ZQ-Zn-Protein} \quad (10)$$

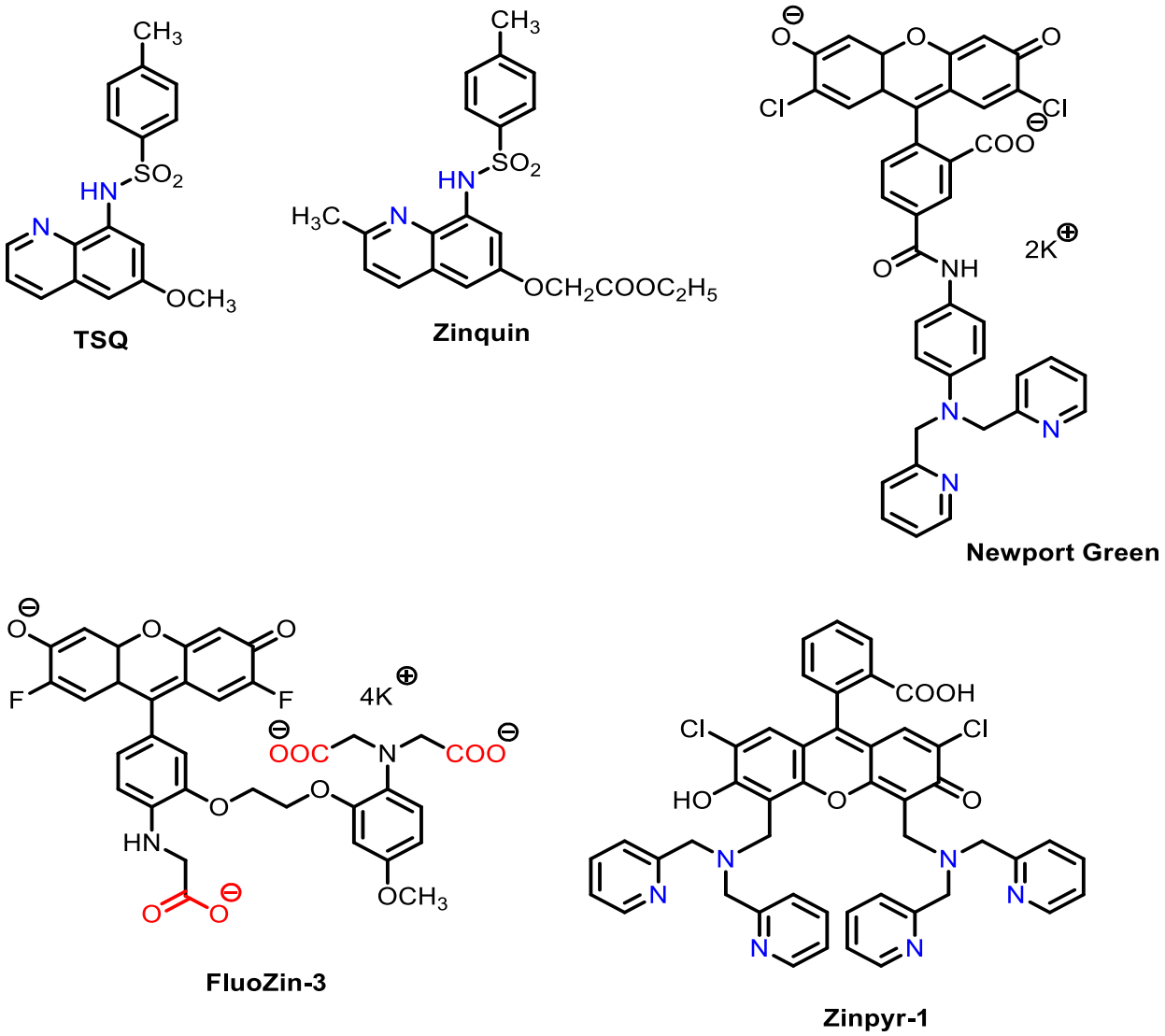

Figure 4. Examples of zinc fluorescent sensors.

These sensors compete with other potential zinc binding ligands, e.g., proteome and glutathione, for intracellular labile zinc, making the cellular chemistry of the sensors more complicated than typically assumed. For example, Newport Green, a weak zinc fluorescent sensor with stability constant of $10^{5\text{-}6}$ M, has been used in a number of studies for imaging intracellular labile zinc [1, 79-84]. However, it has been shown to be outcompeted by high

affinity proteomic ligands for intracellular zinc, and, thus, is able to image intracellular zinc, only when the high affinity proteomic ligands are saturated with zinc [9, 85]. These novel findings of TSQ, Zinquin and Newport Green reveal that a detailed understanding of the cellular chemistry of intracellular zinc sensors that are used to study zinc trafficking is as important as that of understanding cellular zinc trafficking mechanisms.

Herein, we have revisited the zinc buffering study published by Wolfgang Maret research group using a colorimetric zinc sensor, Zincon, and re-interpreted their results on the basis of our findings, to better characterize the non-specific zinc binding sites of Proteome and their interaction with Zincon [9]. Next, we have investigated if the Proteome acts as an intermediate via its adventitious zinc binding sites for intracellular zinc trafficking leading to the generation of native Zn-Proteins. In addition, we have studied if metallothionein individually or in cooperation with Proteome can transfer its strongly bound zinc to apo-proteins. Finally, we have examined if glutathione plays any role in the overall landscape of intracellular zinc trafficking. For trafficking studies, we have used zinc carbonic anhydrase (Zn-CA) as a model zinc protein and studied the reconstitution of Zn-CA mediated by Proteome, metallothionein and glutathione, alone or with the presence of one another. In conclusion, we have presented a detailed intracellular zinc trafficking mechanism, starting from cellular uptake of zinc to the formation of native Zn-Proteins, that involves Proteome, metallothionein and glutathione.

2. MATERIALS AND METHODS

2.1 Chemicals and Reagents

The zinc fluorescent sensors TSQ and FluoZin-3 were purchased from AnaSpec, Inc. and Molecular Probes, respectively, and then dissolved in DMSO and stored in the dark at -20^0 C in small aliquots. N-ethylmaleimide (NEM), glutathione (GSH), buthionine sulfoximine (BSO), ethylenediaminetetraacetic acid (EDTA), 5,5'-dithiobis-(2-nitrobenzoic acid (DTNB) and dansyl amide (DA) were bought from Sigma. Sephadex G-75 and G-25 gel filtration resins were purchased from GE Healthcare Life Sciences. Metallothionein was obtained from Creative Biomart, Inc. The model proteins, bovine serum albumin (BSA), trypsin and carbonic anhydrase were obtained from Sigma in the form of lyophilized powder. The powders were dissolved in degassed 20 mM Tris buffer adjusted to pH 7.4 and stored at -80^0 C. The antibiotics penicillin G and streptomycin sulfate for cell culture were purchased from Fisher Scientific and Sigma, respectively. Fetal calf serum (FCS) was also bought from Fisher Scientific and stored at -80^0 C until use. All the other chemicals and reagents were purchased from either Fisher Scientific or Sigma-Aldrich at the highest grade available.

2.2. Preparation of medium and solutions for cell culture

LLC-PK$_1$ (pig kidney cells) cell line (adherent cell line) was purchased from ATCC and grown in Medium 199 with HEPES modification. Medium powder from the bottle was dissolved in 1L MilliQ water. 2.2 g sodium bicarbonate ($NaHCO_3$) was added to the medium solution and the pH of the solution was adjusted to 7.2. The medium was then supplemented with 50 mg/L

penicillin G and 50 mg/L streptomycin sulfate, and sterile filtered before use. The media solution was stored in 4^0 C.

Confluent LLC-PK_1 cells were released from the culture flask by 10X trypsin-EDTA treatment. To prepare 200 mL 10X trypsin-EDTA solution, 1.0 g trypsin, 0.4 g EDTA tetrasodium salt and 1.8 g sodium chloride (NaCl) were dissolved in MilliQ water. The solution was sterile filtered and stored in 10 mL aliquots at -20^0 C.

2.3 Cell culture

LLC-PK_1 cells were grown in Medium 199 with HEPES modification supplemented with 2.2 g/L $NaHCO_3$, 50 mg/L penicillin G, 50 mg/L streptomycin and 4% fetal calf serum (FCS) (from Fischer Scientific). Each flask of cells contained 15 mL of media mix. The cells were incubated at 37^0 C in the presence of 5% CO_2. The media was changed every 2-3 days until confluence. At the point of confluence, old media was discarded completely, and cells were released by 10X trypsin EDTA solution for 10-15 min in the incubator. Once the cells were released, 0.1-0.2 mL cell suspension was used to make new culture flask and the remaining cells were used for growing cells in 100-mm culture plates. Each plate contained 10 mL of media mix and 0.4 mL of FCS along with cells.

2.4 Cell counting

LLC-PK_1 cells were counted using a hemacytometer. The culture medium from one plate of confluent of cells (ca. 10^7 cells) was discarded and the cells were then incubated with 450 µL of 10X trypsin-EDTA solution for 10-15 min at 37^0 C. 1 mL of DPBS was added to the released cells following trypsin-EDTA incubation. Cells were then transferred to a centrifuge tube containing 550 µL horse serum to make the final volume of 2 mL (450 µL trypsin-EDTA + 1 mL DPBS + 550 µL horse serum) and mixed very well. 10 µL of cells was then transferred to an Eppendorf tube and diluted to 100 µL using DPBS. 10 µL from the final cell suspension was placed onto a hemacytometer and the cells were counted. The counted number was finally multiplied by the dilution factor and the actual number of cells determined.

2.5 Cell viability assay (Trypan blue exclusion assay)

Following incubation with 50 µM $ZnCl_2$ for 48 hours or with 25, 50, 100, 200, 400, 800 and 1600 µM buthionine sulfoximine (BSO) for 24 hours, the culture medium of one plate of LLC-PK_1 cells (ca. 10^7 cells) was completely drained off and the cells were incubated with 1 mL of 10X trypsin-EDTA solution for 10-15 min. The released cells were collected in a centrifuge tube and washed three times with fresh DPBS and finally resuspended in DPBS. 10^4 cells were treated with 0.4% Trypan Blue solution in 1:1 ratio and viable cells were counted immediately using a hemacytometer. Trypan blue is a dye which can penetrate the compromised cell membrane of a dead cell and the cell will in turn look blue under the hemacytometer, while the living cells will appear colorless as Trypan blue is not able to permeate through the cell membrane of an

intact cell [86-88]. The cell viability assay was also used with LLC-PK_1 cells suspended in culture medium. As control, the assay protocol was repeated for untreated LLC-PK_1 cells.

2.6 Fluorescence spectroscopy of BSO-treated LLC-PK_1 cells

LLC-PK_1 cells were treated with 100 μM BSO for 24 hours and grown in 100-mm culture plates until confluence was attained. Culture media from both BSO-treated and untreated (control) plates was then discarded, and the plates washed three times with cold cholate buffer, prepared by dissolving 2.47 g Na_2HPO4, 0.53 g NaH_2PO4, 17.0 g NaCl and 13.33 g choline chloride in 2 L MilliQ water. Cells were then gently scraped from the plates with a rubber cell scraper and pooled in Dulbecco's phosphate buffered saline (DPBS) (0.1 g/L $MgCl_2.6H_2O$, 0.2 g/L KCl, 0.2 g/L KH_2PO_4, 8.0 g/L NaCl, 1.15 g/L anhydrous Na_2HPO_4). Cells were collected by centrifugation at 680 g for 5 min and resuspended in 10 mL DPBS. The cell suspension was then transferred to a cuvette and treated with 20 μM TSQ. Then, over a 30 min period and using an excitation wavelength of 370 nm, emission spectra were recorded between 400 nm and 600 nm with a Hitachi F-4500 fluorescence spectrophotometer.

2.7 Preparation of Sephadex G-75 and G-25 gel filtration column

Sephadex G-75 beads (4-5 g per gel filtration column) and G-25 beads (10-12 g per column) purchased from GE Healthcare were soaked in 20 mM Tris buffer (pH 7.4) for 3 hours (G-25 beads) or 24 hours (G-75 beads). Following on, soaked beads were degassed for an hour and then slowly packed in glass columns to make 0.7 cm x 80 cm Sephadex G-75 and G-25 gel

filtration columns. G-25 and G-75 columns were washed with degassed 0.2 M phosphate buffer or 20 mM Tris buffer (pH 7.4), respectively, each time before use.

2.8 Isolation of cell lysate from LLC-PK_1 cells

Following incubation of LLC-PK_1 cells with 50 µM $ZnCl_2$ for 48 hours or with 100 µM BSO for 24 hours, culture media from both treated and untreated (control) plates was then discarded, and the plates washed three times with cold cholate buffer. Cells were then gently scraped from the plates with a rubber cell scraper and pooled in Dulbecco's phosphate buffered saline (DPBS). Cells were further washed twice with fresh DPBS and centrifuged each time at 680 g for 5 min to separate the pellet from the extracellular medium. The last cell pellet was resuspended in 1 mL of cold MilliQ water. Cells were then lysed by sonication and centrifuged at 47,000 g for 20 min at 4o C to collect the cell supernatant or cell lysate.

2.9 Fractionation of the cell lysate using Sephadex G-75 gel filtration column or Centricon filtration

The cell lysate collected as above was either loaded onto an 80 cm x 0.75 cm gel filtration column of Sephadex G-75 (GE Healthcare) equilibrated with 20 mM Tris buffer (pH 7.4) at room temperature or filtered through a Millipore Centricon Centrifuge filter (3K MW cut off) at 4^{o} C by centrifugation at 13,000 rpm for 30 min to separate the high and low molecular weight fractions. During gel-filtration chromatography, the column was eluted with degassed 20 mM

Tris-Cl (pH 7.4) and 50-60 fractions were collected. The zinc content in each fraction was also detected by flame atomic absorption spectroscopy (AAS).

2.10 Isolation of Proteome Using Sephadex G-75 Chromatography

LLC-PK_1 cells were harvested as described above and finally resuspended in 1 mL cold MilliQ water. Cells were then lysed by sonication and centrifuged at 47,000 g for 20 min to collect the cell supernatant, which was then loaded onto a Sephadex G-75 column equilibrated with degassed 20 mM Tris buffer (pH 7.4). The supernatant was eluted with degassed 20 mM Tris-Cl (pH 7.4) and 1 mL fractions were collected. Fractions within the high molecular weight region having absorbance at 280 nm were pooled. These pooled fractions were referred to as the proteome. Proteome was stored in 1 mL aliquots at -80^0 C until use. On the day of experiment, proteome was ice-thawed.

2.11 Reaction of model proteins (bovine serum albumin and trypsin) with Zincon

The solutions of the model Zn-proteins, such as bovine serum albumin, were prepared by dissolving the lyophilized powder of the Zn-proteins in degassed 20 mM Tris buffer (pH 7.4). The protein solutions were incubated with Zincon and titrated with zinc. The progress of the reaction was monitored by recording absorption spectrum. To identify the absorbing species, the final reaction mixture was fractionated using either Sephadex G-75 gel filtration column or Centricon filtration. For Sephadex G-75 gel filtration, the sample was eluted with degassed 20

mM Tris buffer (pH 7.4) and 50-60 fractions were collected. All the fractions were analyzed for both absorbance, and zinc content using flame atomic absorption spectrophotometry.

2.12 Quantification of zinc

The concentration of Zn^{2+} in solutions was determined by both flame atomic absorption spectrophotometry (AAS) and inductively coupled plasma mass spectrometry (ICP-MS).

For measurement by atomic absorption spectrophotometry, a GBC model 904 instrument that employed an acetylene torch to atomize samples using an 80:20 mixture of compressed air and acetylene was used. Zinc measurements were made with deuterium background correction. The instrument was calibrated before each run using three standard Zn^{2+} solutions of 0.5 ppm, 1.0 ppm and 2.0 ppm. The calibration curve was not considered acceptable until the maximum error was 0.2 µM or less.

In the case of inductively coupled plasma mass spectrometry (ICP-MS), ICPMS 2030 instrument was used. Sample and standard solutions were prepared in 2% nitric acid. For calibration curve, standard zinc solutions of 0.0625, 0.125, 0.25, 0.5, 1.0 and 2.0 ppm were used. A built-in software, LabSolutions ICPMS (version 1.12), was used for data analysis.

2.13 Quantification of sulfhydryl groups

The concentration of sulfhydryl groups was determined with Ellman's Reagent or 5, 5'-dithiobis2-nitrobenzoic acid (DTNB) [89]. To prepare a 10 mM DTNB stock solution, 25 mL

MilliQ water was added to 0.1 g DTNB solid. The mixture was gently stirred. Because DTNB is insoluble at acid pH but oxidizes immediately at pH greater than 8.0, the pH of the solution was monitored while being stirred. Since the pH was around 3.0 to start out and little DTNB powder was in solution, a few crystals of Trizma (Tris) base was added until the pH was between 6.5 and 7.0. The solution was then filtered to remove the residual amount of undissolved DTNB. The filtered DTNB solution was kept into a small brown bottle and stored in dark. The color of the solution was pale yellow.

For measurement of sulfhydryl concentrations, 60 µL of sample was diluted with 540 µL 20 mM Tris-Cl, pH 7.4. 60 µL of 10 mM DTNB was then added to the sample and vortexed immediately. The solution was incubated in dark for 30-60 min before the absorbance at 412 nm was obtained. An extinction coefficient of 13,600 $cm^{-1}M^{-1}$ was used to determine the concentration of reactive thiol groups in the samples.

2.14 Preparation of apo-carbonic anhydrase

Apo-carbonic anhydrase (apo-CA) was prepared according to a published method with some modification [90, 91]. Namely, 100 mg of the holo enzyme (zinc carbonic anhydrase) was dissolved in 5 mL of 0.2 M phosphate buffer (pH 7.0), which contained 0.1 M pyridine-2,6-dicarboxylic acid (dipicolinic acid). Dipicolinic acid is readily dissolved with the addition of solid Tris base with constant stirring. Following incubation for 4 hours, the mixture was loaded onto a Sephadex G-25 gel filtration column and eluted with 10 mM ammonium bicarbonate (NH_4HCO_3) at pH 8.6. The eluted fractions were analyzed by determining absorbance at 280 nm and zinc

concentration using flame atomic absorption spectrophotometry (AAS). The fractions corresponding to apo-carbonic anhydrase were pooled and stored at -80^0 C in small aliquots.

2.15 Apo-carbonic anhydrase assay

The concentration of apo-carbonic anhydrase was determined by measuring absorbance at 280 nm using an extinction coefficient, ε = 5.7 x 10^4 M^{-1} cm^{-1} [92]. The preparation of apo-carbonic anhydrase was confirmed by reaction with dansyl amide (DA). DA forms a ternary complex with native Zn-carbonic anhydrase and exhibits fluorescence at 460 nm but does not react with apo-carbonic anhydrase or free zinc [93].

2.16 Denaturation and renaturation of carbonic anhydrase

Apo-carbonic anhydrase solution in 20 mM Tris buffer (pH 7.4) was denatured by guanidinium hydrochloride. Namely, 100 µM apo-carbonic anhydrase solution was incubated with 4 M guanidinium hydrochloride, resulting in complete denaturation of apo-CA. In order to renature, the denatured apo-CA in 4 M guanidinium hydrochloride was 25-fold diluted using 20 mM Tris buffer (pH 7.4) [94]. Both denaturation and renaturation of apo-carbonic anhydrase were tested by repeating the protocol with native Zn-CA in the presence of dansyl amide. Denaturation caused complete loss of dansyl amide fluorescence at 460 nm, that was originally generated from the formation of ternary complex between dansyl amide and Zn-carbonic

anhydrase. Renaturation of Zn-carbonic anhydrase returned 460 nm fluorescence of dansyl amide.

2.17 Ultraviolet-visible spectroscopy

A Beckman Coulter, DU© 640 spectrophotometer was used to measure the absorption spectra of chromophores in samples or absorbances at their λ_{max}. Measurement of absorbances over time was used for kinetic studies. One-cm quartz or plastic cuvettes were used for UV (200 -400 nm) and Visible (400 - 700nm) measurements, respectively.

3. RESULTS

3.1 Characterization of proteome's non-specific zinc binding

Recent studies have reported that beyond its structural and catalytic role in various proteins, zinc can act as a secondary messenger in cellular signaling, meaning that cells maintain a mobile or dynamic zinc pool [53-59]. For example, cellular nitric oxide can react with sulfhydryl groups of high molecular weight Zn-proteins and thus liberate zinc, which in turn participates in the downstream cellular processes [33, 95 - 99]. Over the past couple of decades, a number of colorimetric and fluorescent zinc sensors with a wide range of structures and zinc binding affinity have been developed to monitor this cellular pool of mobile zinc. Although these sensors are thought to image only intracellular free zinc, recently published articles concluded that some of these sensors do not image free zinc in cells. For instance, TSQ and Zinquin (ZQ), two widely used fluorescent zinc sensors, predominantly image cellular Zn-Proteins, not free zinc [76-78]. They form ternary complexes with Zn-Proteins, TSQ-Zn-Proteins or ZQ-Zn-Proteins, characterized by emission maxima at 470 nm, while their binary complexes with free zinc, $Zn(TSQ)_2$ or $Zn(ZQ)_2$, display an emission maximum at 490 nm [76-78].

$$2\ TSQ/ZQ + Zn^{2+} \leftrightarrows Zn(TSQ/ZQ)_2 \quad (490\ nm) \qquad (11)$$

$$TSQ/ZQ + Zn\text{-}Protein \leftrightarrows (TSQ/ZQ)\text{-}Zn\text{-}Protein \quad (470\ nm) \qquad (12)$$

Additionally, Newport Green, another fluorescent sensor used to image intracellular free zinc, was found to be weakly efficient in imaging intracellular free zinc in the proteomic environment [85]. These interesting findings about some of the zinc sensors question the performance of

other sensors in sensing intracellular free zinc and thus support the need for re-examination of the mode of action of these fluorescent probes.

Wolfgang Maret's research group characterized the proteome's zinc buffering capacity using Zincon (ZI), a colorimetric sensor used to image free zinc [9]. ZI has only a modest affinity for Zn^{2+} with a stability constant at pH 7.4 of $10^{4.9}$ [9]. According to their published study, a simple titration of ZI with Zn^{2+} resulted in a linear increase of absorbance at 620 nm, indicating the formation of the Zn-ZI complex. However, when ZI was titrated with Zn^{2+} in the presence of HT-29 cell Proteome, no absorbance at 620 nm was observed until about 2 µM Zn^{2+} was added, suggesting that the initially added Zn^{2+} was bound to some of the Proteome's non-specific zinc binding sites, rather than picked up by ZI. Once the proteome's zinc buffering capacity was saturated, with the addition of more zinc, the absorbance at 620 nm gradually increased, which was interpreted as the formation of Zn-ZI complex (**Figure 5**). However, Maret research group apparently ignored that the slope of straight line following the initial flat region is not the same as that of the control line, i.e. titration of ZI with Zn^{2+} in the absence of Proteome. Therefore, it cannot represent the simple titration of ZI with Zn^{2+}; at least the altered slope suggests that Proteome and ZI are competing for Zn^{2+}.

This chapter focuses on re-examining of Maret's Proteome experiment and re-interpreting the results of the experiment.

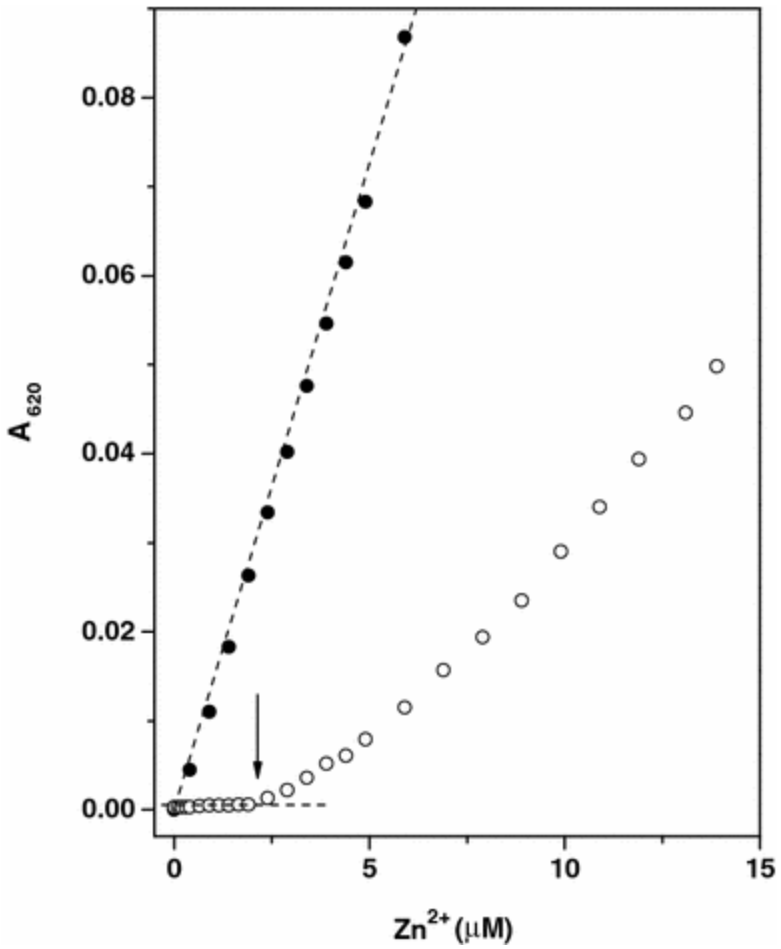

Figure 5. Spectrophotometric zinc titration of HT-29 cell homogenates after centrifugation at 100,000g in the presence of 200 µM Zincon. Homogenates (500 µL) derived from 6x106 cells were titrated with zinc sulfate in HEPES-Na, pH 7.4 (open circles). Titration in the absence of homogenate under the same conditions as control (filled circles). [Krezel et al. (2006), J Biol Inorg Chem]

3.1.1 Spectral properties of ZI and Zn-ZI

Zincon (ZI) solution in 20 mM Tris (pH 7.4) showed an absorption maximum at about 490 nm. In the presence of Zn^{2+}, the absorption maximum shifted to 620 nm (**Figure 6A**). When 40 µM ZI in 20 mM Tris (pH 7.4) was titrated with Zn^{2+}, its absorbance reached the maximum at equimolar concentration of Zn^{2+} (**Figure 6 B** and **C**), suggesting that ZI formed a 1:1 complex with Zn^{2+}.

$$Zn^{2+} + ZI \leftrightarrows Zn\text{-}ZI \quad \text{(absorption maximum 620 nm)} \qquad (13)$$

An isosbestic point at 531 nm characterized the reaction, indicative of the straightforward conversion of ZI into Zn-ZI.

A.

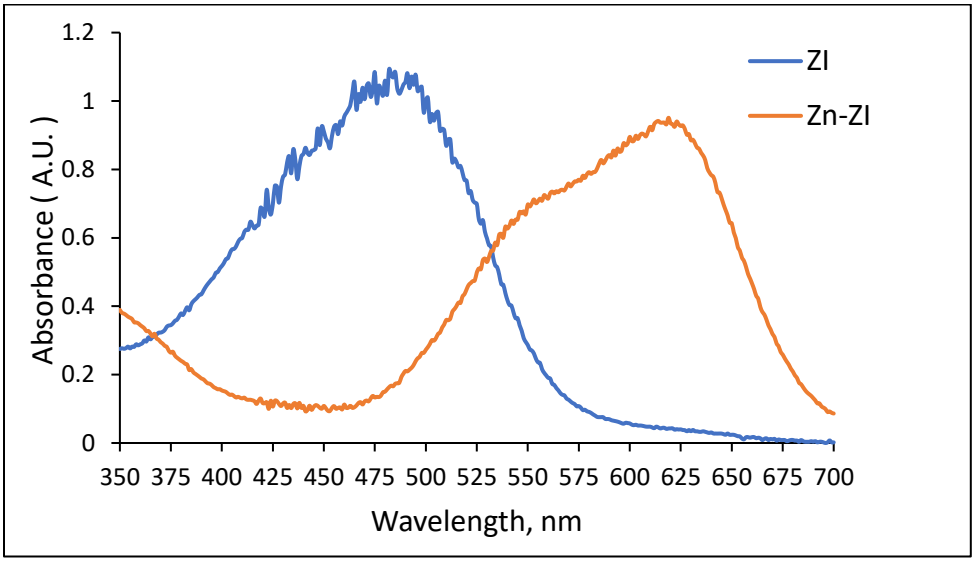
1.2
1
0.8
0.6
0.4
0.2
0
Absorbance (A.U.)
350 375 400 425 450 475 500 525 550 575 600 625 650 675 700
Wavelength, nm
ZI
Zn-ZI

B.

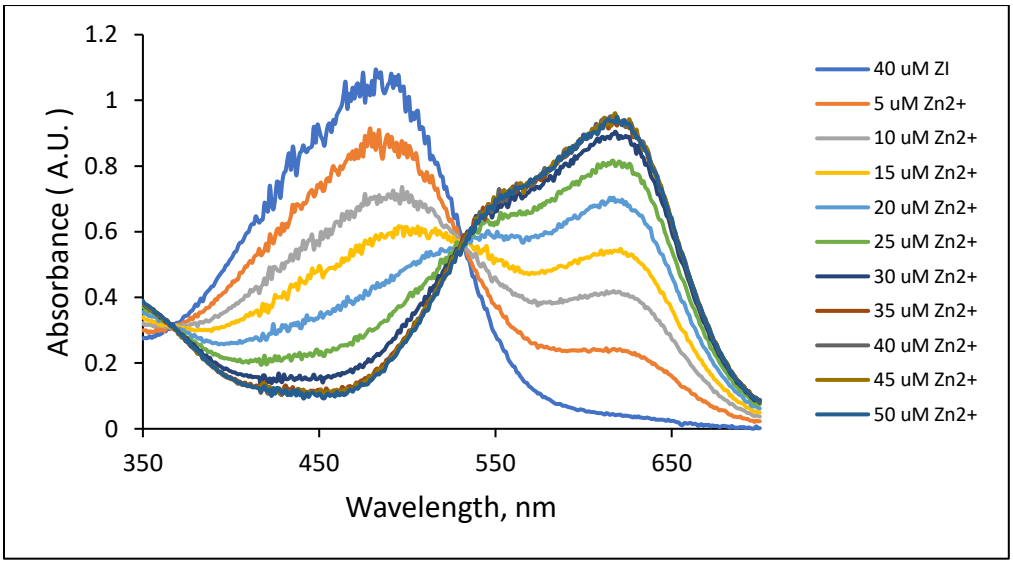
1.2
1
0.8
0.6
0.4
0.2
0
Absorbance (A.U.)
350
450
550
650
Wavelength, nm
40 uM ZI
5 uM Zn2+
10 uM Zn2+
15 uM Zn2+
20 uM Zn2+
25 uM Zn2+
30 uM Zn2+
35 uM Zn2+
40 uM Zn2+
45 uM Zn2+
50 uM Zn2+

C.

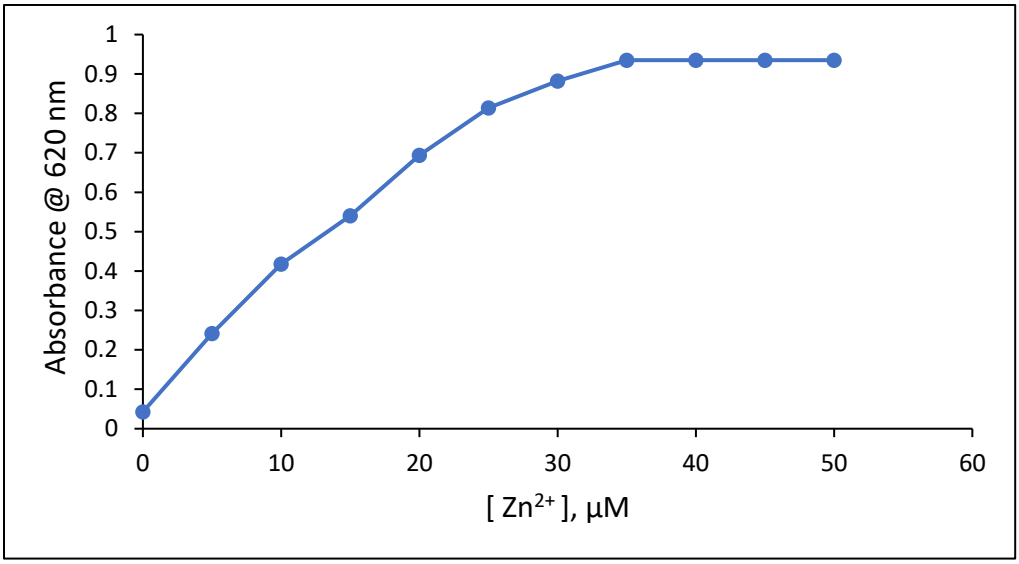

Figure 6. Spectral properties of ZI and Zn-ZI. (A) Absorption spectrum of 40 µM ZI in 20 mM Tris (pH 7.4) and the reaction mixture of 40 µM ZI and 40 µM Zn^{2+}. (B) Absorption spectra of titration of 40 µM ZI with Zn^{2+}. (C) Change of 620 nm absorbance with increasing concentration of Zn^{2+}.

3.1.2 Titration of ZI with Zn^{2+} in the presence of proteome

The titration experiment in the presence of Proteome done by Maret's research group was repeated. Proteome containing 4.5 µM native Zn^{2+} was incubated with 40 µM ZI followed by the addition of increasing concentrations of added Zn^{2+}. Before the addition of exogenous Zn^{2+}, ZI displayed an absorption maximum at 490 nm in the presence of Proteome, suggesting that ZI does not react with native Zn-proteins (**Figure 7**). No significant change in the absorption spectrum was observed, until about 10 µM of the extra Zn^{2+} was added (**Figure 7**). This initial unaltered absorbance re-confirmed that the first 10 µM of the added Zn^{2+} was strongly buffered by Proteome via its non-specific, high affinity zinc binding sites and that when Zn^{2+} was bound, they were unreactive with ZI. A similar lack of reactivity of Proteome•Zn was observed at the beginning of the titration of Proteome with Zn^{2+} in the presence of Newport Green, another sensor with low affinity for Zn^{2+} (stability constant at pH 7.4, 10^6 [85].

As more Zn^{2+} was added, the 490 nm absorbance started decreasing. Surprisingly, a concurrent increase of absorbance at 640 nm, not 620 nm, was observed with the increasing concentration of added Zn^{2+} (**Figure 7**). Moreover, the slope of this straight line plot of absorbance vs. Zn^{2+} concentration was manifestly different from that of control line. In addition, the quantum yield was significantly less than that of control titration. Finally, the titration was not characterized by a precise isosbestic point, indicating that more than two absorbing species were present during part of the reaction. All these discrepancies clearly indicated that (i) the process was more complicated than the simple titration of ZI with Zn^{2+} as that would yield a slope similar to that of the control, and (ii) the generated species is not Zn-ZI, as this would show an absorption maximum at 620 nm. These results conflicted with the interpretation of the Maret research

group, that claimed the production of the Zn-ZI complex following the saturation of Proteome's zinc buffering capacity. The requirement of about 100 µM Zn^{2+}, as opposed to only 40 µM for the control experiment, for the absorbance to reach its maximum value suggested a possible competition between Proteome's non-specific, relatively low affinity zinc binding sites and ZI for added Zn^{2+} (reactions 14-16).

To further characterize the absorbing species, in a separate experiment, 50 µM ZI was titrated with Zn^{2+} in the presence of Proteome and the final reaction mixture was filtered using a Centricon 3K molecular weight cut-off filter. Both retentate and filtrate were analyzed for absorbance and zinc content. Interestingly, almost all of the absorbance and zinc content were found in the retentate. The absorption spectrum of the retentate was centered at 640 nm (**Figure 8 A**). These findings were consistent with the generation of a ternary complex of Proteome, Zn^{2+} and ZI, Proteome•Zn-ZI or Proteome(Zn-ZI), in which Zn-ZI binds to Proteome through the ZI ligand.

$$\text{Proteome} + Zn^{2+} \leftrightarrows \text{Proteome}\bullet\text{Zn} \quad \text{(higher affinity binding sites, buffering region)} \qquad (14)$$

$$\text{Proteome}\bullet\text{Zn} + \text{ZI} \leftrightarrows \text{Proteome}\bullet\text{Zn-ZI} \quad \text{(lower affinity binding sites, 640 nm absorbance)} \qquad (15)$$

$$\text{Proteome} + \text{Zn-ZI} \leftrightarrows \text{Proteome}\bullet\text{Zn-ZI} \quad \text{(lower affinity binding sites, 640 nm absorbance)} \qquad (16)$$

Finally, the introduction of TPEN, a strong zinc chelator with a conditional stability constant at pH 7.4 of $10^{15.6}$, abolished the 640 nm absorbance and regenerated 490 nm absorbance. The result of TPEN experiment indicated that the generated ternary complex was Proteome•Zn-ZI.

However, the unexpected feature of this titration was the fact that instead of being a stoichiometric ligand exchange reaction, a large excess of TPEN was needed to displace ZI from Zn^{2+}. Considering that the conditional stability constants of Zn-TPEN and Zn-ZI differ by $10^{10\text{-}11}$, the titration results show that Zn^{2+} in the Proteome•Zn-ZI ternary complex is not readily accessible to TPEN. (**Figure 8 B** and **C**).

$$\text{Proteome•Zn-ZI} + \text{TPEN} \leftrightarrows \text{Proteome} + \text{Zn-TPEN} + \text{ZI} \qquad (17)$$

Therefore, this experiment suggested that proteome contains two types of non-specific zinc binding sites – i) sites with relatively higher affinity for Zn^{2+} that are unreactive with ZI, and ii) sites with lower affinity for Zn^{2+} that permit the binding of Zn^{2+} to ZI. The proteomic non-specific zinc binding sites with higher affinity are more important for the Proteome's zinc buffering capacity, while other sites permit the formation of ternary complexes with Zn-ZI.

A.

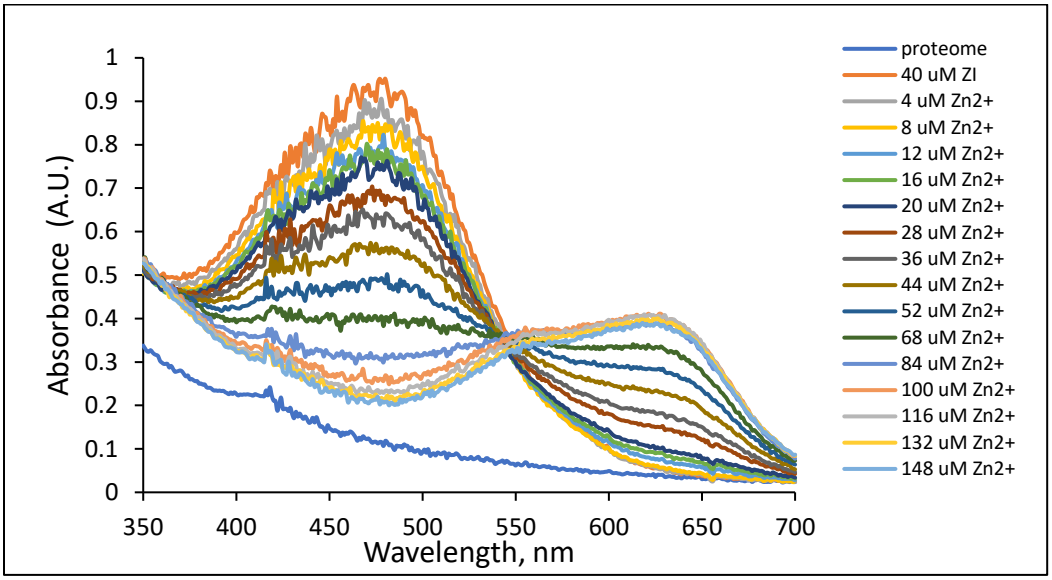

B.

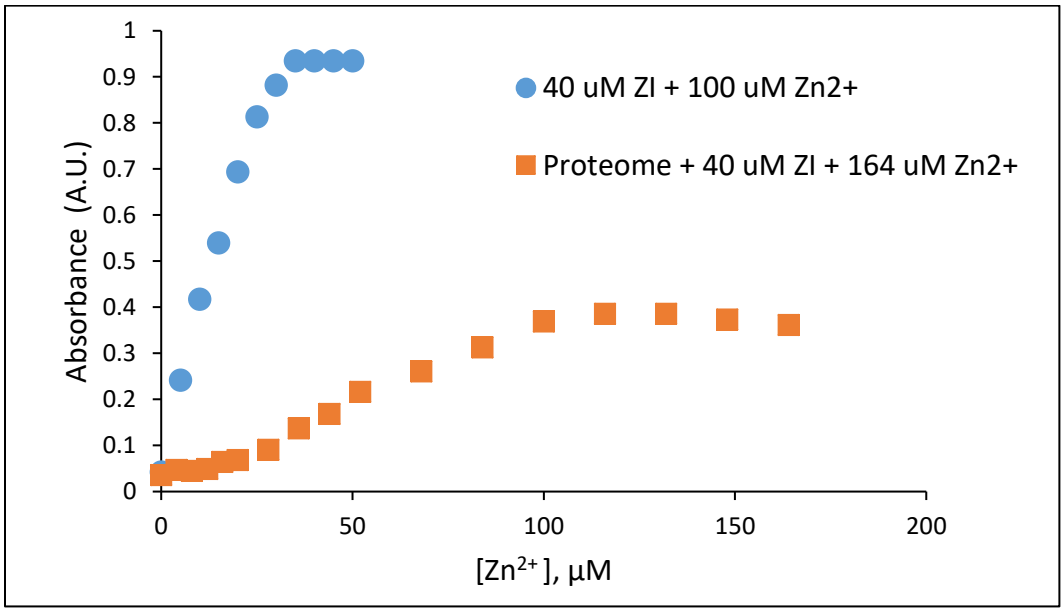

Figure 7. Titration of ZI with Zn^{2+} in presence of proteome. (A) Proteome (4.5 µM native Zn^{2+}) isolated from LLC-PK_1 cells was treated with 40 µM ZI followed by titration with Zn^{2+}. The reaction progress was monitored by recording the absorbance between 350- 700 nm. (B) Control: change of absorbance at 620 nm with titration of 40 µM ZI with Zn^{2+}. Proteome: change of absorbance at 640 nm from the titration experiment in presence of proteome.

A.

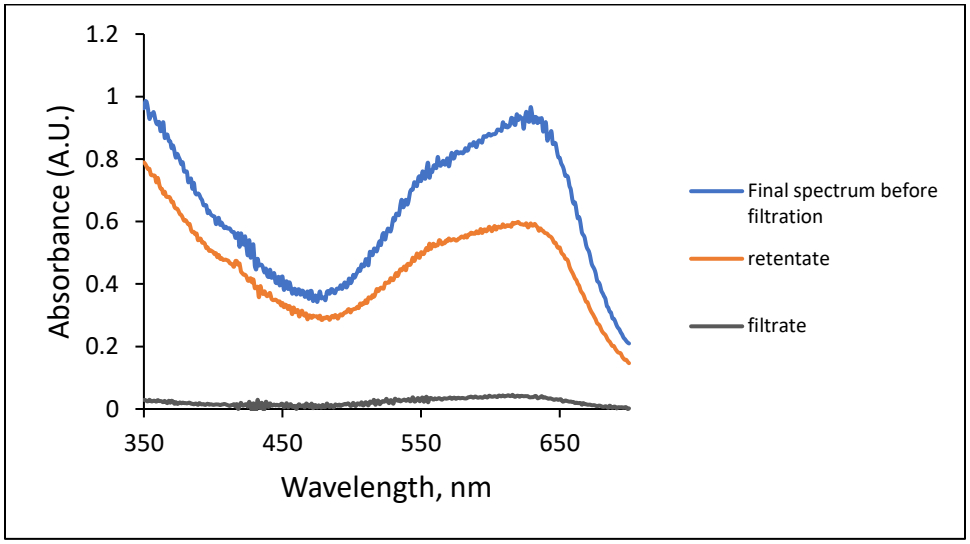
1.2
1
0.8
0.6
0.4
0.2
0
Absorbance (A.U.)
350
450
550
650
Wavelength, nm
Final spectrum before filtration
retentate
filtrate

B.

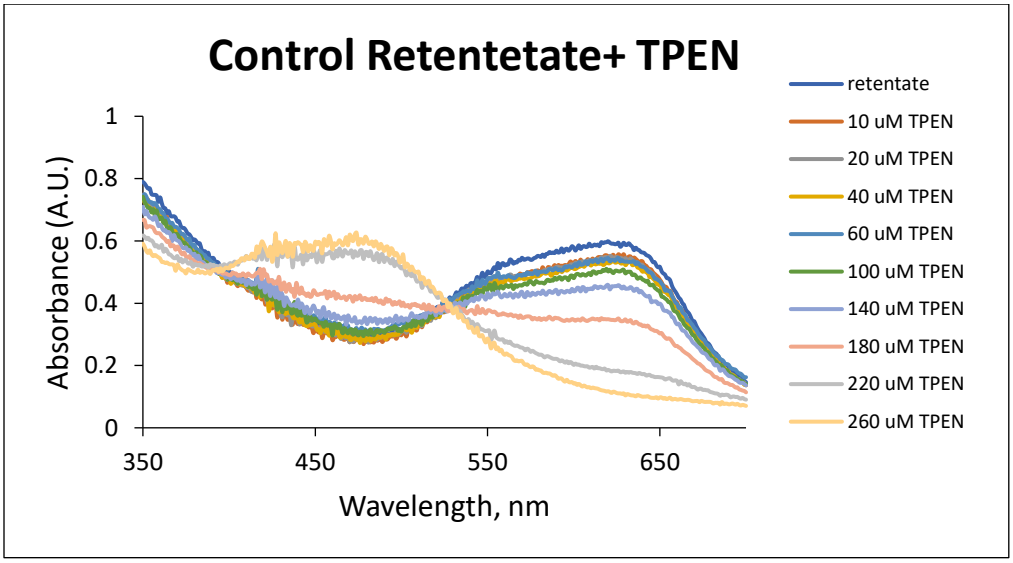
Control Retentetate+ TPEN
1
0.8
0.6
0.4
0.2
0
Absorbance (A.U.)
350
450
550
650
Wavelength, nm
retentate
10 uM TPEN
20 uM TPEN
40 uM TPEN
60 uM TPEN
100 uM TPEN
140 uM TPEN
180 uM TPEN
220 uM TPEN
260 uM TPEN

C.

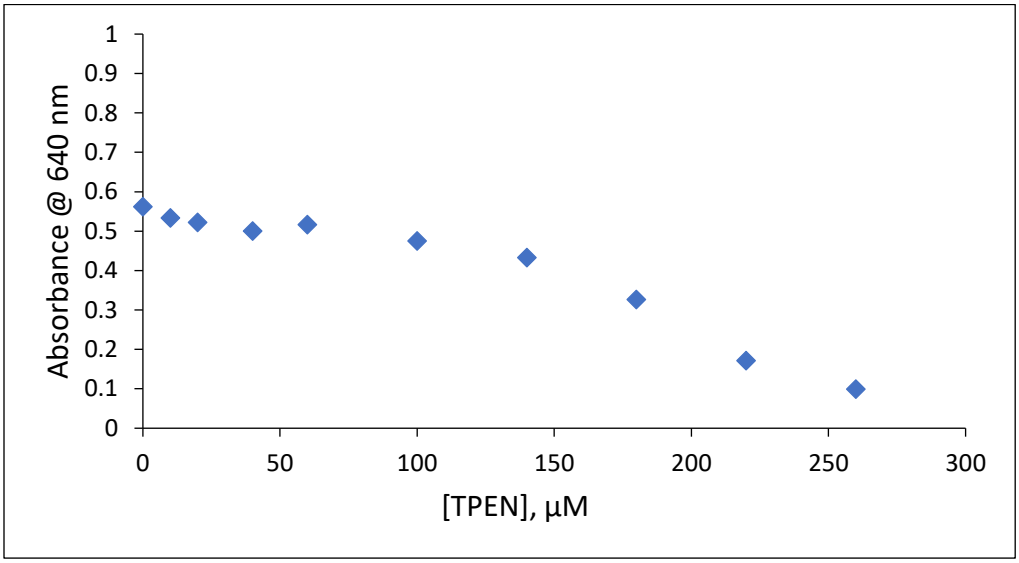

Figure 8. Characterization of 640 nm absorbing species. (A) 50 µM ZI was titrated with Zn^{2+} (final 240 µM) in the presence of Proteome. Thereafter, the final reaction mixture was filtered using a Centricon 3K molecular weight cut-off filter to separate the high molecular weight and low molecular weight fractions. (B) Retentate fraction was titrated with TPEN. (C) Change of 640 nm absorbance of the retentate following addition of TPEN.

3.1.3 Reaction of Proteome•Zn-ZI with TSQ

The formation of ternary complex, Proteome•Zn-ZI, between proteome's lower affinity zinc binding sites and Zn-ZI was tested another way. A widely used fluorescent zinc sensor, TSQ forms ternary complexes with both native Zn-proteins and with zinc that is adventitiously bound to proteome's non-specific zinc binding sites [77]. Therefore, the pre-formed ternary complex Proteome•Zn-ZI was reacted with TSQ to see if it replaces ZI from the ternary complex and makes new ternary complex, Proteome•Zn-TSQ.

$$\text{TSQ} + \text{Zn-Protein} \leftrightarrows \text{TSQ-Zn-Protein} \qquad (18)$$

$$\text{TSQ} + \text{Proteome•Zn} \leftrightarrows \text{Proteome•Zn-TSQ} \qquad (19)$$

For this purpose, first, Proteome•Zn-ZI was formed by titrating 40 µM ZI with Zn^{2+} in the presence of isolated proteome. As expected, a gradual increase in absorbance at 640 nm was observed with the addition of Zn^{2+} after Proteome's high affinity zinc binding sites were saturated, indicating the generation of Proteome•Zn-ZI ternary complex (**Figure 9 A** and **B**).

$$\text{Proteome} + \text{Zn-ZI} \leftrightarrows \text{Proteome•Zn-ZI (640 nm absorbance)} \qquad (20)$$

Subsequently, the final reaction mixture was treated with increasing concentrations of TSQ. Interestingly, with the increment in TSQ concentration to the reaction mixture, absorbance at 640 nm slowly decreased (**Figure 9 C** and **D**). At about 80 µM TSQ, 640 nm absorbance was almost completely lost. The displacement of ZI from the ternary complex, Proteome•Zn-ZI, by TSQ and by inference the generation of a new ternary complex, Proteome•Zn-TSQ, was consistent with the loss of absorbance at 640 nm with addition of TSQ. Since TSQ shows

negligible absorbance in the 500-650 nm range, the change in the spectrum could be solely attributed to the dissociation of Zn-ZI in the ternary complex with the Proteome.

$$\text{Proteome}\bullet\text{Zn-ZI} + \text{TSQ} \leftrightarrows \text{Proteome}\bullet\text{Zn-TSQ} + \text{ZI} \quad (21)$$

This result further supported that ZI forms ternary complex with zinc adventitiously bound to proteome's lower affinity non-specific binding sites

A.

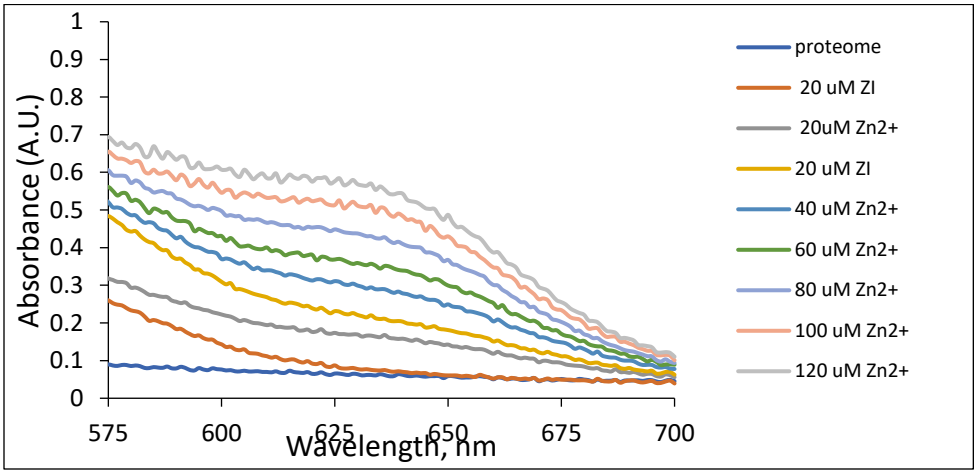
Absorbance (A.U.)
1
0.9
0.8
0.7
0.6
0.5
0.4
0.3
0.2
0.1
0
575
600
625
650
675
700
Wavelength, nm
proteome
20 uM ZI
20uM Zn2+
20 uM ZI
40 uM Zn2+
60 uM Zn2+
80 uM Zn2+
100 uM Zn2+
120 uM Zn2+

B.

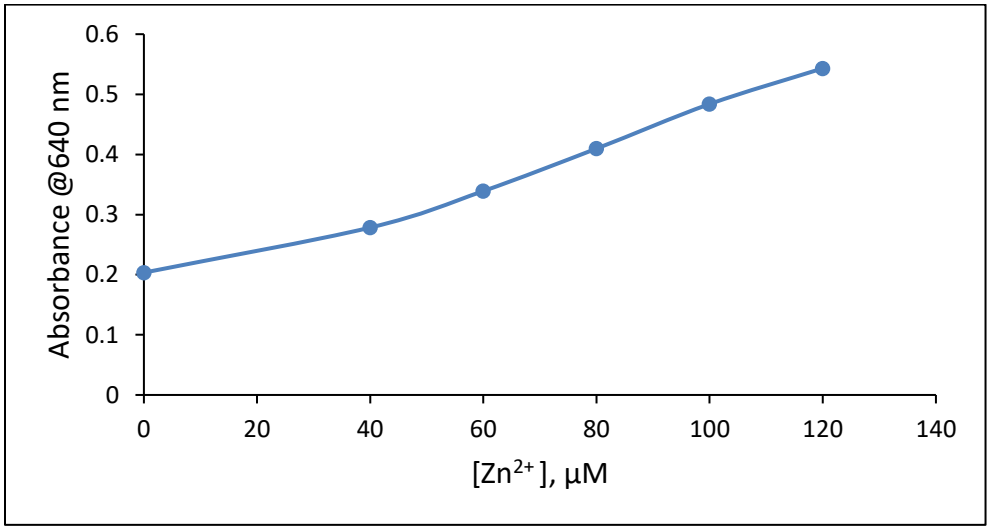
Absorbance @640 nm
0.6
0.5
0.4
0.3
0.2
0.1
0
0
20
40
60
80
100
120
140
[Zn2+], µM

C.

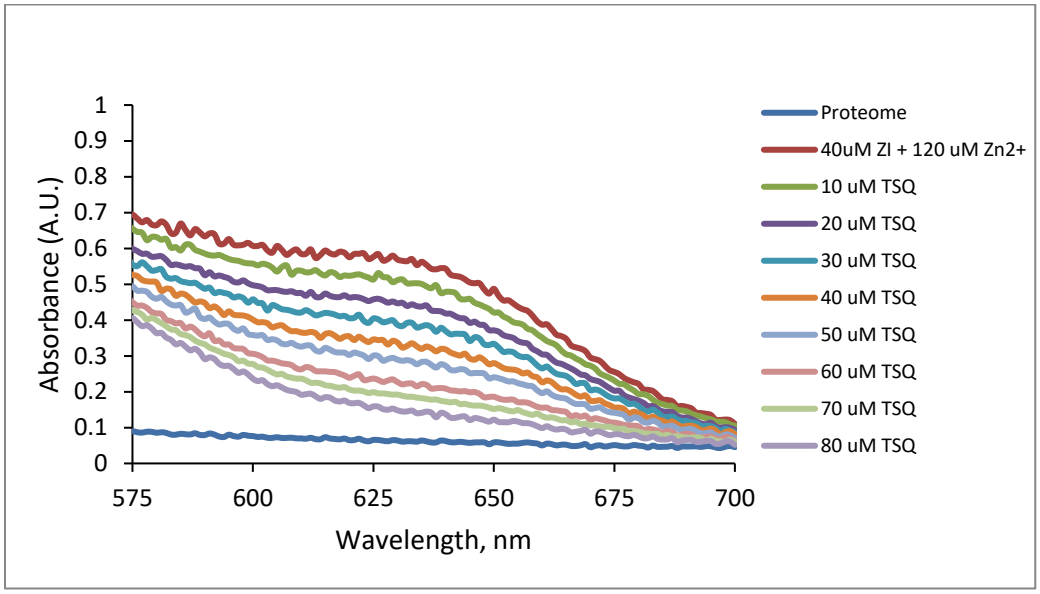

D.

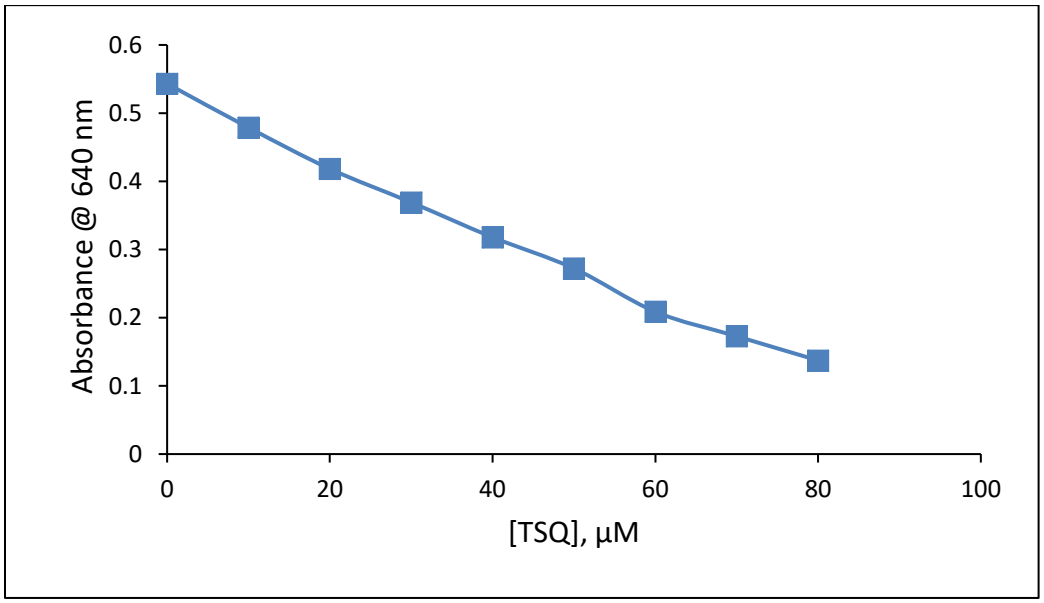

Figure 9. Reaction of Proteome•Zn-ZI with TSQ. (A) 40 µM ZI was titrated with Zn^{2+} in the presence of isolated Proteome. (B) Change of absorbance at 640 nm with the increasing concentration of added Zn^{2+}. (C) The final reaction mixture of (A) was titrated with TSQ. (D) Change of absorbance at 640 nm with the increasing concentration of TSQ.

3.1.4 Reaction of Zn-ZI with a model zinc binding protein

The results of the reaction of Zn^{2+} and ZI with Proteome were consistent with the formation of the ternary adduct, Proteome•Zn-ZI. Next, we repeated the experiment with a model protein, bovine serum albumin (BSA). BSA was chosen as the model protein for this experiment, because it has been reported to have a zinc binding sites that are variably occupied with Zn^{2+} [100]. Therefore, its ability to bind Zn^{2+} reversibly seems to model proteomic binding of Zn^{2+}. To test its interaction with Zn^{2+} and ZI, 10 µM BSA in 20 mM Tris (pH 7.4) was first treated with 50 µM ZI (**Figure 10 A**). As expected, in the presence of BSA, ZI showed an absorption maximum at 490 nm, and no noticeable absorbance at 640 nm. However, as the mixture of 10 µM BSA and 50 µM ZI was titrated with Zn^{2+}, a gradual increase of absorbance at 640 nm appeared, with the disappearance of absorbance at 490 nm (**Figure 10 A** and **B**). This simultaneous increase of absorbance at 640 nm and decrease at 490 nm suggested that BSA forms ternary complexes, BSA•Zn-ZI, with ZI and Zn^{2+} bound to its non-specific zinc binding sites.

$$BSA + ZI + Zn^{2+} \leftrightarrows BSA\bullet Zn\text{-}ZI \quad (640\ nm\ absorbance) \qquad (22)$$

At the end of titration, the final reaction mixture was filtered using a Centricon 3K molecular weight cut-off filter to separate the high molecular weight (retentate) and low molecular weight (filtrate) fractions. Both fractions were analyzed for absorbance and zinc content. The retentate displayed an absorption maximum at 640 nm and retained virtually all of the added Zn^{2+} during titration, further confirming the formation of ternary complex, BSA•Zn-ZI (**Figure 10 C** and **D**).

A.

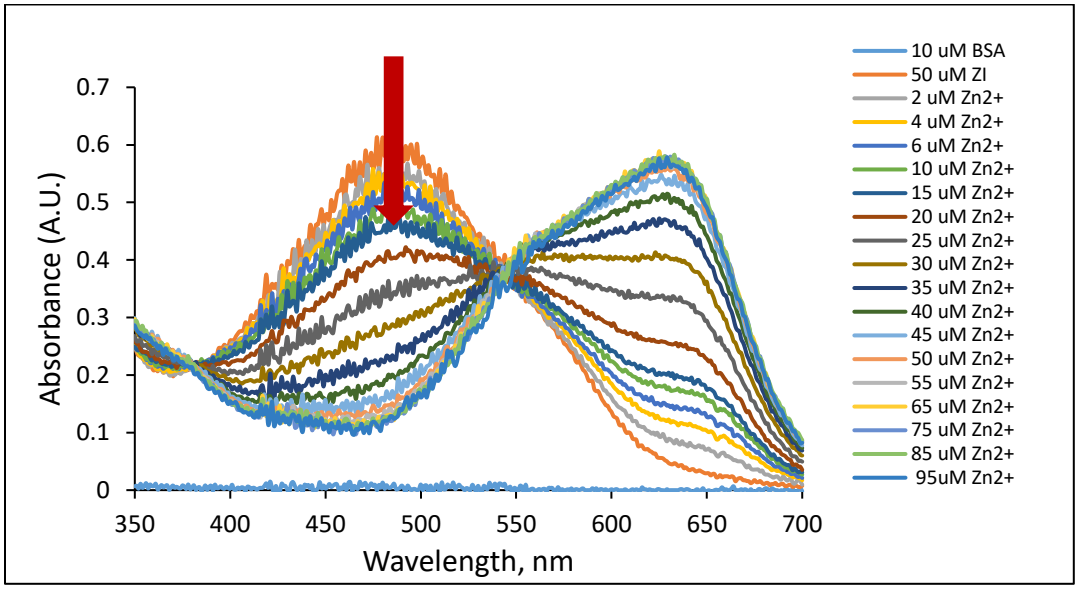
Absorbance (A.U.)
0.7
0.6
0.5
0.4
0.3
0.2
0.1
0
350
400
450
500
550
600
650
700
Wavelength, nm
10 uM BSA
50 uM ZI
2 uM Zn2+
4 uM Zn2+
6 uM Zn2+
10 uM Zn2+
15 uM Zn2+
20 uM Zn2+
25 uM Zn2+
30 uM Zn2+
35 uM Zn2+
40 uM Zn2+
45 uM Zn2+
50 uM Zn2+
55 uM Zn2+
65 uM Zn2+
75 uM Zn2+
85 uM Zn2+
95uM Zn2+

B.

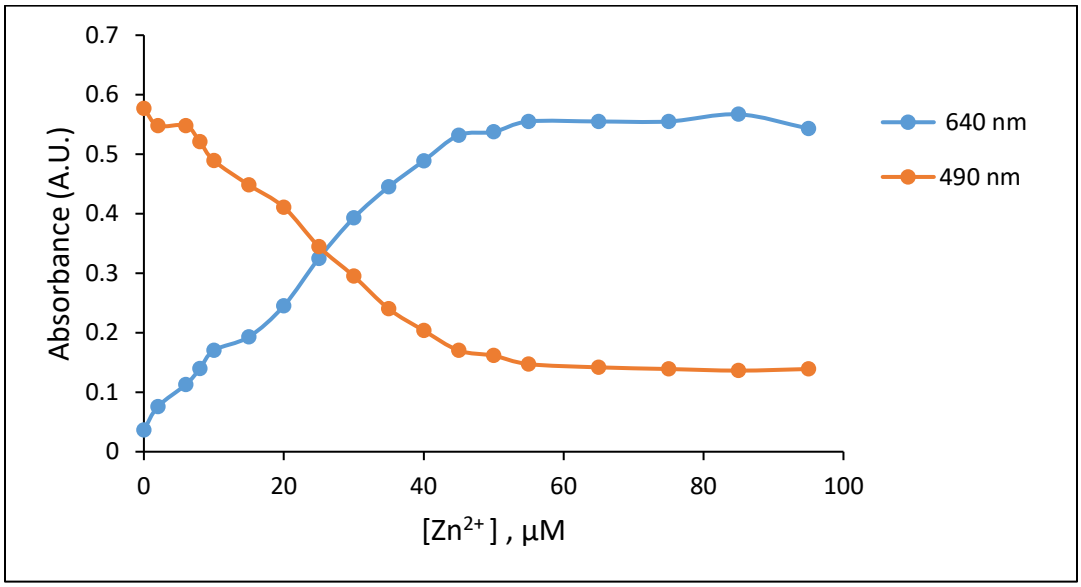
Absorbance (A.U.)
0.7
0.6
0.5
0.4
0.3
0.2
0.1
0
0
20
40
60
80
100
[Zn2+] , µM
640 nm
490 nm

C.

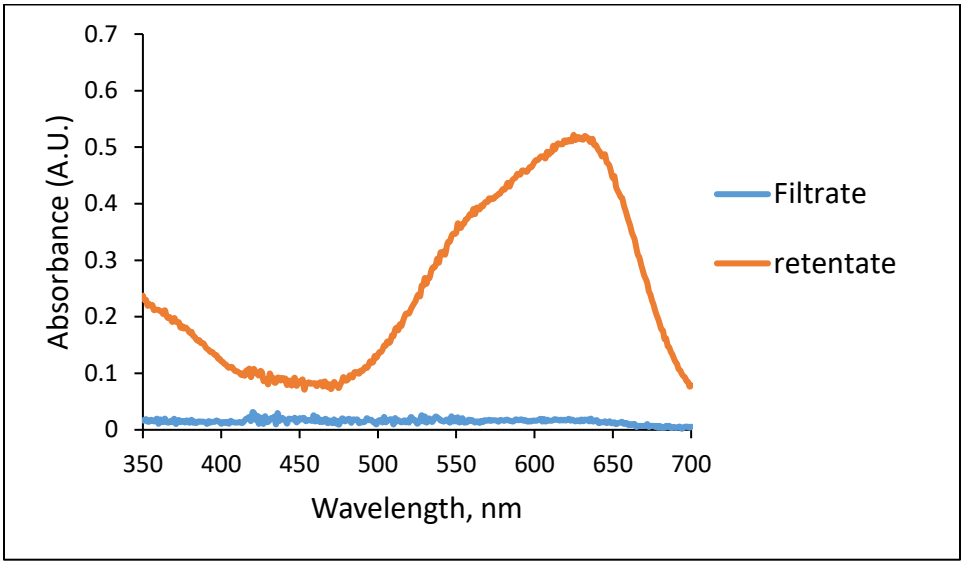

D.

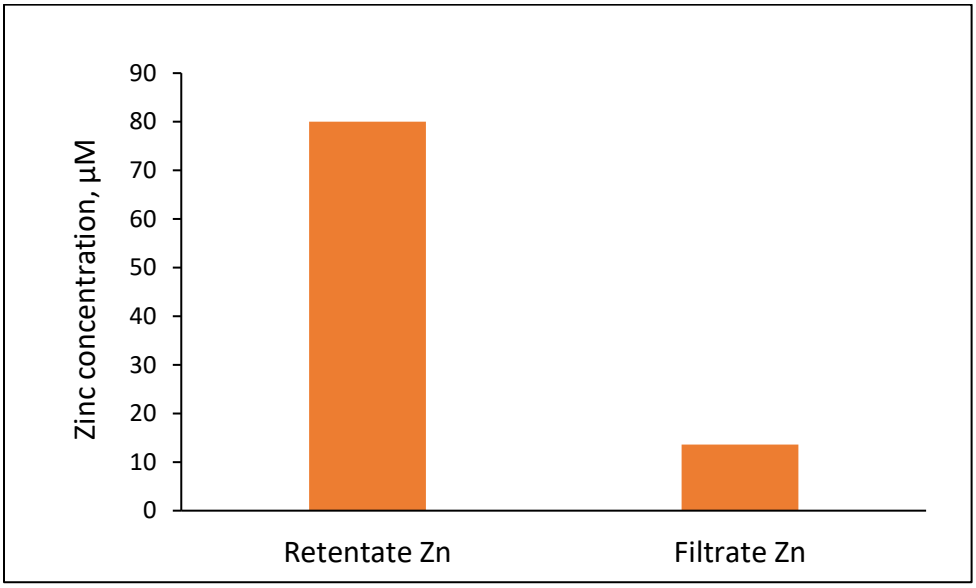

Figure 10. Reaction of BSA with ZI and Zn^{2+}. (A) 10 µM BSA in 20 mM Tris (pH 7.4) was treated with 50 µM ZI followed by titration with Zn^{2+}. (B) Change of absorbance at 490 nm and 640 nm with the increasing concentration of Zn^{2+}. (C) Absorption spectrum of retentate and filtrate following filtration of the final reaction of (A) using a Centricon 3K molecular weight cut-off filter. (D) Zinc content of the retentate and filtrate fractions.

The stoichiometry of BSA and Zn^{2+} was identified as well. 5 µM BSA in 20 mM Tris buffer (pH 7.4) was incubated with 13 different concentrations of Zn^{2+} between 2 – 80 µM. Subsequently, each of the 13 reaction mixtures was filtered using Centricon 3K molecular weight cut-off filter to separate the retentate and filtrate fractions. Zinc content in both retentate and filtrate fractions was quantified. The amount of zinc in retentate and filtrate fractions was labelled as 'bound zinc' and 'free zinc', respectively. Total added zinc was plotted against the bound zinc to identify the stoichiometry between BSA and zinc (**Figure 11**). From the plot, it appeared that 35-40 nmol of zinc was required to saturate the zinc binding sites of 5 nmol of BSA, meaning that each BSA molecule can potentially bind 7-8 zinc ions.

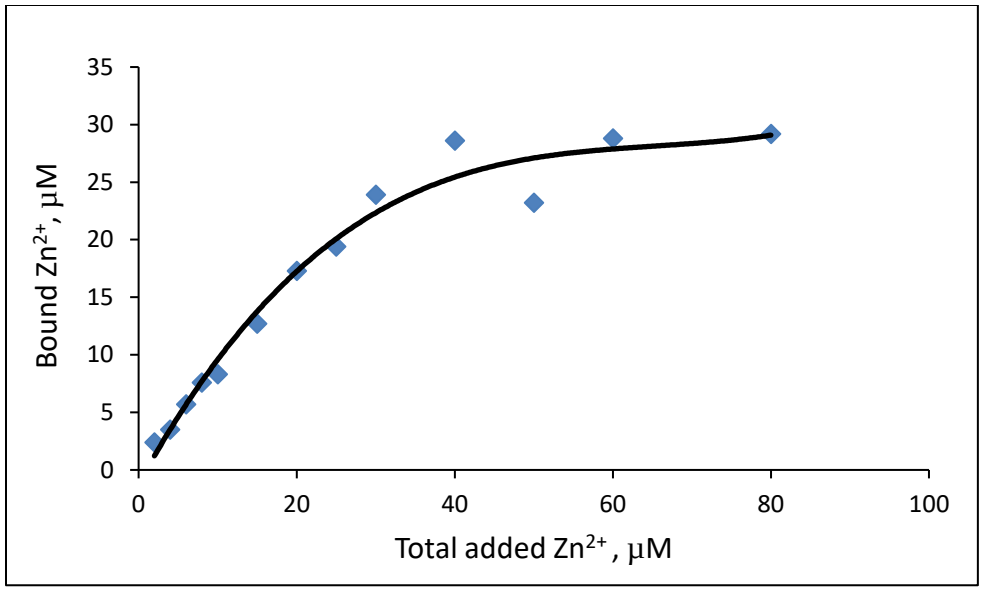

Figure 11. Zinc binding of BSA. 5 µM BSA in 20 mM Tris buffer (pH 7.4) was incubated with varying concentrations of zinc, and each mixture was then filtered using a Centricon 3K molecular weight cut-off filter to separate the retentate from the filtrate fraction. Zinc content was quantified in each fraction. Zinc content in the retentate fractions for each mixture (bound zinc) was plotted against the total added zinc in each mixture.

As a negative control, ternary complex formation experiment was conducted with trypsin to test if ternary complex formation is independent of the existence of zinc binding site in a protein. Trypsin was chosen because it has no potential zinc binding sites. First, interaction of ZI with trypsin was examined by incubating 10 µM trypsin in 20 mM Tris buffer (pH 7.4) with 40 µM ZI. ZI did not display any interaction with trypsin, as evident from its absorption spectrum centered at 490 nm (**Figure 12 A**). In addition, following filtration of the reaction mixture using a Centricon 3K molecular weight cut-off filter, most of the absorbance was confined to the filtrate (**Figure 12 A**), further indicating the lack of interaction between trypsin and ZI.

When the reaction mixture of 10 µM trypsin and 40 µM ZI was titrated with Zn^{2+}, an increase of absorbance at 620 nm was observed (**Figure 12 B**), suggesting the formation of Zn-ZI binary complex. Moreover, change of absorbance at 620 nm with increasing concentration of Zn^{2+} was in alignment with that of control titration, i.e. titration of 40 µM ZI with Zn^{2+} in the absence of trypsin (**Figure 12 C**). And the presence or an isosbestic point at – nm demonstrated that the simple conversion of ZI to Zn-ZI had occurred in the titration. These results confirmed that proteins need to have potential zinc binding sites for non-specific zinc binding.

A.

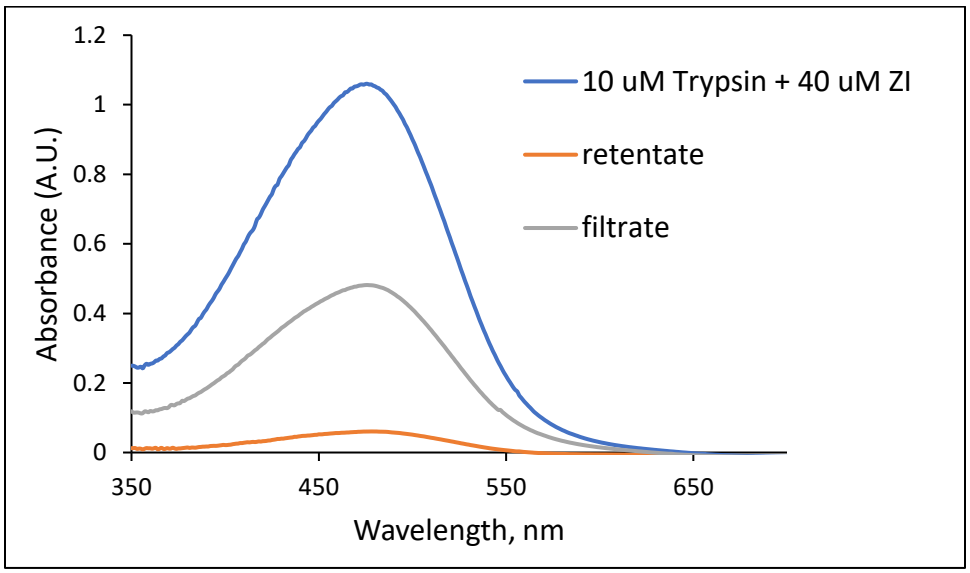
1.2
1
0.8
0.6
0.4
0.2
0
Absorbance (A.U.)
350
450
550
650
Wavelength, nm
10 uM Trypsin + 40 uM ZI
retentate
filtrate

B.

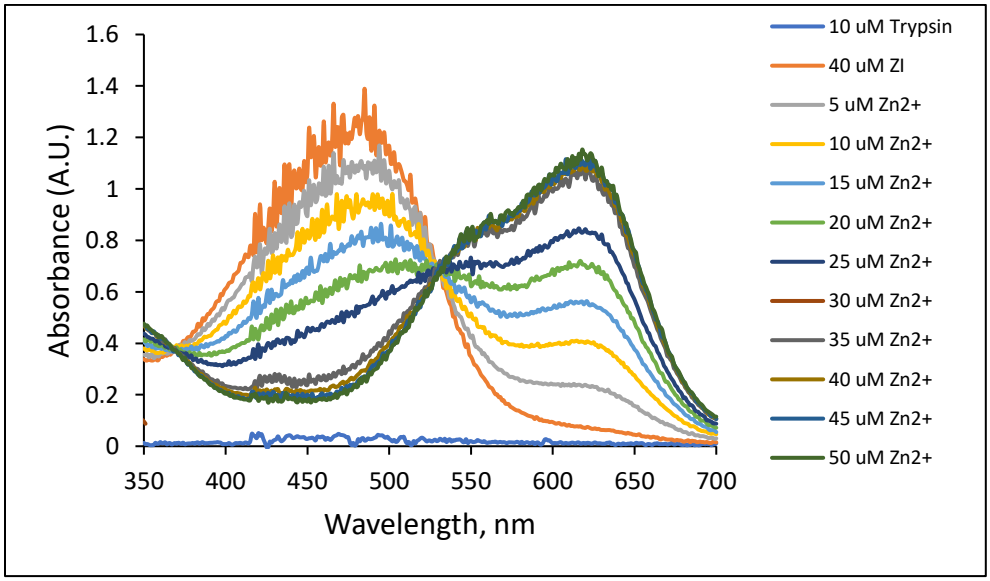
1.6
1.4
1.2
1
0.8
0.6
0.4
0.2
0
Absorbance (A.U.)
350
400
450
500
550
600
650
700
Wavelength, nm
10 uM Trypsin
40 uM ZI
5 uM Zn2+
10 uM Zn2+
15 uM Zn2+
20 uM Zn2+
25 uM Zn2+
30 uM Zn2+
35 uM Zn2+
40 uM Zn2+
45 uM Zn2+
50 uM Zn2+

C.

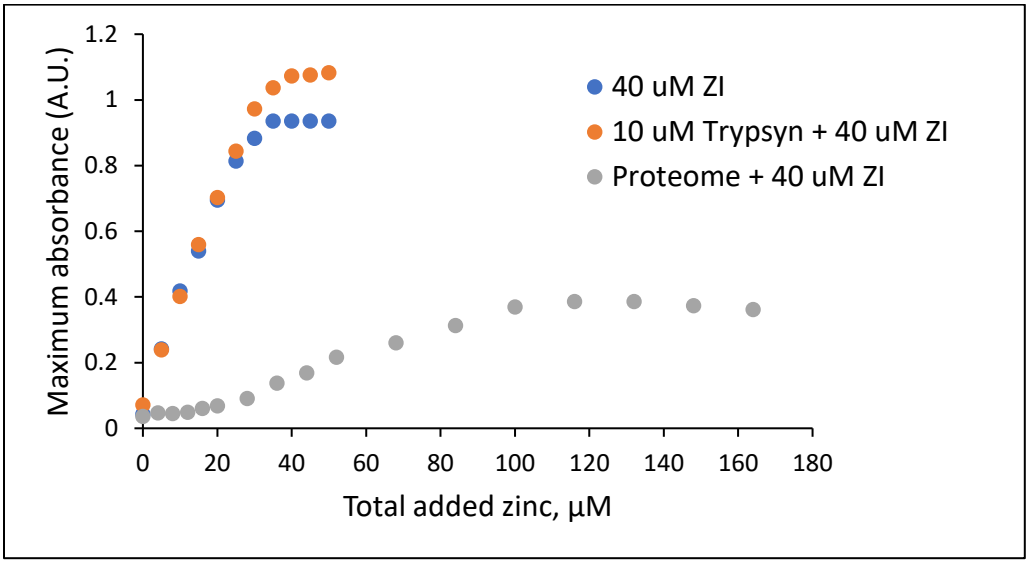

Figure 12. Titration of ZI with Zn2+ in the presence of trypsin. (A) Absorption spectra of the reaction mixture of 10 µM trypsin and 40 µM ZI, and the retentate and filtrate following filtration of the reaction mixture using a Centricon 3K molecular weight cut-off filter. (B) Titration of 40 µM ZI with Zn^{2+} in the presence of 10 µM trypsin. (C) Change of absorbance with increasing concentration during titration of 40 µM ZI with Zn^{2+} in the presence or absence of Proteome or 10 µM trypsin.

3.1.5 Absorption spectrum of Zn-ZI in different solvents

We considered the possibility that the shift of absorption maximum to 640 nm following the addition of Zn^{2+} to the mixture of proteome and ZI originated from the presence of Zn-ZI complex in a distinctive proteomic microenvironment, not from Proteome•Zn-ZI ternary complex formation. To test this possibility, Zn-ZI solution was prepared in different solvents of varying polarity and their absorption spectrum was recorded (**Figure 13**). In none of the cases did Zn-ZI display an absorption spectrum similar to that obtained in the presence of Proteome or Albumin, suggesting that the shift of absorption maximum to 640 nm during titration of ZI with Zn^{2+} in presence of proteome was due to proteome•Zn-ZI ternary complex formation.

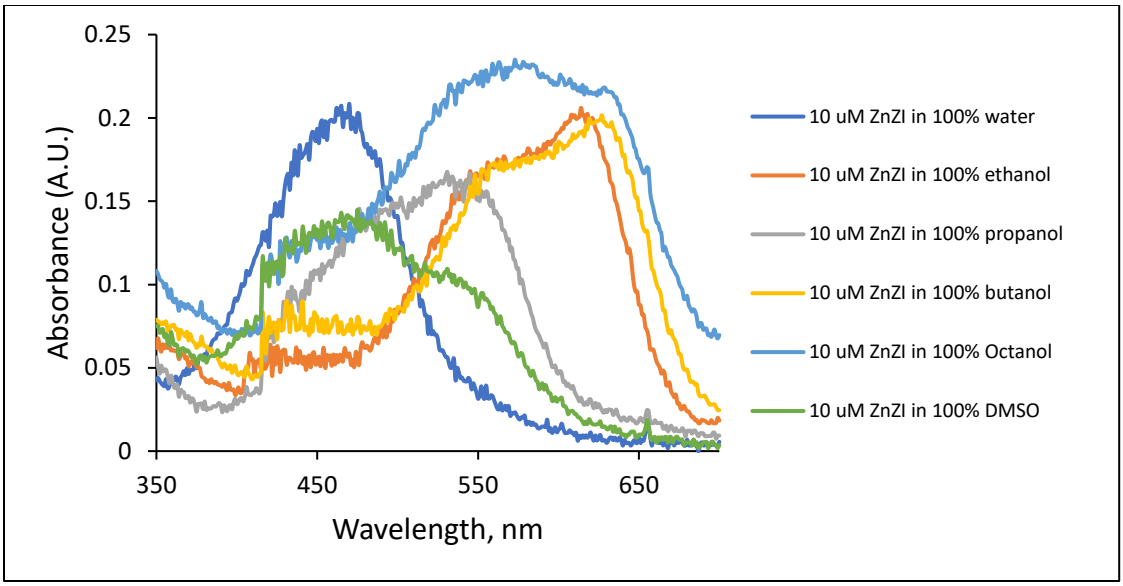

Figure 13. Zn-ZI solution in different solvents. 10 µM Zn-ZI was prepared in various solvents and absorption spectra were recorded

3.1.6. Effect of N-ethylmaleimide (NEM) on proteome's non-specific zinc binding

To further characterize proteome's non-specific zinc binding, we attempted to identify the proteomic components involved in adventitious zinc binding. Because cysteine residues are predominantly present in zinc binding sites of native Zn-proteins, we hypothesized that Proteome's adventitious zinc binding sites involve sulfhydryl groups as well. To test the hypothesis, Proteome's zinc buffering capacity was examined following pre-incubation with N-ethylmaleimide (NEM), a thiol-binding reagent that blocks the sulfhydryl groups [101]. Isolated Proteome was first pre-treated with 500 µM NEM for an hour and then titrated with Zn^{2+} in the presence of 40 µM ZI. A control experiment was done proteome without any pre-treatment with NEM. As expected, the control titration displayed zinc buffering capacity by Proteome, as evident from very small increase of absorbance at the beginning of titration (**Figure 14**). However, in case of NEM-treated Proteome, the increase in absorbance was immediate and did not include the initial lag phase of the control titration (**Figure 14**), indicating that NEM pre-treatment significantly reduced proteome's high affinity non-specific zinc binding capacity. Apart from this impact, the rest of the two curves are similar. While about 50 µM Zn^{2+} was needed to reach mid-point of the control titration, only about 30 µM Zn^{2+} was needed in case of NEM-treated proteome experiment. These results clearly suggested that Proteome uses sulfhydryl groups for high affinity, non-specific zinc binding. Once NEM has reacted with the SH groups, there are lower affinity sites that are available for reaction with Zn and ZI. These are the ones that yield the 640 nm absorbance.

$$\text{Proteome-SH} + Zn^{2+} \leftrightarrows \text{Proteome-S}\bullet\text{Zn (high affinity)} \qquad (23)$$

$$\text{Proteome-SH} + \text{NEM} \leftrightarrows \text{Proteome-S-NEM} \qquad (24)$$

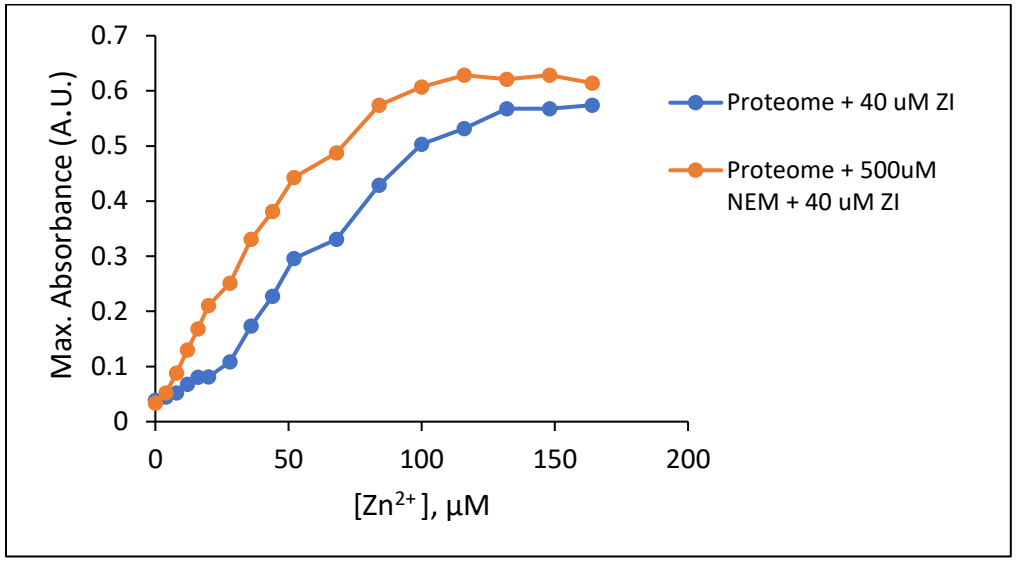

Figure 14. Effect of NEM on proteome's non-specific zinc binding. Proteome was pre-treated with 500 µM NEM for an hour. NEM-treated proteome was then reacted with 40 µM ZI followed by titration with Zn^{2+}. A control experiment was done with Proteome without any pre-treatment with NEM. The absorbance increase of both titration experiments with the increasing concentration of Zn^{2+} was plotted.

3. 2 Proteome mediated reconstitution of Zn-carbonic anhydrase

A eukaryotic cell contains about 3000 zinc proteins, among which zinc can have either structural or catalytical role [4, 14]. Recent studies have reported that zinc can act as a secondary messenger as well and participate in cellular signaling [53-57]. However, the trafficking pathways that lead to the formation of thousands of native Zn-proteins following the entry of zinc into the cytosol are not well understood. A few studies have reported that metallothionein, a widely expressed protein with variable Zn content, can act as an intermediate in cellular zinc trafficking and signaling [15, 31, 37, 38, 45]. Metallothionein (MT) has the ability to bind seven zinc with very strong affinity and can transfer these zinc ions to apo-proteins to generate native, specific Zn-proteins [34, 36]. However, metallothionein-null, MT gene knock-out cells were found to proliferate normally, suggesting that metallothionein is not absolutely necessary for the formation of Zn-proteins, which are critically important for cell survival [52]. Therefore, the mechanism of zinc's trafficking pathway remains unanswered.

As we have seen in the zincon study (section 3.1 above), the cellular proteome possesses a large number of adventitious zinc binding sites, that involve primarily sulfhydryl groups. The binding constant of the high affinity sites was calculated to be on the order of 10^{10} M, which is within the range of the stability constants (10^{9} – 10^{12} M) of native Zn-proteins [11, 12]. Therefore, we have hypothesized that these proteomic, non-specific zinc binding sites participate in trafficking zinc to the target proteins to generate native Zn-proteins. According to our hypothesis, following the entry into cytosol, zinc trafficking via proteomic binding occurs in two steps: (i) zinc binds to proteome at various non-specific sites primarily through sulfhydryl

groups, and (ii) zinc is then transferred from these proteomic non-specific sites to apo-proteins to make native, specific Zn-proteins via ligand substitution.

$$Zn^{2+}_{out} \leftrightarrows Zn^{2+}_{in} \quad \text{(transport into cells)} \tag{25}$$

$$Zn^{2+}_{in} + \text{Proteome-SH} \leftrightarrows \text{Proteome-S}\bullet\text{Zn} + H^{+} \text{ (step I)} \tag{26}$$

$$\text{Proteome-S}\bullet\text{Zn} + \text{apo-proteins} + H^{+} \leftrightarrows \text{Proteome-SH} + \text{Zn-proteins (step II)} \tag{27}$$

This part of the thesis describes the experiments and their results to investigate the above-mentioned zinc trafficking hypothesis.

Step 1 of zinc trafficking hypothesis: Non-specific zinc binding by Proteome

3.2.1 Cellular distribution of extra Zn^{2+} after entry into cytosol

In order to probe the first step of our hypothesis that following the entry into cytosol, zinc first binds at various non-specific zinc binding sites, LLC-PK_1 cells were treated with 50 µM Zn^{2+} for 48 hours. Subsequently, cells were washed thoroughly to remove the extracellular residual zinc, and the cellular supernatant was collected after sonication followed by centrifugation. The cytosol was then fractionated using size exclusion chromatography with Sephadex G-75. A control experiment was done with LLC-PK_1 cells untreated with excess Zn^{2+}, in which almost all the cellular zinc (61 µM) was found to be associated with high molecular proteome fractions and an insignificant pool of metallothionein zinc (2 µM) was observed (**Figure 5**). The result of untreated LLC-PK_1 cells was expected, because almost all the endogenous zinc in eukaryotic cells is bound to various proteins, and LLC-PK_1 cells express very little metallothionein under basal conditions.

Next, cells were exposed to 50 µM Zn^{2+} for 24 h and then examined for the distribution of zinc. The treatment of cell with excess zinc did not affect the cell viability (**Figure 15 A**). According to the Sephadex G-75 chromatogram, the total zinc content was measured be to 2 nmol/10^7 cells more than that of the control fractions, meaning that 2 nmol/10^7 cells of the added 200 nmol/10^7 cells could get into the cells (**Figure 15 B and C**). Moreover, high molecular weight proteome fractions from the treated cells had 0.5 nmol/10^7 cells more Zn^{2+} than those from control cells, indicating that 0.5 nmol/10^7 cells of the extra 2 nmol/10^7 cells Zn^{2+} (26%) ended up being bound to proteome. Since the native zinc binding sites are already by 61 µM Zn^{2+}, this

extra 10 μM Zn^{2+} is assumed to be bound at non-specific sites of proteome. In addition, the treatment of LLC-PK_1 cells with zinc induced the synthesis of a significant amount of metallothionein. About 1.45 nmol/10^7 cells more zinc was associated with metallothionein fractions collected from treated cells (1.5 nmol/10^7 cells) than from control cells, meaning that 1.45 nmol/10^7 cells of the extra 2 nmol/10^7 cells Zn^{2+} (73%) was captured by the induced metallothionein.

This is a very interesting finding, because this model reaction seems to support the first step of our zinc trafficking hypothesis that zinc can bind at adventitious sites of proteome as well as to metallothionein after making its way into the cytosol or cell supernatant. Although this type of experiment has been done innumerable times, showing that Zn transported into cells induces and then binds to MT, this is perhaps the first documenting that Zn associates both with MT and the proteome. Nevertheless, what was not resolved is the form of the extra Zn in the proteomic fractions. It could be Proteome•Zn (reaction 6) or it might be an adduct, Proteome-S-Zn_7-MT, that provides additional zinc to the proteome via the association of Zn_7-MT with proteomic sulfhydryl groups (reaction 7).

$$\text{Proteome-SH} + Zn_7\text{-MT} \leftrightarrows \text{Proteome-S}\bullet Zn_n + Zn_{(7-n)}\text{-MT} \qquad (28)$$

$$\text{Proteome-SH} + Zn_7\text{-MT} \leftrightarrows \text{Proteome-S-}Zn_7\text{-MT} \qquad (29)$$

A.

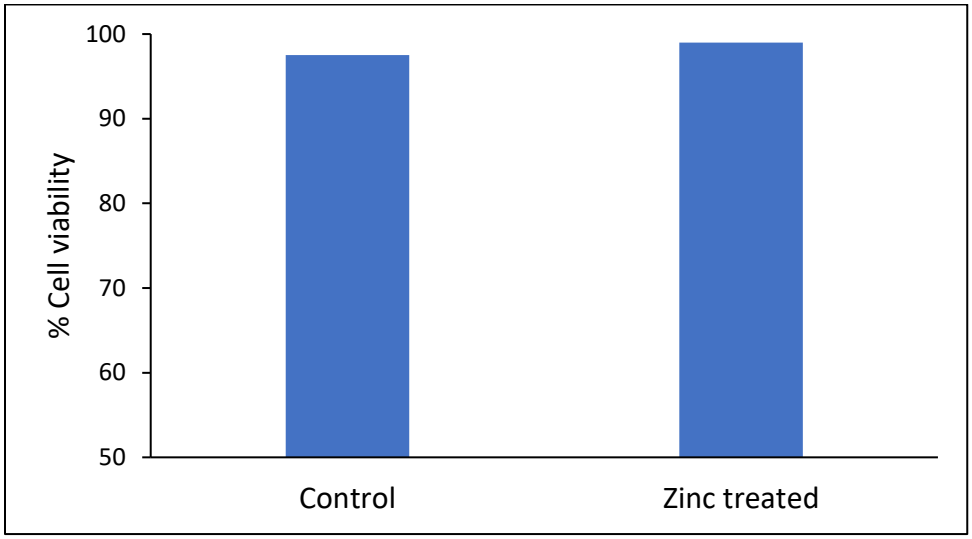
100
90
80
70
60
50
% Cell viability
Control
Zinc treated

B.

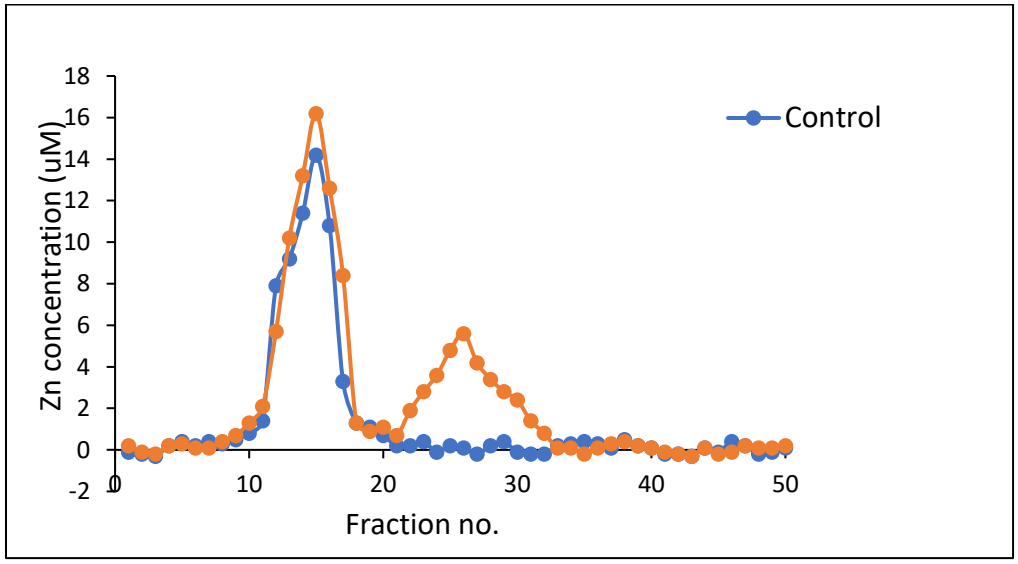
18
16
14
12
10
8
6
4
2
0
-2
Zn concentration (uM)
0
10
20
30
40
50
Fraction no.
Control

C.

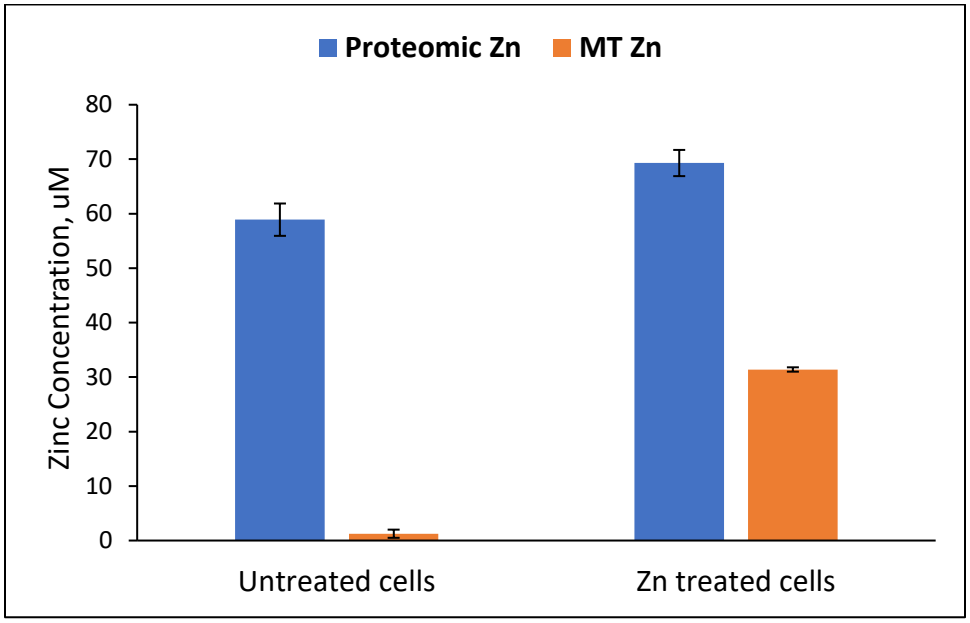

Figure 15. Distribution of added zinc between cellular proteome and metallothionein. (A) Cells were released from one confluent plate of control and zinc treated cells by trypsin treatment and stained with trypan blue to measure the cell viability. (B) $2x10^8$ LLC-PK_1 cells were incubated in culture media supplemented with or without (control) 50 µM $ZnCl_2$ for 48 hours. Following incubation, cells were harvested, washed, sonicated and centrifuged to collect the supernatant, which was then fractionated using a Sephadex G-75 column. Zinc content in each of the fractions was quantified using flame AAS. (C) Comparison of total proteomic and metallothionein zinc in control and zinc treated cells. Error bar indicated standard deviation.

3.2.2 Reaction of TSQ and proteome isolated from LLC-PK_1 cells treated with exogenous Zn^{2+}

According to **Figure 15**, we have found that 0.5 nmol/10^7 cells of 2 nmol/10^7 cells Zn^{2+} which entered into cells was associated with high molecular weight proteome fractions. We have shown that this extra zinc was bound to proteome at various adventitious zinc binding sites. To test whether the additional Zn in the Proteome stems from Proteome-S•Zn or Proteome-S-Zn_7-MT, proteome collected from zinc treated cells was reacted with TSQ, a fluorescent sensor that specifically binds to Zn-proteins as well as Zn^{2+}. TSQ reacts with 15-20% of the native Zn-proteins to form TSQ-Zn-protein ternary complex, evidenced by the slow increase of fluorescence with an emission maximum of 470 nm [76]. It does not react with Zn_7-MT. With non-specifically bound proteomic zinc, Proteome-S•Zn, TSQ reacts with a rapid enhancement of fluorescence at 470 nm. **Figure 16** shows the different reaction rate of native Zn-Proteins and Proteome-S•Zn with TSQ. In contrast, Zn-MT is unreactive with TSQ. Therefore, the different rate of TSQ fluorescence increase at 470 nm can differentiate between specifically (Zn-proteins) and non-specifically bound proteomic zinc (Proteome-S•Zn) as well as Proteome-S-Zn_7-MT (no fluorescent contribution).

Zn-protein + TSQ ⇆ TSQ-Zn-protein (ternary complex, 470 nm, slow) (30)

Proteome-S•Zn + TSQ ⇆ Proteome-S•Zn-TSQ (ternary complex, 470 nm, fast) (31)

Proteome-S-Zn_7-MT + TSQ ⇆ no reaction (32)

The reaction of control proteome (12.2 µM native Zn^{2+}) collected from untreated LLC-PK1 cells and 20 µM TSQ resulted in the slow increase of fluorescence centered at 470 nm, as expected, indicative of the formation of TSQ-Zn-protein ternary complex with native Zn-proteins (**Figure 17 A and C**). On the other hand, proteome collected from cells treated with extra zinc (50 µM) LLC-PK1 displayed a rapid two-fold increase of fluorescence at 470 nm, when reacted with 20 µM TSQ (**Figure 17 B and C**). This abrupt enhancement of TSQ fluorescence suggested that extra zinc was non-specifically bound to proteome and TSQ formed ternary complexes, proteome-S•Zn-TSQ, with them, which accounted for the fluorescence increase. This experiment further supported the hypothesis that after entering into the cytosol, a significant fraction of zinc binds proteomic adventitious sites, along with and perhaps in competition with metallothionein.

A.

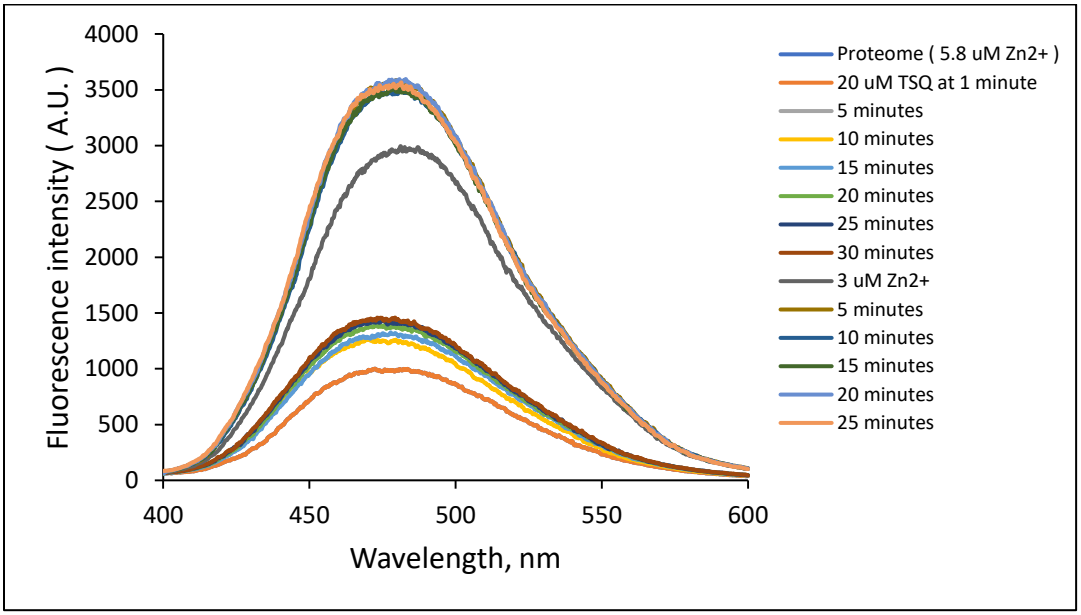

B.

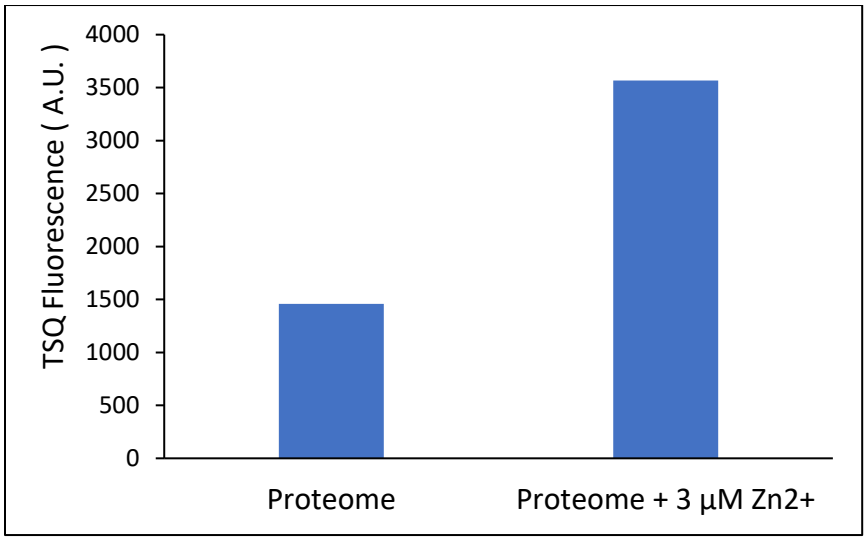

Figure 16. Reaction of zinc proteins with TSQ. (A) Isolated proteome containing 5.8 µM native zinc was reacted with 20 µM TSQ, followed by the addition of 3 µM excess zinc. (B) Comparison TSQ fluorescence before and after addition of 3 µM excess zinc.

A.

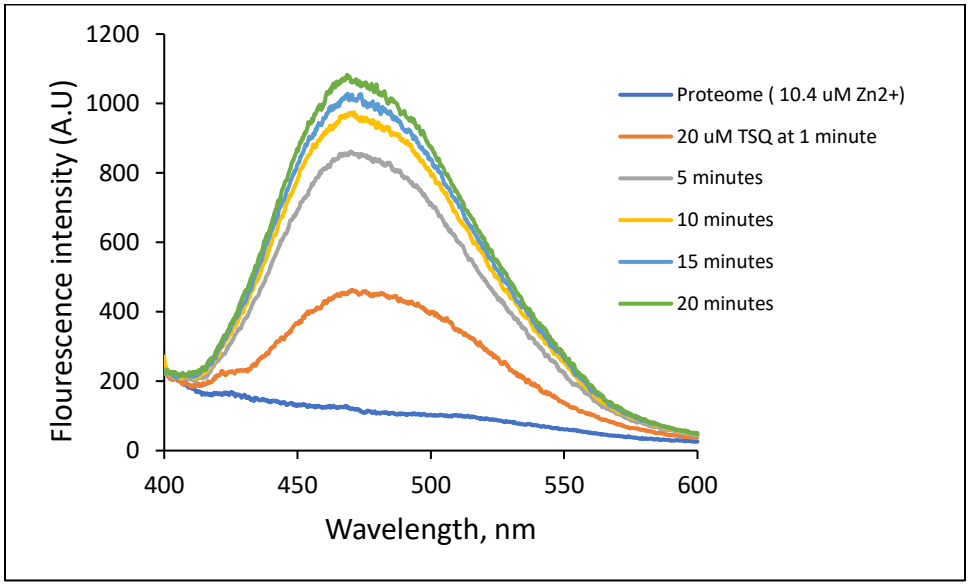
Flourescence intensity (A.U)
1200
1000
800
600
400
200
0
400
450
500
550
600
Wavelength, nm
Proteome (10.4 uM Zn2+)
20 uM TSQ at 1 minute
5 minutes
10 minutes
15 minutes
20 minutes

B.

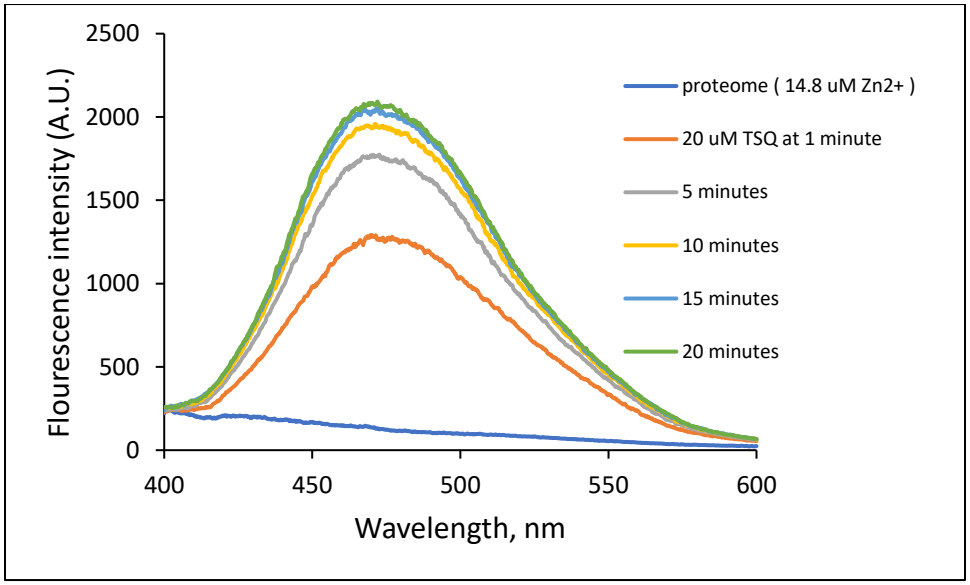
Flourescence intensity (A.U.)
2500
2000
1500
1000
500
0
400
450
500
550
600
Wavelength, nm
proteome (14.8 uM Zn2+)
20 uM TSQ at 1 minute
5 minutes
10 minutes
15 minutes
20 minutes

C.

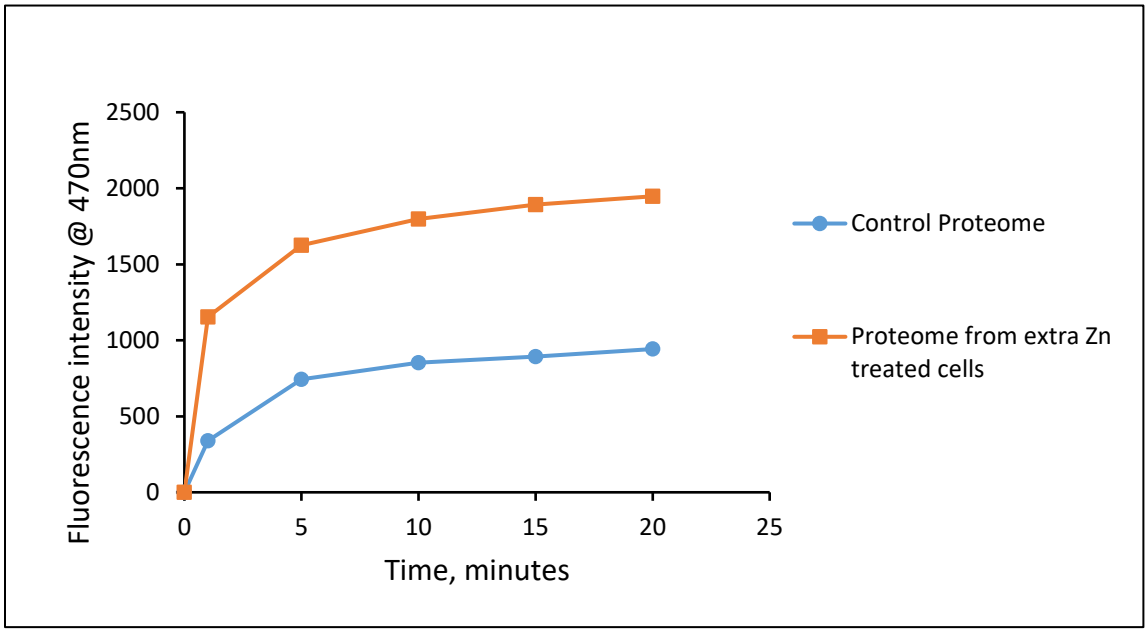

Figure 17. Reaction of proteome isolated from extra zinc treated cells with TSQ. (A and B) $2x10^8$ LLC-PK_1 cells were incubated in culture media supplemented with or without (control) 50 µM excess $ZnCl_2$ for 48 hours. Following incubation, cells were harvested, washed, sonicated and centrifuged to collect the supernatant, which was then fractionated using a Sephadex G-75 column. Proteome fractions were pooled together and reacted with 20 µM TSQ for 20 min. Fluorescence spectra were recorded from 400 nm to 600 nm following excitation at 370 nm. (C) Change of fluorescence at 470 nm with time from the reaction of proteome with TSQ.

Step 2 of zinc trafficking hypothesis: Zinc transfer from non-specific binding sites of Proteome to apo-Proteins

3.2.3. Reconstitution of a model apo-carbonic anhydrase with Proteome•Zn

The finding that Proteome-SH and Zn-MT establish an equilibrium distribution of Zn^{2+} reinforced the hypothesis that Zn^{2+} bound to Proteome plays a central role in the intracellular trafficking of Zn^{2+} that leads to the constitution of native Zn-proteins from precursor apo-proteins. To examine this hypothesis, we chose Zn-carbonic anhydrase as a model Zn-protein and studied the reaction of apo-carbonic anhydrase with Proteome•Zn.

$$\text{Proteome-S•Zn + apo-CA} \leftrightarrows \text{Proteome-SH + Zn-CA} \qquad (33)$$

Carbonic anhydrase was chosen for the following reasons.

- Known structure
- Known Zn stability constant
- Readily available

It does have the drawback that the apo-protein fully refolds into the native Zn-protein structure even in the absence of Zn^{2+} [102]. Its preformed, relatively rigid structure prevents zinc ligand flexibility as apo-CA reacts with Zn^{2+} bound to proteomic sites. Such lack of flexibility may act as a steric barrier to accomplishing the ligand substitution reaction.

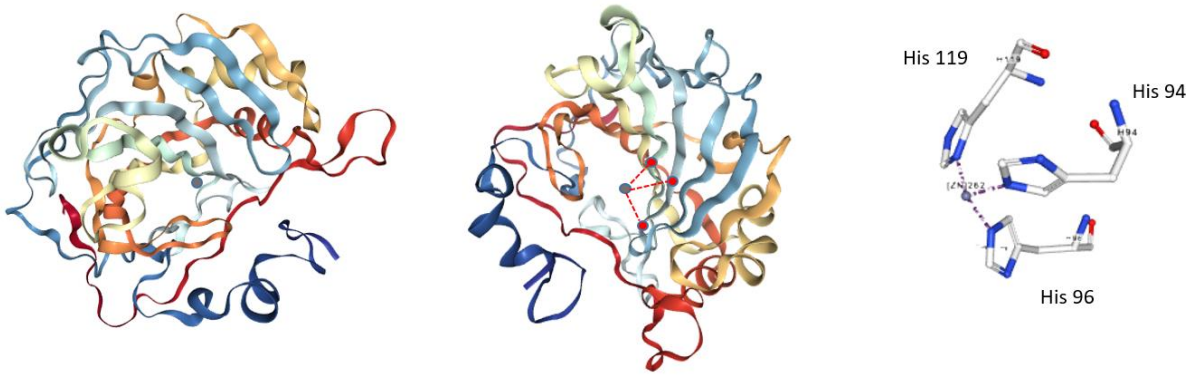

Zn/Apo-Carbonic anhydrase

Zn-His_3 site

Figure 18. Structure of Carbonic Anhydrase [102]

3.2.4 Preparation of apo-carbonic anhydrase (apo-CA) from Zn-carbonic anhydrase (Zn-CA)

Apo-carbonic anhydrase (apo-CA) was prepared from Zn-carbonic anhydrase (Zn-CA) following the protocol as described in methods [90, 91]. The extent of formation of apo-CA by the reaction of the preparation with dansyl amide (DA), which is used as a fluorescent sensor for Zn-CA [93].

$$\text{Zn-CA} + \text{DA} \leftrightarrows \text{DA-Zn-CA} \qquad (34)$$

When excited at 320 nm, DA, itself, displays a minor fluorescence emission with an emission maximum at 540 nm. When reacted with free zinc, the emission maximum remains unaltered. However, in the presence of Zn-CA, it forms a ternary complex, DA-Zn-CA, that causes a blue shift of its emission maximum to 460 nm. As the prepared apo-carbonic anhydrase was reacted with DA, emission maximum was found to be 540 nm and no significant fluorescence observed at 460 nm, indicating that the protocol successfully removed zinc from Zn-CA and apo-CA was formed (**Figure 19**). Direct measurement of Zn by atomic absorption spectrophotometry demonstrated that apo-CA preparations typically contained 6% of their original content of zinc. By contrast, the reaction of Zn-CA and DA produced fluorescence centered at 460 nm, indicating the formation of ternary complex, DA-Zn-CA (**Figure 19**). A titration of Zn-CA with DA showed that about 1.6 µM DA was needed to completely react with 1 µM Zn-CA (**Figure 20**). The reaction of 1 µM Zn-CA and 1.6 µM DA was fast and displayed about 1900±100 fluorescence units under the conditions of the measurements (reaction 12 and **Figure 19**).

$$Zn^{2+} + \text{DA} \leftrightarrows \text{No reaction (emission maximum 540 nm)} \qquad (35)$$

$$\text{apo-CA} + \text{DA} \leftrightarrows \text{No reaction (emission maximum 540 nm)} \qquad (36)$$

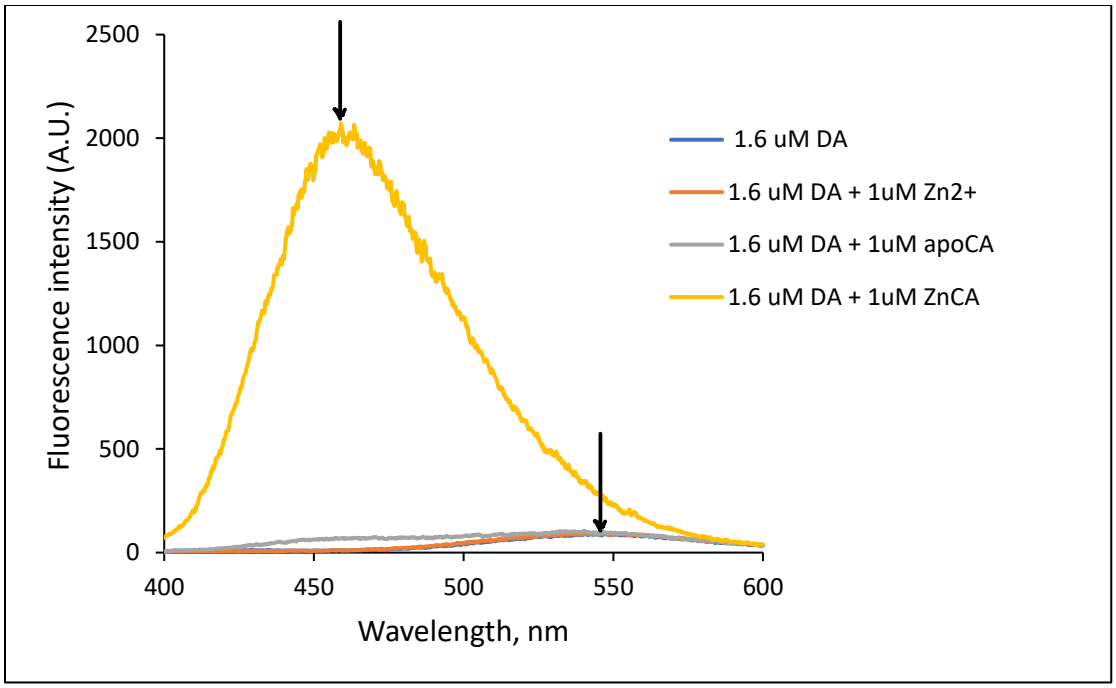

Figure 19. Emission spectra of dansyl amide (DA) in the presence of free zinc, apo-CA or Zn-CA. 1.6 µM dansyl amide (DA) in 20 mM Tris (pH 7.4) was treated with 1 µM Zn^{2+} or apo-CA or Zn-CA. The resulting solutions were then excited at 320 nm and fluorescence spectra were recorded from 400 nm to 600 nm.

A.

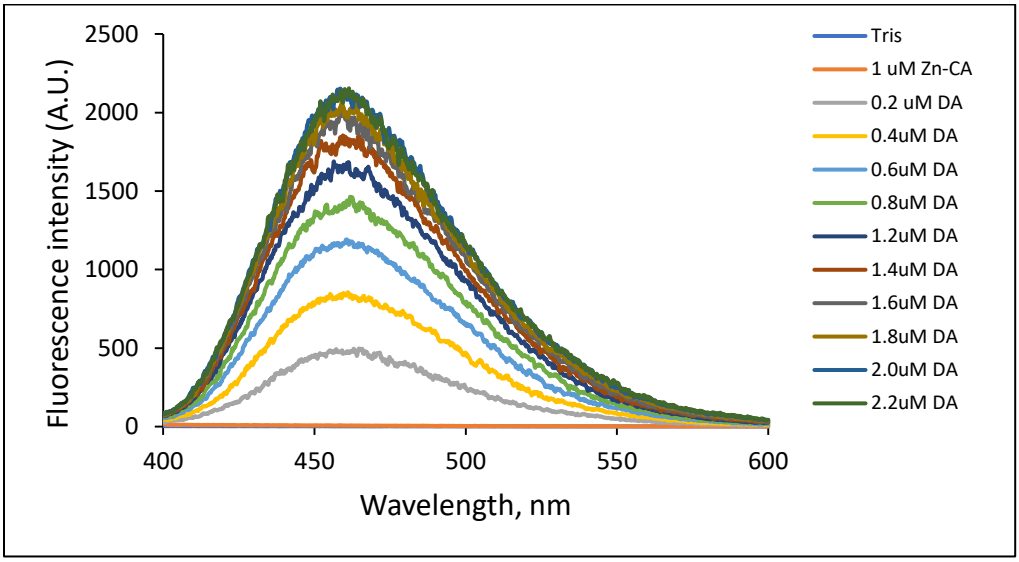

B.

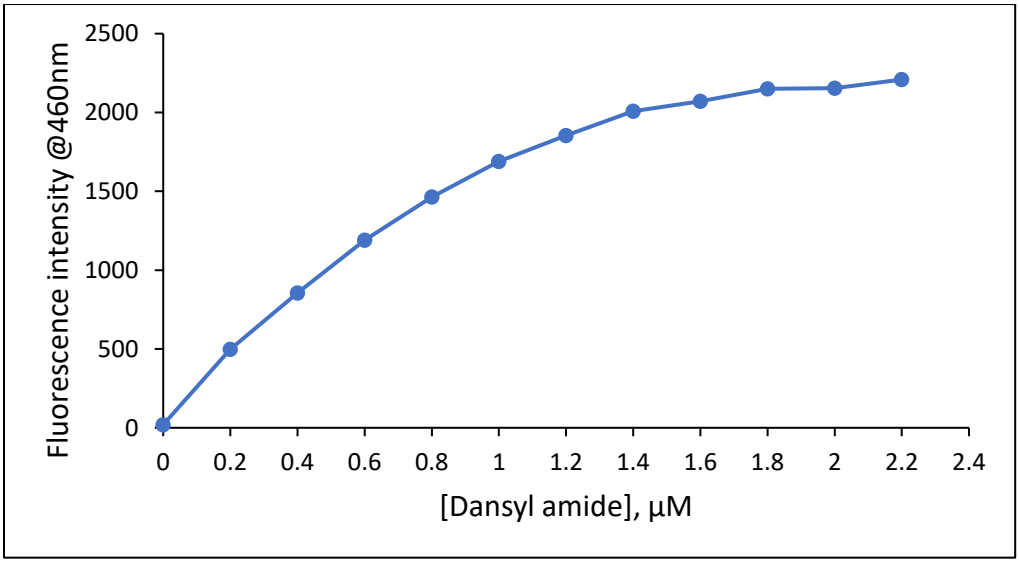

Figure 20. Titration of Zn-CA with dansyl amide. (A) 1 µM Zn-carbonic anhydrase (Zn-CA) in 20 mM Tris (pH 7.4) was titrated with the increasing concentrations of dansyl amide (DA). Following each addition, the reaction mixture was excited at 320 nm and fluorescence was recorded from 400 to 600 nm. (B) Maximum fluorescence of each spectrum from (A) was plotted against the concentration of dansyl amide.

3.2.5 Reaction of apo-carbonic anhydrase (apo-CA) with Zn^{2+} in the presence of dansyl amide (DA)

The prepared apo-carbonic anhydrase was tested for reconstitution of Zn-CA by reacting with Zn^{2+} and monitoring product formation with dansyl amide (DA) (**Figure 21**). When 1 µM Zn^{2+} was added to 1.6 µM DA, no change of fluorescence was observed, as expected. However, upon addition of 1 µM apo-CA, a dramatic increase of fluorescence occurred, and the emission maximum immediately shifted from 540 nm to 460 nm, indicative of the formation of Zn-CA (**Figure 21**). The final measurement of fluorescence units indicated that almost 100% Zn-CA was reconstituted from this reaction. Direct measurement of the zinc content of the product confirmed the reconstitution of Zn-CA.

A.

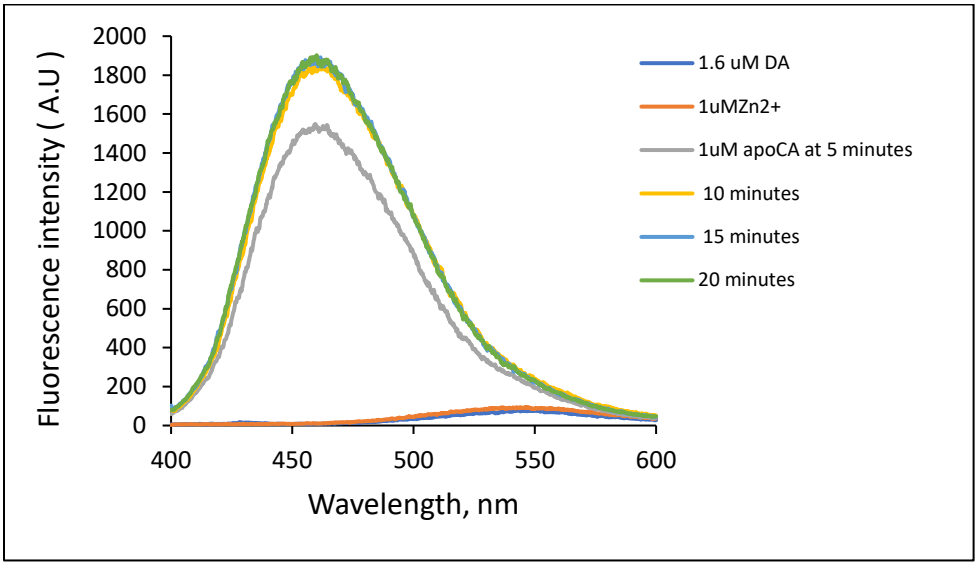

B.

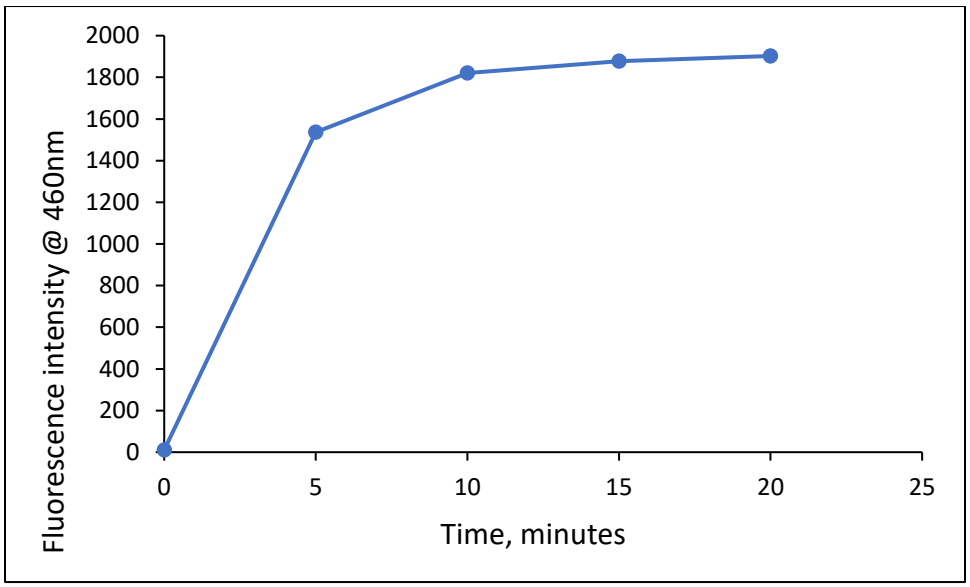

Figure 21. Reaction of apo-CA and Zn2+ to reconstitute Zn-CA in the presence of dansyl amide. (A) 1.6 µM dansyl amide was treated with 1 µM $ZnCl_2$ followed by the addition of 1 µM apo-CA. Fluorescence spectra of the reaction mixture from 400 – 600 nm (excitation 320 nm) was recorded every 5 min for 20 min. (B) Fluorescence at 460 nm of the spectra from (A) was plotted against time.

3.2.6 Reconstitution of Zn-carbonic anhydrase (Zn-CA) mediated by proteome

To test whether proteome can mediate zinc transfer to apo-carbonic anhydrase via its non-specific zinc binding sites and thus reconstitute Zn-carbonic anhydrase, first, isolated proteome containing 5 µM native Zn^{2+} was reacted with 1.6 µM dansyl amide (**Figure 22**). The emission maximum was found to be 540 nm, suggesting that either (i) isolated proteome contained very low concentration of Zn-CA in its native Zn-protein pool, or (ii) even if proteome had noticeable amount of Zn-CA, the reaction is very slow in the proteomic environment. This experiment also indicated that dansyl amide does not display significant reactivity with other native Zn-proteins. Next, 2 µM exogenous Zn^{2+} was added in the form of $ZnCl_2$ to the mixture of proteome and dansyl amide. Since proteome can bind extra Zn^{2+} via non-specific zinc binding sites involving primarily sulfhydryl groups, 2 µM proteome-S•Zn was assumed to be formed following the addition of 2 µM Zn^{2+}. The unchanged fluorescence at 525 nm indicated that DA did not react with free Zn^{2+} or non-specifically bound proteomic zinc, Proteome•Zn (**Figure 22**). Subsequently, 1 µM apo-CA was added to the reaction mixture of Proteome•Zn and dansyl amide. Following the addition, dansyl amide fluorescence started to increase slowly, the emission maximum the fluorescence blue-shifted from 525 nm to 460 nm, clearly indicating reconstitution of Zn-CA resulting from the transfer of zinc to apo-CA from proteome's non-specific sites. The progress of the experiment can be summarized by the following reactions.

$$\text{Proteome} + Zn^{2+} \leftrightarrows \text{Proteome}\bullet\text{Zn} \quad (37)$$

$$\text{Proteome}\bullet\text{Zn} + \text{apo-CA} \leftrightarrows \text{Proteome} + \text{Zn-CA} \quad (38)$$

$$\text{Zn-CA} + \text{DA} \leftrightarrows \text{DA-Zn-CA (460 nm)} \quad (39)$$

A.

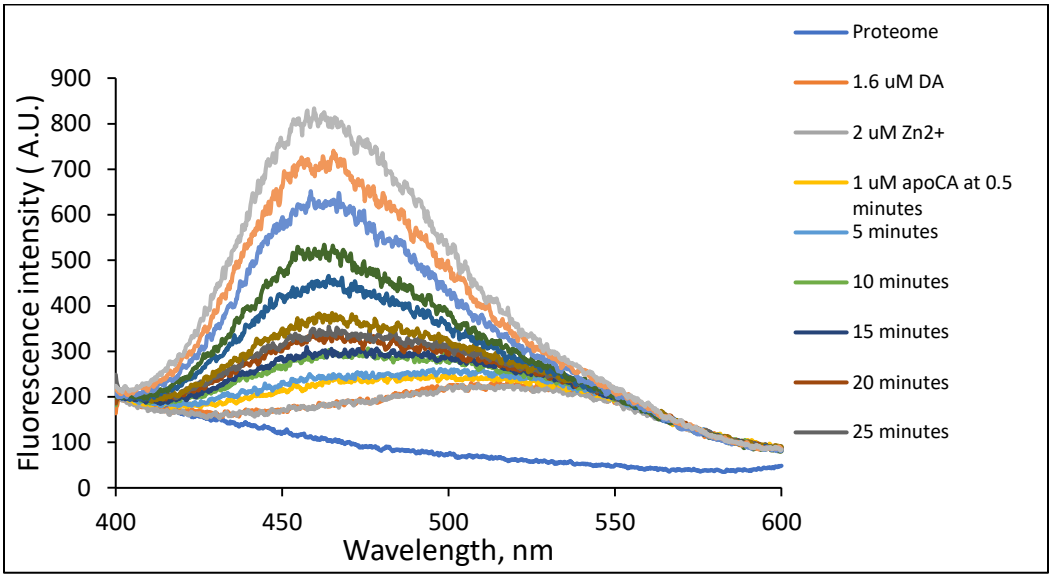

B.

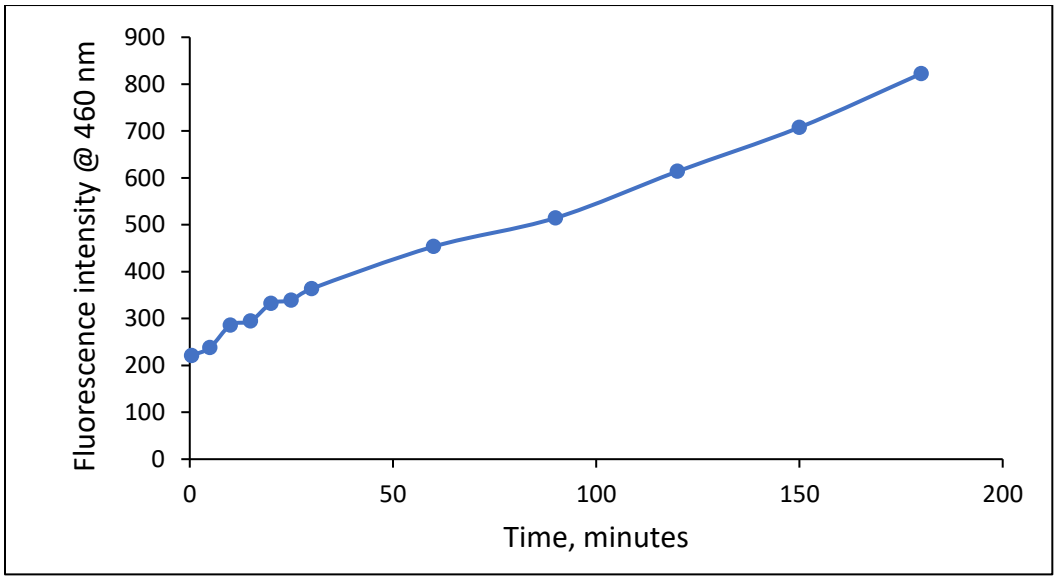

Figure 22. Proteome-mediated reconstitution of Zn-CA from apo-CA. (A) Isolated proteome containing 5.2 µM native Zn^{2+} was treated with 1.6 µM DA followed by the addition of 2 µM exogenous Zn^{2+} and 1 µM apo-CA. Fluorescence spectra of the reaction mixture (excitation 320 nm, emission 400-600 nm) was monitored for 3 hours. (B) Change of fluorescence at 460 nm with time.

As shown in **Figure 22**, the reconstitution of Zn-CA in presence of proteome is very slow. While in the absence of proteome, almost 100% reconstitution occurred rapidly, it took several hours for only about 50% Zn-CA reconstitution to occur in presence of proteome. Evidently, binding zinc to the Proteome markedly slowed the kinetics of the reaction. In addition, it makes the energetics of the reaction much less favorable. Also considering that Zn^{2+} bound to Proteome•Zn probably has a full complement of ligands in its coordination sphere (≥4), the complete ligand substitution reaction is complex and may be slowed simply because of the difficulty in exchanging, sequentially, multiple ligands between two large, bulky ligand sets, which must involve the formation of an intermediate (reaction 40).

$$\text{Proteome•Zn + apo-CA} \leftrightarrows \text{Proteome•Zn-CA} \leftrightarrows \text{Proteome + Zn-CA} \qquad (40)$$

To further explore role of energetics in the proteome-mediated reconstitution of Zn-CA, 1 µM apo-CA was reacted with 1 µM exogenous Zn^{2+} in the presence of various concentrations of proteome and their reaction monitored with dansyl amide. Proteome containing 9 µM native Zn^{2+} was serially diluted and used in this reaction. **Figure 23** shows that with increasing concentration of Proteome, both the extent and the rate of Zn-CA reconstitution declined. The inverse relationship of Proteome concentration and the fraction of Zn-CA reconstitution can be explained by the hypothesis that at higher concentration, Proteome possesses larger number of non-specific zinc binding sites, possibly sulfhydryl groups, and thus provides stronger competition for exogenous Zn^{2+} with apo-CA, leading to the smaller regeneration of Zn-CA.

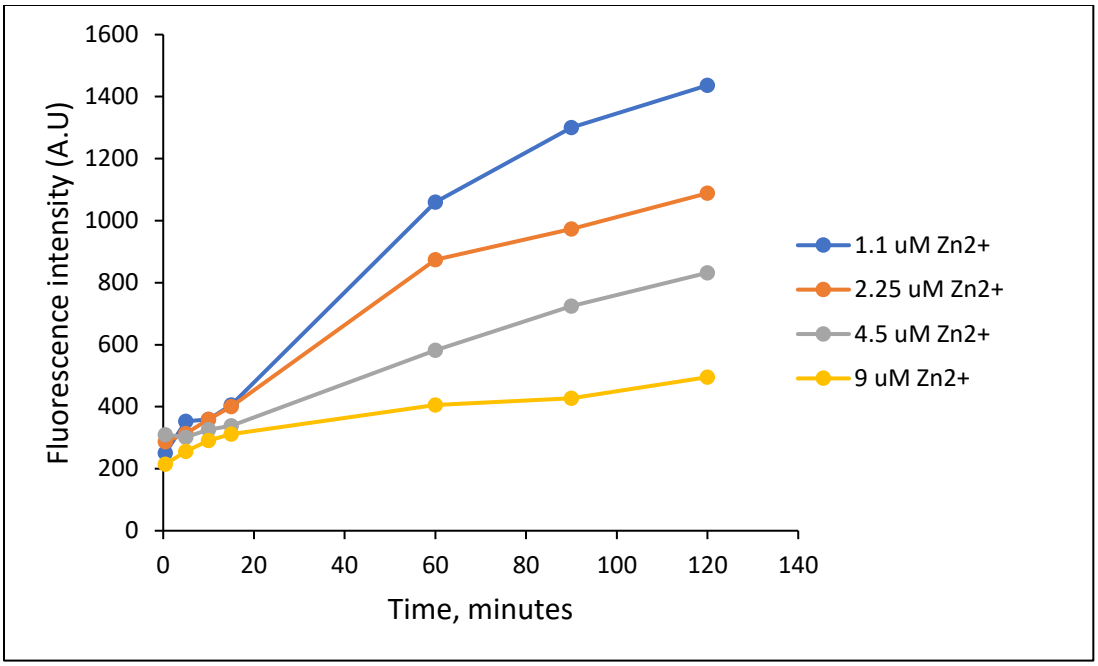

Figure 23. Effect of proteome concentration on proteome-mediated Zn-CA reconstitution. Isolated proteome containing 9 µM native Zn^{2+} was serial diluted in 20 mM Tris buffer (pH 7.2). Proteome solution containing 9 µM, 4.5 µM, 2.25 µM or 1.1 µM native Zn^{2+} was treated with 1.6 µM DA followed by the addition of 1 µM exogenous Zn^{2+} and 1 µM apo-CA. Fluorescence spectra of the reaction mixture (excitation 320 nm, emission 400-600 nm) was monitored for 2 hours. Fluorescence at 460 nm of the spectra was plotted against time.

These results are in good agreement with the $K_{Proteome•Zn}$ determined in the reaction of FluoZin-3 with Proteome•Zn (Karim and Petering, unpublished data). That fact supports the view that the reaction of apo-CA with Proteome•Zn can be treated as a straight-forward ligand substitution process between the protein and Zn^{2+} bound in equilibrium fashion to a number of proteomic sites.

The decline in rate of reaction as one of the reactant concentrations was reduced suggests that the kinetics of the ligand substitution process has second order character, first order in each reactant. Section **3.2.10** examines the kinetics of reaction 10.

3.2.7. Effect of N-ethylmaleimide (NEM) on proteome mediated reconstitution of Zn-CA

According to previous work as well as current studies of the reaction of Zincon with Proteome•Zn, the high affinity zinc binding sites in the Proteome include sulfhydryl groups. Experiments were conducted to confirm that reaction 10 involves Zn^{2+} bound to proteomic thiolate groups. In particular, the effect of N-ethylmaleimide (NEM), a thiol binding reagent, on proteome mediated reconstitution of Zn-CA was examined.

$$\text{Proteome-SH + NEM} \leftrightarrows \text{Proteome-S-NEM} \qquad (41)$$

In doing so, isolated proteome containing 4 µM native Zn^{2+} was pre-incubated with different concentrations of NEM for 30 min. Reaction mixture was then filtrated using a 3K molecular weight cut-off filter to remove residual NEM. The retentate proteome was subsequently reacted with 1 µM exogenous Zn^{2+} and 1 µM apo-CA. As displayed in **Figure 24**, the pre-treatment of Proteome with increasing concentrations of NEM caused a large, progressive increase in the rate of Zn-CA regeneration, confirming that proteomic sulfhydryl groups are implicated in non-specific zinc binding and in competition with apo-CA for exogenous Zn^{2+}. NEM abolished proteomic sulfhydryl groups and high affinity, non-specific zinc binding sites, which weakened but did not abolish the Proteome's competition with apo-CA for Zn^{2+}. In place of Proteome-SH, Zn^{2+} became bound to sites containing ligands other than sulfhydryl groups, such as imidazole and carboxylate groups. In this situation the energetics are more favorable for the formation of Zn-CA and clearly the kinetics of reaction are faster.

$$\text{Proteome-S•Zn + apo-CA} \leftrightarrows \text{Proteome-S}^- + \text{Zn-CA (slow)} \qquad (42)$$

$$\text{Proteome-S}^- + \text{NEM} \leftrightarrows \text{Proteome-S-NEM} \qquad (43)$$

$$\text{Proteome}\bullet Zn_{\text{weak sites}} + \text{apo-CA} \leftrightarrows \text{Zn-CA} + \text{Proteome (fast)} \quad (44)$$

As the concentration of NEM was increased, favoring the titration of sulfhydryl groups, the number of residual proteomic SH groups decreased though not in a linear fashion.

A.

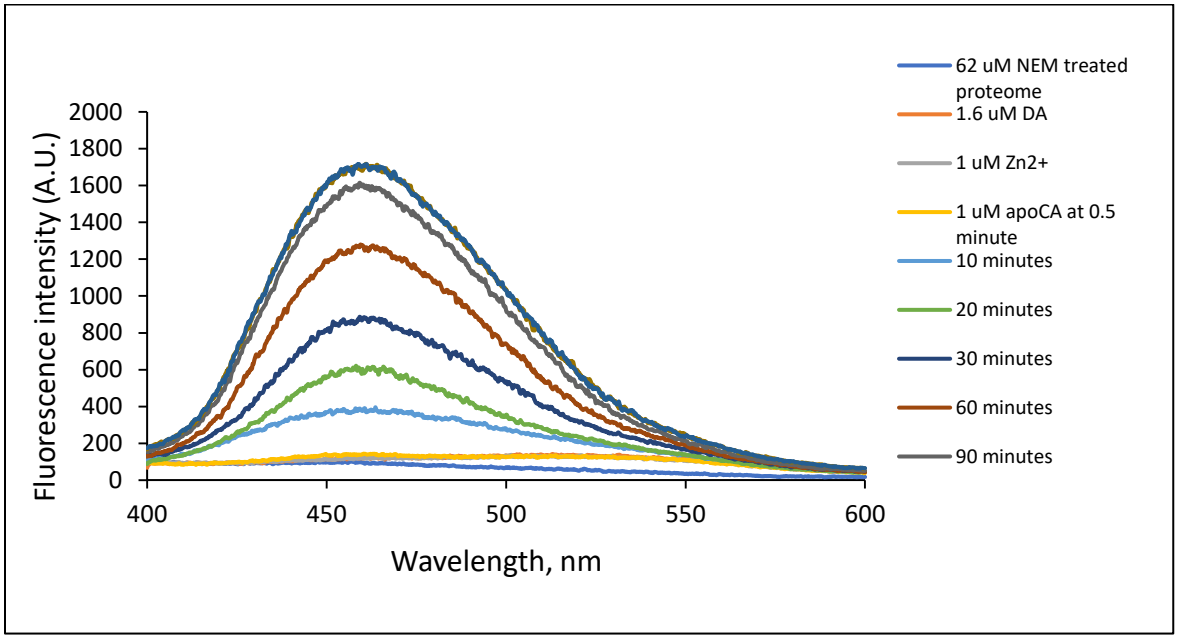
Fluorescence intensity (A.U.)
2000
1800
1600
1400
1200
1000
800
600
400
200
0
400
450
500
550
600
Wavelength, nm
62 uM NEM treated proteome
1.6 uM DA
1 uM Zn2+
1 uM apoCA at 0.5 minute
10 minutes
20 minutes
30 minutes
60 minutes
90 minutes

B.

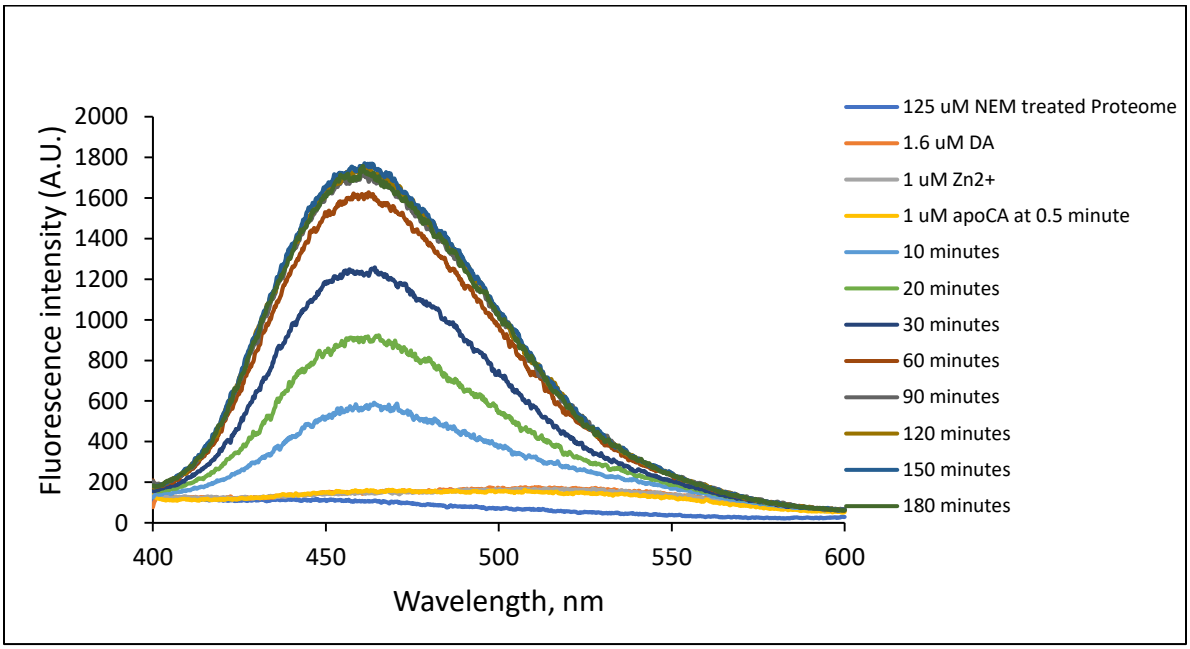
Fluorescence intensity (A.U.)
2000
1800
1600
1400
1200
1000
800
600
400
200
0
400
450
500
550
600
Wavelength, nm
125 uM NEM treated Proteome
1.6 uM DA
1 uM Zn2+
1 uM apoCA at 0.5 minute
10 minutes
20 minutes
30 minutes
60 minutes
90 minutes
120 minutes
150 minutes
180 minutes

C.

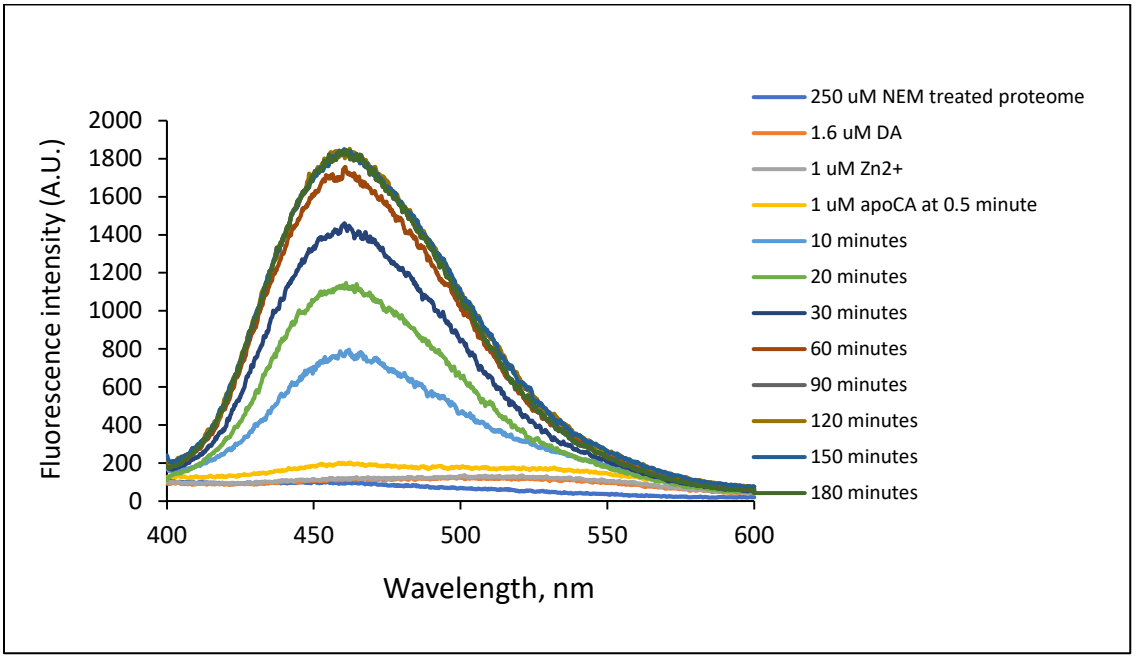
Fluorescence intensity (A.U.)
2000
1800
1600
1400
1200
1000
800
600
400
200
0
400
450
500
550
600
Wavelength, nm
250 uM NEM treated proteome
1.6 uM DA
1 uM Zn2+
1 uM apoCA at 0.5 minute
10 minutes
20 minutes
30 minutes
60 minutes
90 minutes
120 minutes
150 minutes
180 minutes

D.

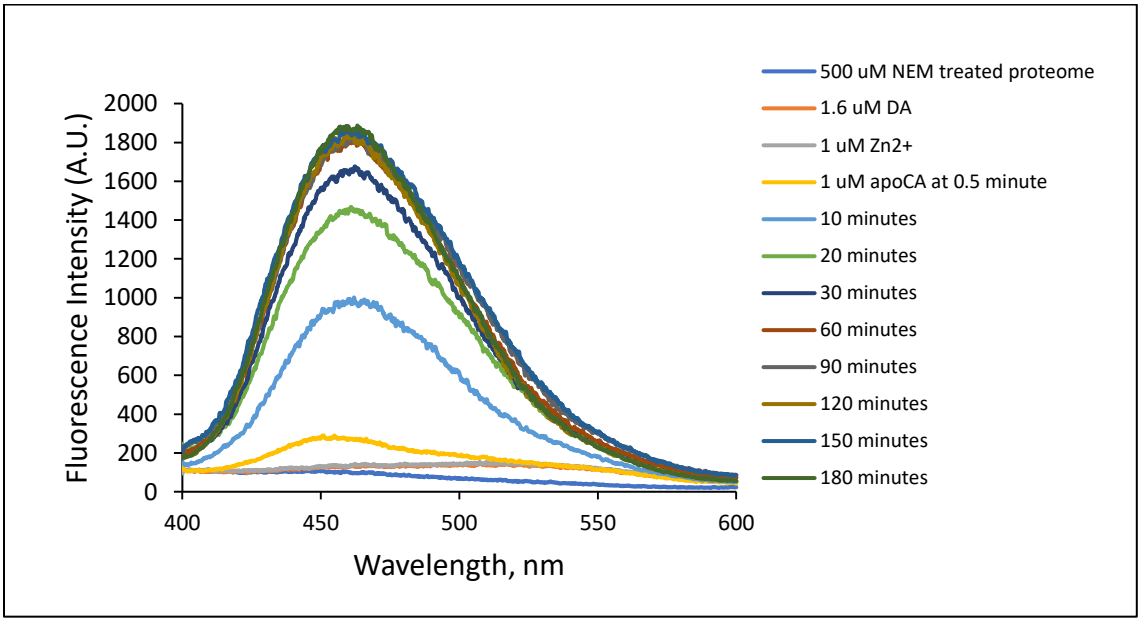
Fluorescence Intensity (A.U.)
2000
1800
1600
1400
1200
1000
800
600
400
200
0
400
450
500
550
600
Wavelength, nm
500 uM NEM treated proteome
1.6 uM DA
1 uM Zn2+
1 uM apoCA at 0.5 minute
10 minutes
20 minutes
30 minutes
60 minutes
90 minutes
120 minutes
150 minutes
180 minutes

E.

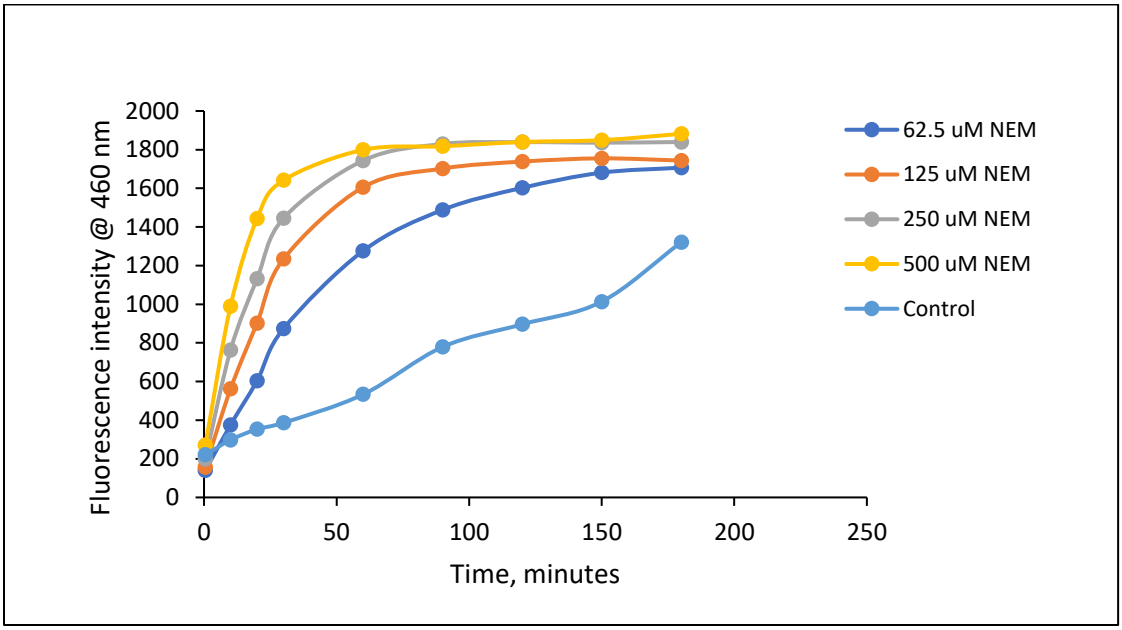

Figure 24. Effect of N-ethylmaleimide (NEM) on proteome mediated reconstitution of Zn-CA. (A-D) Isolated proteome containing 4 µM native Zn^{2+} was pre-incubated with (A) 62.5 µM, (B) 125 µM, (C) 250 µM or (D) 500 µM N-ethylmaleimide (NEM) for 1 hour. Subsequently, each of the four reaction mixtures was filtered using 3K molecular weight cut-off filter in order to remove unreacted and residual NEM. NEM-treated and filtered proteome was then treated with 1.6 µM dansyl amide followed by the addition of 1 µM exogenous Zn^{2+} and 1 µM apo-CA. Fluorescence spectra of the reaction mixture (excitation 320 nm, emission 400 – 600 nm) was recorded for 3 hours. As control, proteome without NEM treatment was reacted with 1.6 µM dansyl amide, 1 µM exogenous Zn^{2+} and 1 µM apo-CA. (E) Fluorescence at 460 nm of the reactions (A – D) was plotted against time.

3.2.8. Reaction of Proteome-S•Zn with denatured apo-CA_d

One likely difference in these *in vitro* experiments and native, cellular conditions is that the *in vitro* experiment used pre-folded, native apo-CA for reconstitution (reaction 45), while under native conditions zinc possibly binds to unfolded apo-CA to form native, folded Zn-CA (reaction 46). The latter case may thermodynamically favor the reaction and thus facilitate the generation of Zn-CA. It might also enhance the kinetic rate of reaction by making available a set of flexible ligands to react with Proteome-S•Zn instead of the highly constrained trio of imidazole ligands present in native apo-CA.

$$\text{Proteome-S•Zn} + \text{apo-CA}_{\text{native}} \leftrightarrows \text{Proteome-SH} + \text{Zn-CA} \quad \text{(slow)} \qquad (45)$$

$$\text{Proteome-S•Zn} + \text{apo-CA}_{\text{unfolded}} \leftrightarrows \text{Proteome-SH} + \text{Zn-CA} \quad \text{(fast)} \qquad (46)$$

Therefore, the proteome-assisted Zn-CA reconstitution experiment was repeated with denatured (unfolded) apo-CA, instead of already folded, native apo-CA, to see if the extent and rate of reconstitution becomes faster.

Apo-CA was denatured by guanidinium hydrochloride treatment. To verify this denaturation protocol, 25 µM native Zn-CA was treated with 4M guanidium hydrochloride in the presence of 25 µM dansyl amide (**Figure 25**). The complete loss of DA fluorescence following addition of guanidinium hydrochloride demonstrated that this protocol could successfully denature Zn-CA. Moreover, 25-fold dilution of guanidinium hydrochloride abolished its denaturing capacity and thus resulted in reconstitution of Zn-CA, evidenced from the gradual increase of dansyl amide fluorescence at 460 nm (**Figure 26 A**). The final fluorescence intensity was comparable to that of 1 µM $\text{Zn-CA}_{\text{native}}$ (**Figure 26 B**) . The result was also consistent with the control experiment, in

which 1 µM denatured apo-CA was reacted with 1 µM Zn^{2+} in the presence of 1.6 µM dansyl amide. The lower fluorescence intensity in this experiment relative to the previous experiments under identical condition resulted from the different settings of the fluorometer parameters used in the two experiments.

A.

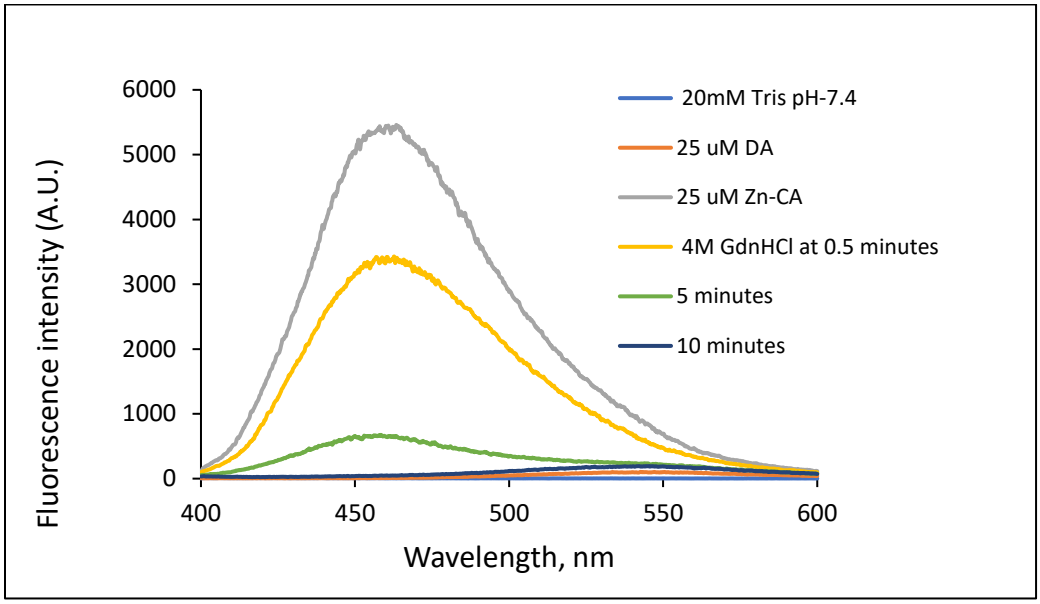

B.

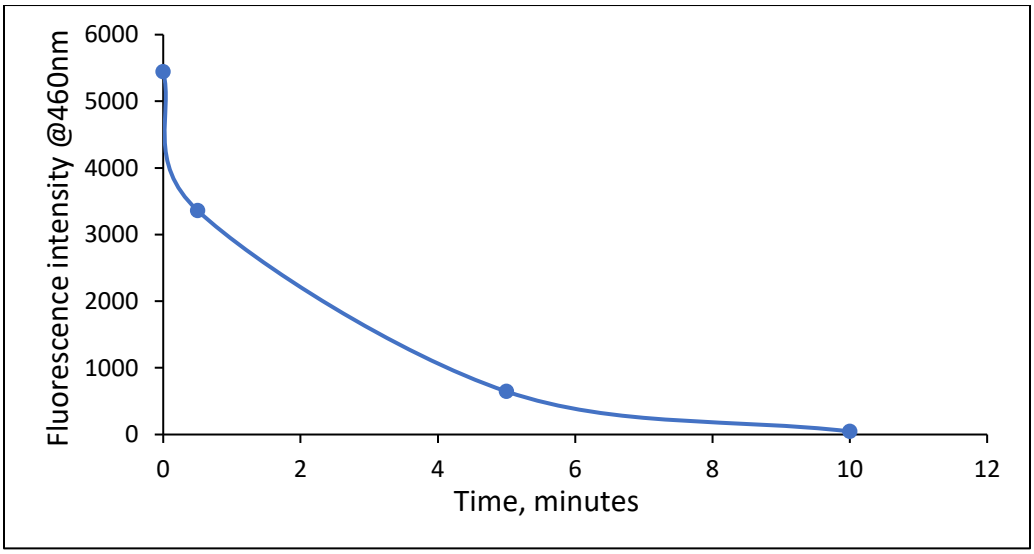

Figure 25. Denaturation of Zn-CA by guanidinium hydrochloride treatment. (A) 25 µM Zn-CA was reacted with 25 µM dansyl amide followed by the addition of 4 mM guanidinium hydrochloride for 10 min. Fluorescence spectra were recorded using excitation wavelength 320 nm and emission wavelength 400 – 600 nm. (B) Change of 460 nm fluorescence with time following the addition of guanidinium hydrochloride.

A.

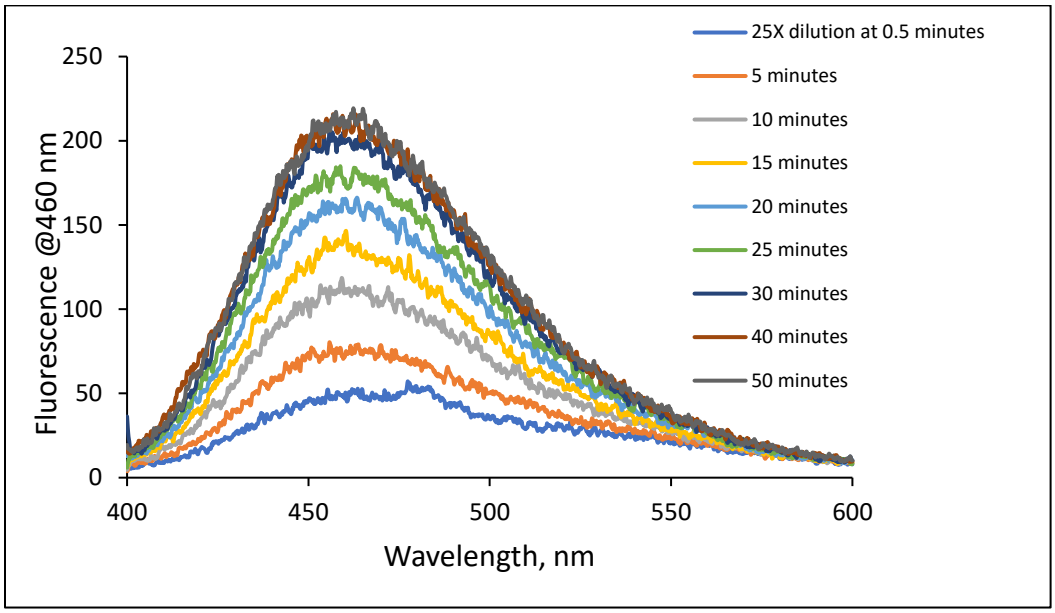
25X dilution at 0.5 minutes
5 minutes
10 minutes
15 minutes
20 minutes
25 minutes
30 minutes
40 minutes
50 minutes
Fluorescence @460 nm
0
50
100
150
200
250
400
450
500
550
600
Wavelength, nm

B.

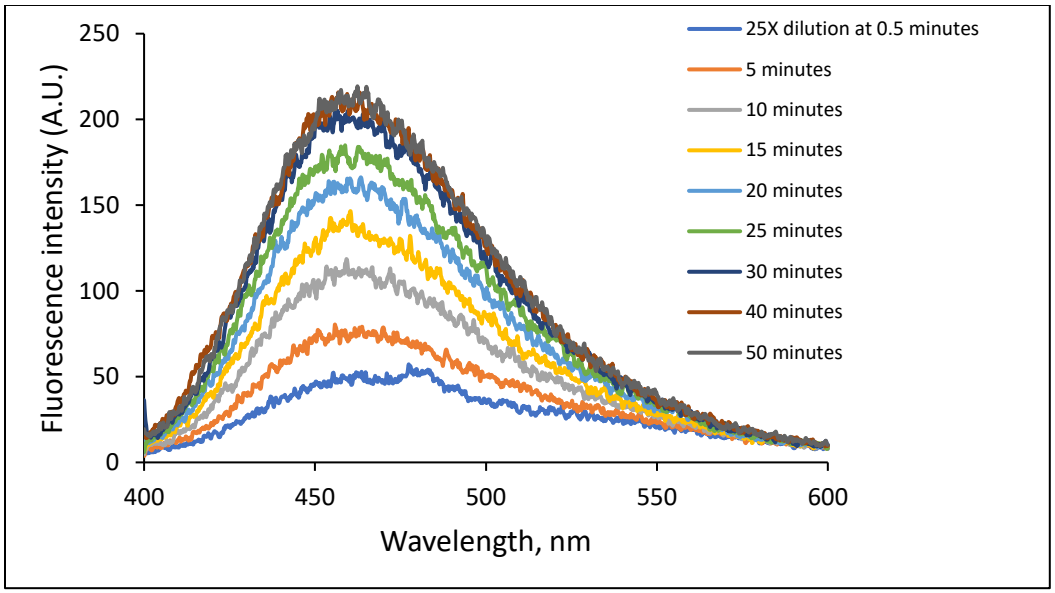
25X dilution at 0.5 minutes
5 minutes
10 minutes
15 minutes
20 minutes
25 minutes
30 minutes
40 minutes
50 minutes
Fluorescence intensity (A.U.)
0
50
100
150
200
250
400
450
500
550
600
Wavelength, nm

C.

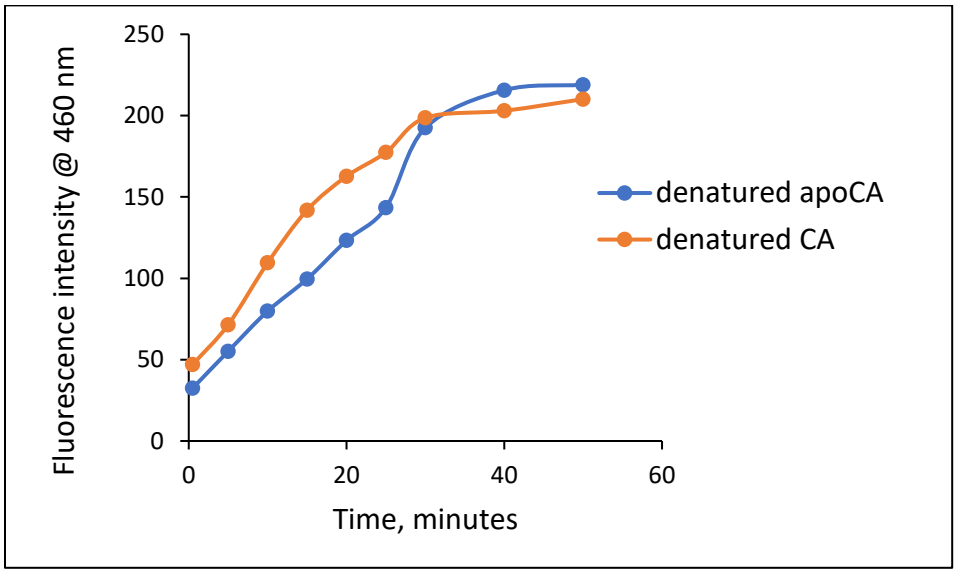

Figure 26. Renaturation of Zn-CA in the presence of diluted guanidinium hydrochloride. (A) The final reaction mixture of 25 µM Zn-CA, 25 µM dansyl amide and 4 mM guanidinium hydrochloride was diluted 25-fold with 25 mM Tris buffer (pH 7.4). Dansyl amide fluorescence was recorded using excitation wavelength 320 nm and emission wavelength 400 – 600 nm. (B) Reaction of 1 µM denatured apo-CA and 1 µM Zn^{2+} in the presence of 1.6 µM dansyl amide. (C) Comparison of the kinetics of the reactions (A) and (B).

Apo-CA was denatured using the same protocol and 1 μM denatured apo-CA was then reacted with 1 μM Zn^{2+} in the absence (**Figure 27**) or presence of proteome (**Figure 28**). Interestingly, the rate of proteome-assisted reconstitution of Zn-CA from denatured apo-CA was not significantly different from that with native apo-CA (**Figure 28**). But the extent of reconstitution of the denatured protein was only about half as much as that of native apo-CA.

A.

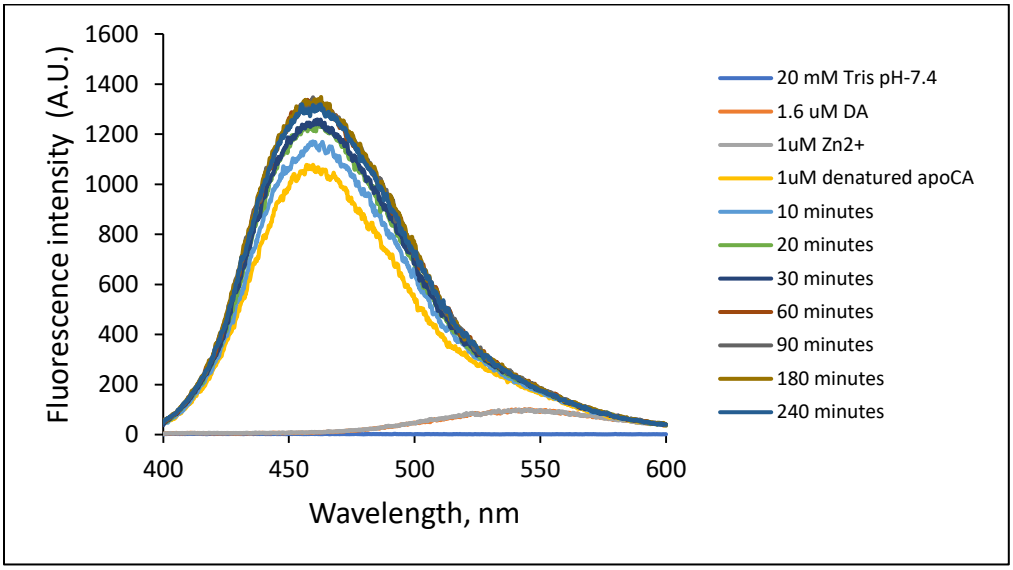

B.

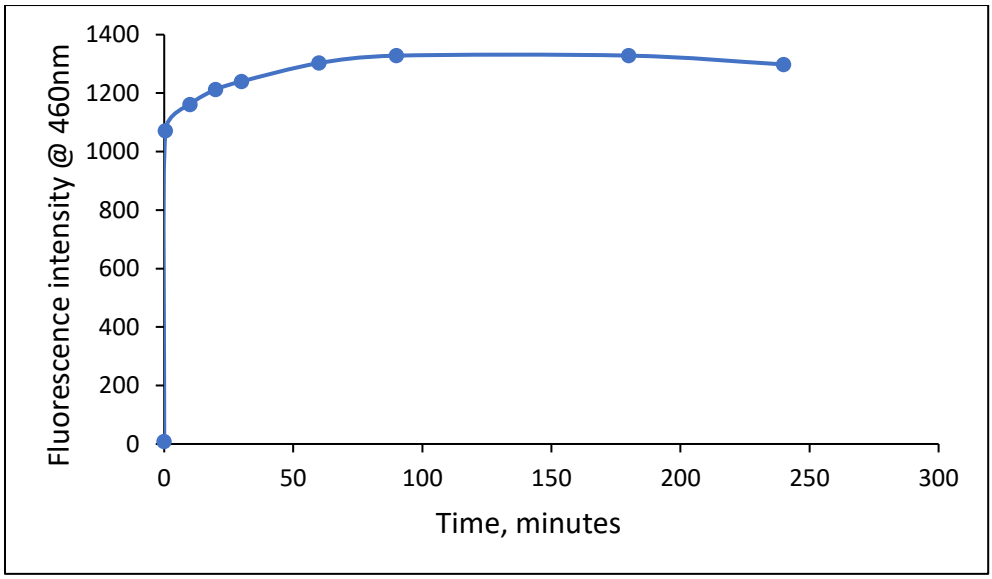

Figure 27. Reaction of denatured apo-CA and Zn^{2+} in the presence of dansyl amide. (A) 1 µM denatured apo-CA was reacted with 1 µM Zn^{2+} in the presence of 1.6 µM dansyl amide. Fluorescence spectra at excitation wavelength 320 nm and emission wavelength 400 – 600 nm were recorded for 90 min. (B) Change of 460 nm fluorescence with time

A.

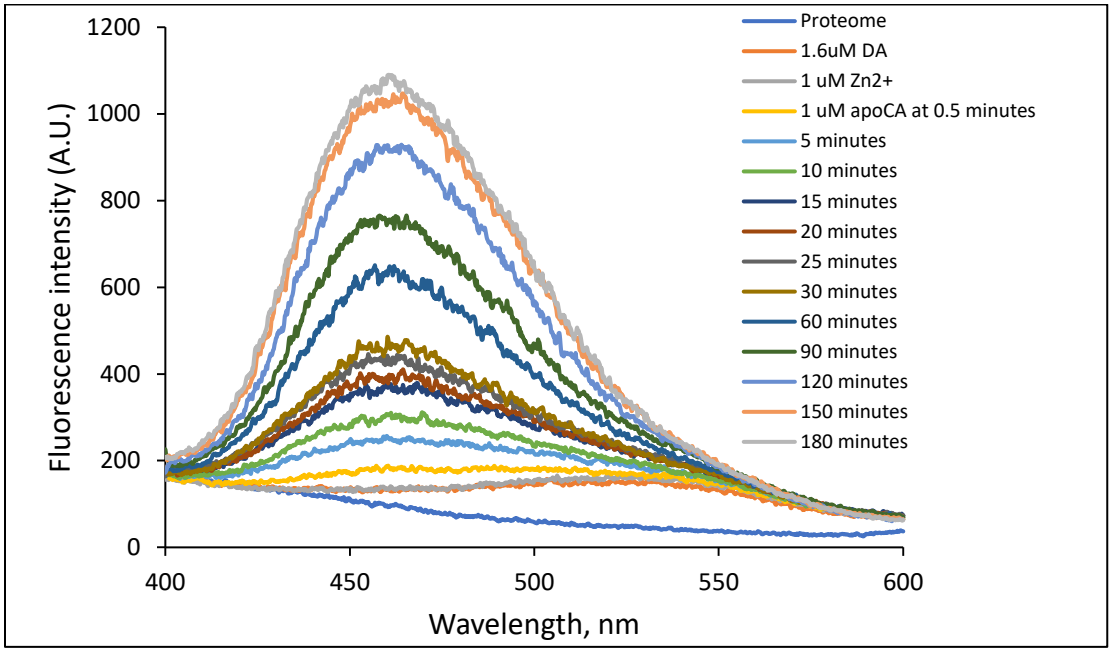
Fluorescence intensity (A.U.)
1200
1000
800
600
400
200
0
400
450
500
550
600
Wavelength, nm
Proteome
1.6uM DA
1 uM Zn2+
1 uM apoCA at 0.5 minutes
5 minutes
10 minutes
15 minutes
20 minutes
25 minutes
30 minutes
60 minutes
90 minutes
120 minutes
150 minutes
180 minutes

B.

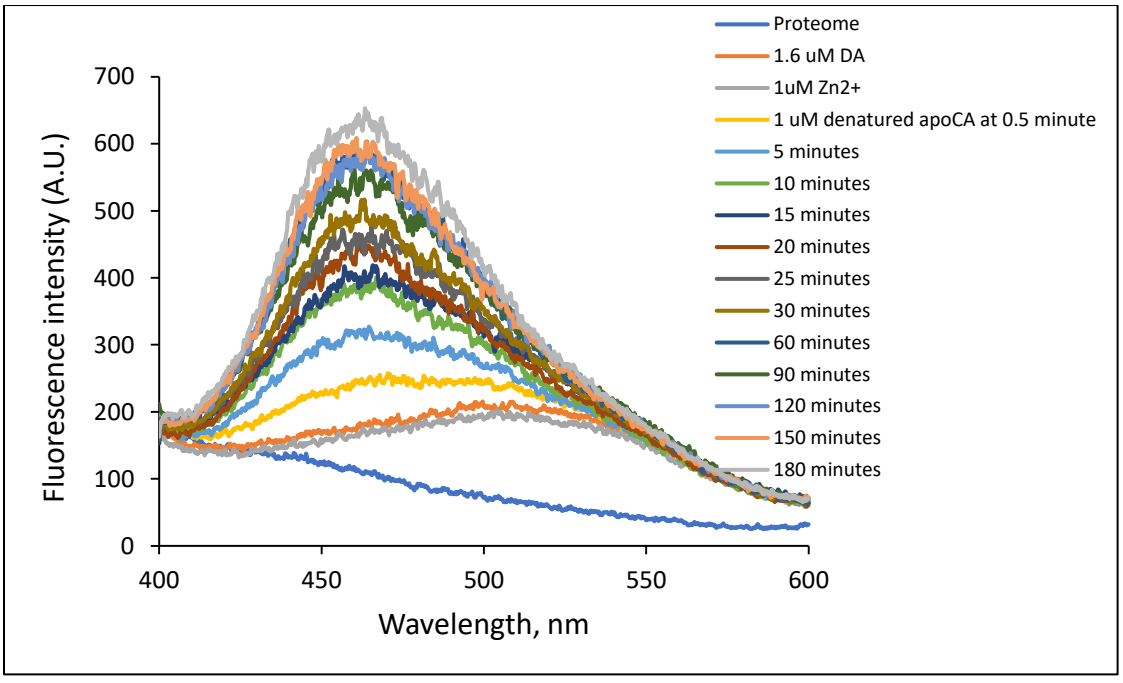
Fluorescence intensity (A.U.)
700
600
500
400
300
200
100
0
400
450
500
550
600
Wavelength, nm
Proteome
1.6 uM DA
1uM Zn2+
1 uM denatured apoCA at 0.5 minute
5 minutes
10 minutes
15 minutes
20 minutes
25 minutes
30 minutes
60 minutes
90 minutes
120 minutes
150 minutes
180 minutes

C.

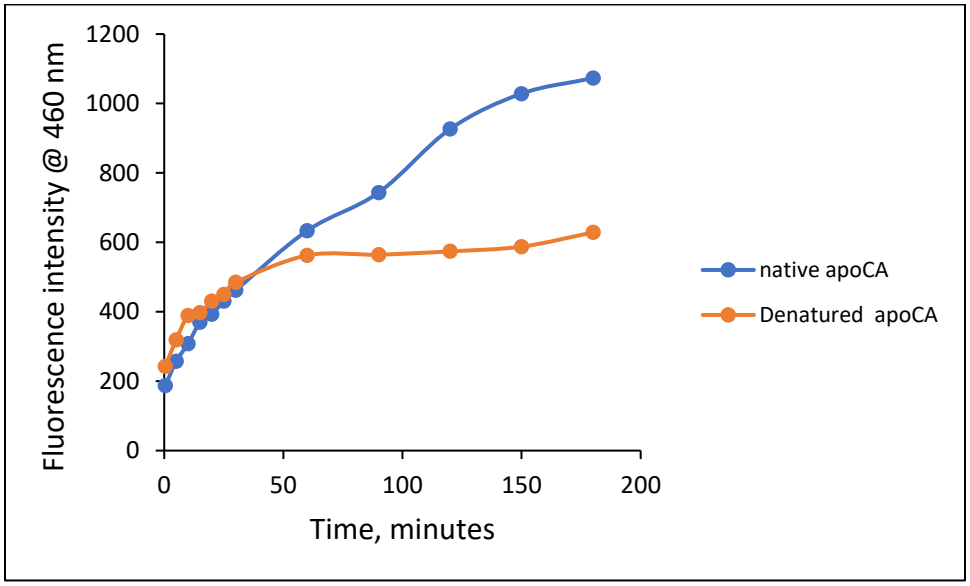

Figure 28. Comparison of proteome-mediated Zn-CA reconstitution from native and denatured apo-CA. Isolated proteome was treated with 1.6 µM DA followed by the addition of 1 µM exogenous Zn^{2+} and (A) 1 µM denatured or (B) native apo-CA. Fluorescence spectra of both reactions (excitation 320 nm, emission 400-600 nm) was recorded. (C) Comparison of rate of Zn-CA reconstitution from native and denatured apo-CA.

3.2.9 Reaction kinetics of proteome mediated reconstitution of Zn-CA

In the native environment, i.e., in cells, the rate of formation of Zn-proteins might be expected to be relatively fast as considered in the Discussion (section 4). If so, then the apparent slow rate of reconstitution of apo-CA observed in **Figure 22** may suggest that the direct reaction of apo-CA with Proteome-S•Zn is not kinetically competent to serve as the direct pathway for the constitution of apo-Zn proteins *in vivo*.

In order to gain deeper insight into the reconstitution of Zn-CA mediated by the Proteome, the kinetics of Zn-CA formation from the reaction of apo-CA and Proteome-S•Zn were investigated. Potentially, the involvement of multiple reactants within Proteome-S•Zn make the kinetic study of this reaction complicated. A pseudo-first order rate study was done by using a large excess of apo-CA relative to Proteome-S•Zn. First, 1 µM proteome-S•Zn was generated by reacting proteome containing - µM native Zn^{2+} with 1 µM exogenous Zn^{2+}. Then, 10, 20 or 30 µM apo-CA was added and the progress of reaction was monitored with 1.6 µM DA. As anticipated, increased rate of Zn-CA regeneration was observed with increasing concentration of apo-CA (**Figure 29 A-D**). Initially, we hypothesized that this reaction was second order, first order in both reactants, apo-CA and Proteome-S•Zn.

$$\text{Rate of Zn-CA reconstitution} = k\,[\text{Proteome-S•Zn}]\,[\text{apo-CA}] \qquad (47)$$

where k is the second order rate constant.

Since [apo-CA] was used in large excess relative to [Proteome-S•Zn], [apo-CA] was assumed to be constant for the pseudo-first order reaction. Therefore, the above rate equation can be modified as below.

$$\text{Rate of Zn-CA reconstitution} = k' [\text{Proteome-S}\bullet\text{Zn}] \quad (48)$$

$$\text{or} \quad d[\text{Proteome-S}\bullet\text{Zn}]/dt = -k' [\text{Proteome-S}\bullet\text{Zn}] \quad (49)$$

$$\text{where} \quad k' = \text{observed rate constant} = k [\text{apo-CA}] \quad (50)$$

The integrated form of equation (48) can be re-written as,

$$\ln[\text{proteome-S}\bullet\text{Zn}]_t = \ln[\text{Proteome-S}\bullet\text{Zn}]_0 - k't \quad (51)$$

$$\text{where} \quad [\text{Proteome-S}\bullet\text{Zn}]_t = \text{concentration of Proteome-S}\bullet\text{Zn at time t} \quad (52)$$

Next, for each of these three reactions, the concentration of Proteome-S•Zn, $[\text{Proteome-S}\bullet\text{Zn}]_t$, was calculated at different time points for the first 20 minutes using the following equation.

$$[\text{Proteome-S}\bullet\text{Zn}]_t = [\text{Proteome-S}\bullet\text{Zn}]_0 - [\{(F_{max} - F_t) / (F_{max} - F_{min})\}*[\text{proteome-S}\bullet\text{Zn}]_0] \quad (53)$$

F_{max} = maximum fluorescence units upon completion of the reaction; F_t = fluorescence units at time t; and F_{min} = background fluorescence before the addition of apo-CA. $[\text{proteome-S}\bullet\text{Zn}]_0$ = initial concentration of Proteome-S•Zn = 1 µM

A plot of $\ln[\text{proteome-S}\bullet\text{Zn}]_t$ versus t was made for each of three reactions (**Figure 29 E**). The slopes of the resulting straight lines were calculated to find the values of observed rate constants, k' for each reaction. Finally, the observed rate constants, k', were plotted against the concentration of apo-CA, [apo-CA], producing another straight line (**Figure 29 F**). According to equation (50), the slope of this straight line is the actual rate constant, k. The value of k was measured to be 23 $M^{-1}s^{-1}$.

A.

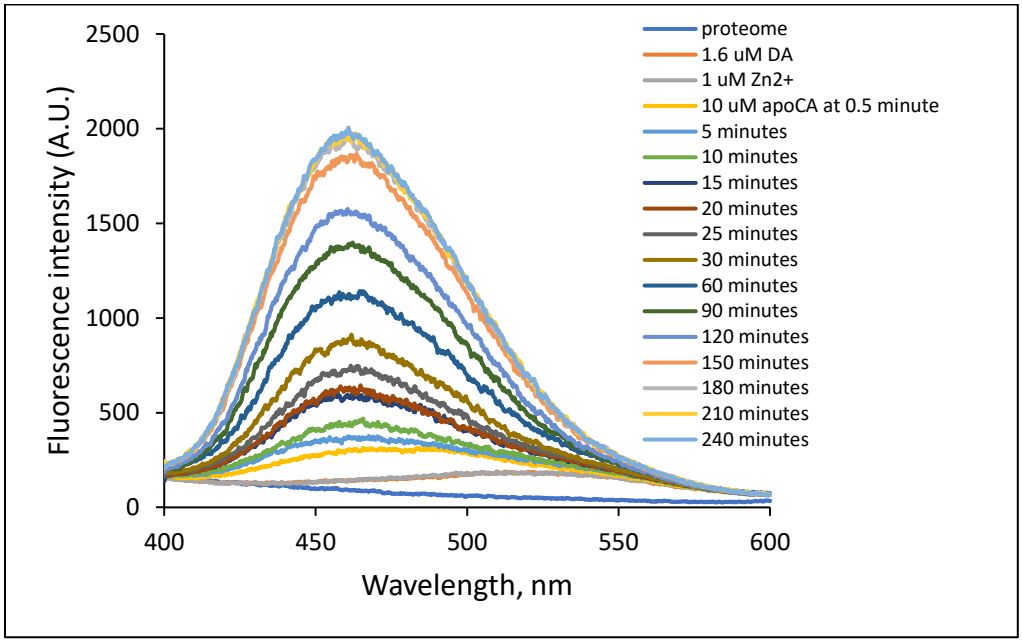
Fluorescence intensity (A.U.)
2500
2000
1500
1000
500
0
400
450
500
550
600
Wavelength, nm
proteome
1.6 uM DA
1 uM Zn2+
10 uM apoCA at 0.5 minute
5 minutes
10 minutes
15 minutes
20 minutes
25 minutes
30 minutes
60 minutes
90 minutes
120 minutes
150 minutes
180 minutes
210 minutes
240 minutes

B.

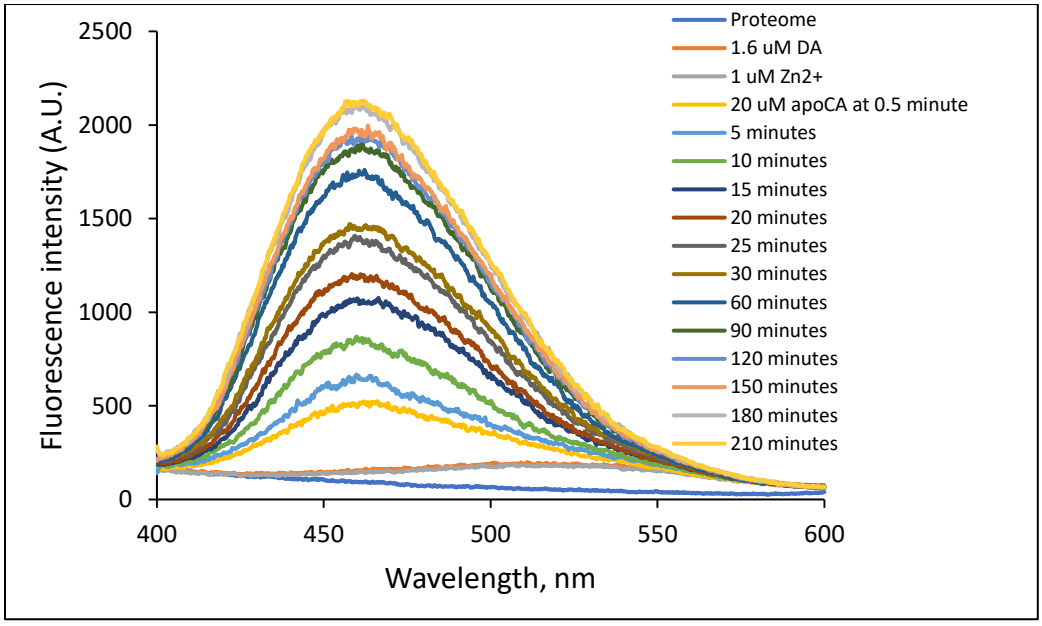
Fluorescence intensity (A.U.)
2500
2000
1500
1000
500
0
400
450
500
550
600
Wavelength, nm
Proteome
1.6 uM DA
1 uM Zn2+
20 uM apoCA at 0.5 minute
5 minutes
10 minutes
15 minutes
20 minutes
25 minutes
30 minutes
60 minutes
90 minutes
120 minutes
150 minutes
180 minutes
210 minutes

C.

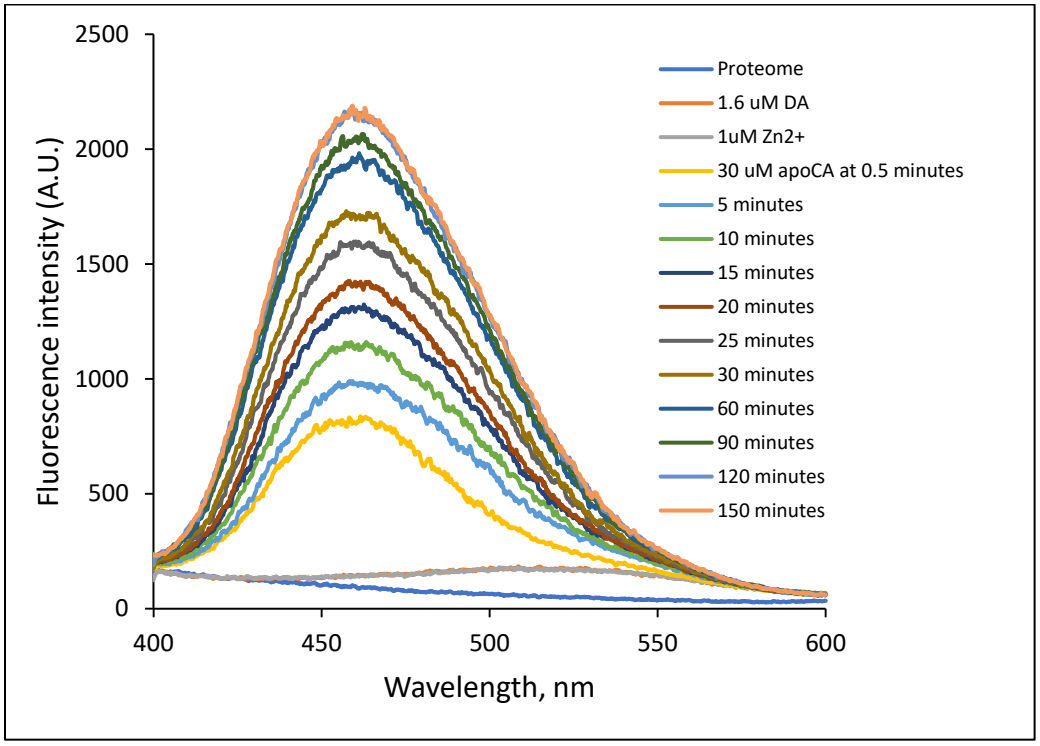
Fluorescence intensity (A.U.)
2500
2000
1500
1000
500
0
400
450
500
550
600
Wavelength, nm
Proteome
1.6 uM DA
1uM Zn2+
30 uM apoCA at 0.5 minutes
5 minutes
10 minutes
15 minutes
20 minutes
25 minutes
30 minutes
60 minutes
90 minutes
120 minutes
150 minutes

D.

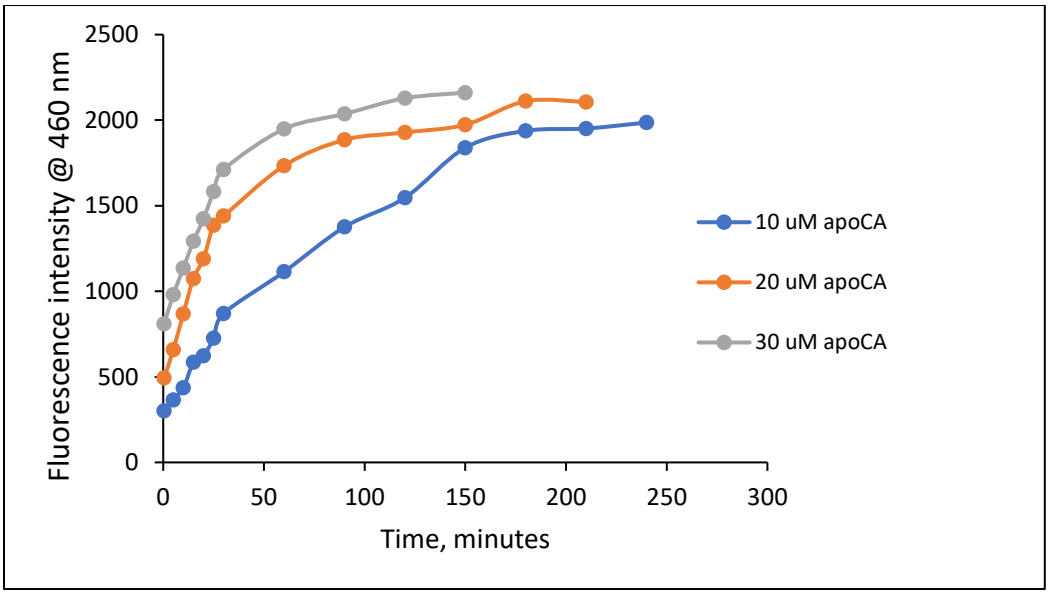
Fluorescence intensity @ 460 nm
2500
2000
1500
1000
500
0
0
50
100
150
200
250
300
Time, minutes
10 uM apoCA
20 uM apoCA
30 uM apoCA

E.

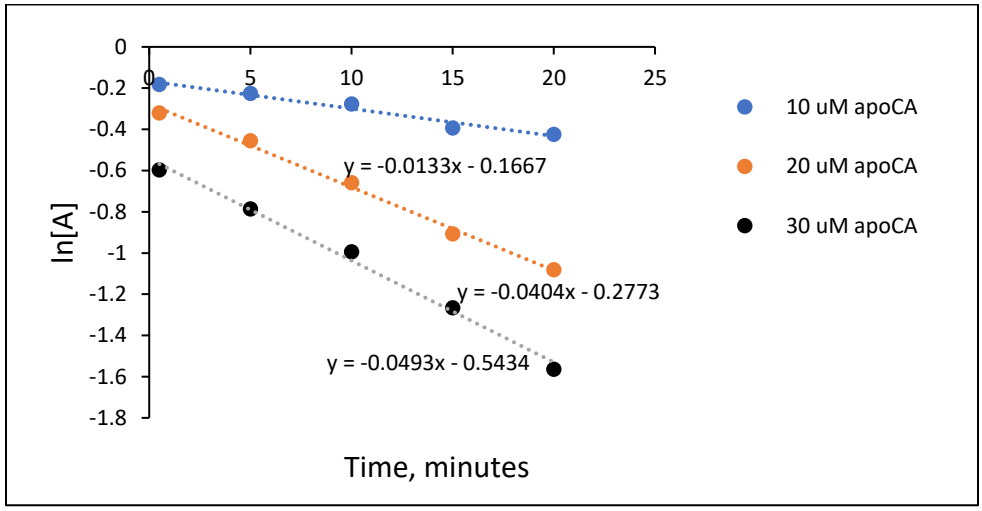

F.

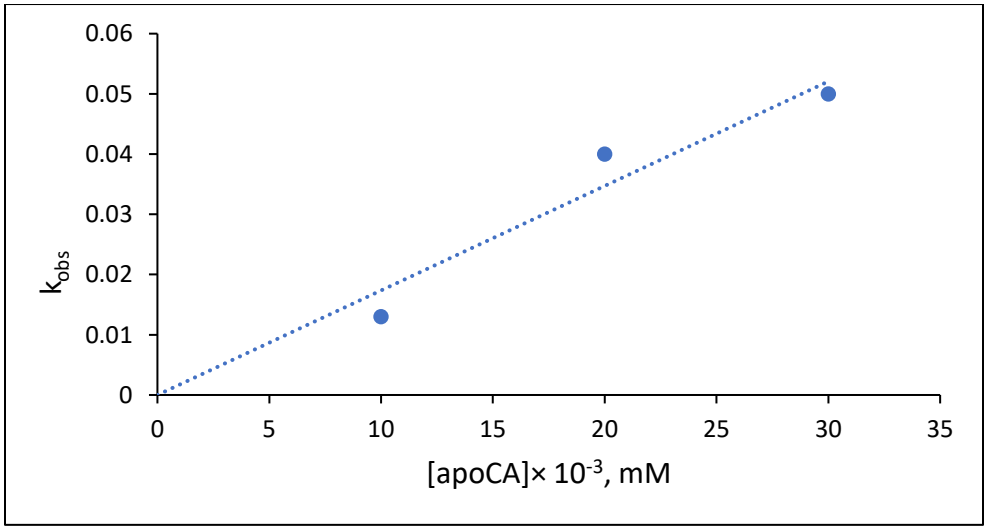

Figure 29. Reaction kinetics of proteome-mediated reconstitution of Zn-CA. (A – C) Isolated proteome was treated with 1.6 µM dansyl amide followed by the introduction of 1 µM exogenous Zn^{2+} and (A) 10 µM, (B) 20 µM or (C) 30 µM apo-CA. Fluorescence spectra of the reactions (excitation 320 nm, emission 400 – 600 nm) were recorded. (D) Fluorescence at 460 nm of each of the three reactions (A – C) was plotted against time. (E) Concentration of proteome-S•Zn (lnA) was calculated for each of three reactions for first 20 minutes and plotted against time. (F) The slope of the straight lines (k_{obs}) from (E) was plotted against the concentration of apo-CA.

3.3 Metallothionein-mediated reconstitution of Zn-CA

We examined two possible reasons to explain the slow rate of Zn-CA reconstitution in presence of proteome. Since formation of native Zn-proteins in the cellular environment is supposed to occur faster, we hypothesized that cellular components other than proteome protein, e.g., metallothionein, glutathione, etc., that may be more kinetically reactive, are involved, as well, in proteome-mediated zinc trafficking to generate native Zn-proteins.

Metallothionein is a small protein with very strong binding affinity for Zn^{2+} [29, 31]. It has 60 amino acid residues, of which 20 are cysteine residues [34, 35]. Each metallothionein molecule can bind up to seven zinc ions with stability constant of $10^{11\text{-}12}$ [37, 38]. Due to this high affinity, some studies have claimed that metallothionein acts as a thermodynamic sink for zinc following cellular uptake. Various studies have reported that metallothionein plays important role in cellular zinc trafficking and thus in the formation of native, specific Zn-proteins [15, 31, 37, 38, 45]. Therefore, it is expected that metallothionein will possibly have an impact on proteome-assisted zinc trafficking. It can either directly transfer its zinc to the apo-proteins producing Zn-proteins (reaction 54), or can establish an equilibrium with proteome, eventually transferring zinc to apo-proteins (reactions 55 and 56).

$$Zn_7\text{-MT} + \text{apo-protein} \leftrightarrows Zn_{(7\text{-}n)}\text{-MT} + \text{Zn-protein} \quad (54)$$

$$Zn_7\text{-MT} + \text{Proteome-SH} \leftrightarrows Zn_{(7\text{-}n)}\text{-MT} + \text{Proteome-S}\bullet\text{Zn} \quad (55)$$

$$\text{Proteome-S}\bullet\text{Zn} + \text{apo-protein} \leftrightarrows \text{Proteome-SH} + \text{Zn-protein} \quad (56)$$

In this chapter, we have investigated metallothionein-mediated reconstitution of Zn-CA either in the absence or presence of proteome. The interaction of metallothionein with proteome was probed, too. For this purpose, Zn_7-MT purchased from Creative Biomart was employed. However, before using it in reactions, its zinc and sulfhydryl content and zinc binding affinity were characterized.

3.3.1 Characterization of Zn_7-MT purchased from Creative Biomart

The seven zinc ions of metallothionein should be tightly bound to it with equal or similar affinity, first it was confirmed if the purchased metallothionein has any free or loosely bound zinc in it. In doing so, the purchased metallothionein containing 5 µM was reacted with 5 µM FluoZin-3, a fluorescent zinc sensor with relatively high stability constant (K_d 15 nM). FluoZin-3 forms a 1:1 complex, Zn-FluoZin3, with zinc and shows a significant enhancement of fluorescence at 518 nm, when excited at 492 nm. However, it does not display any noticeable reactivity with the tightly bound zinc of metallothionein.

$$Zn^{2+} + \text{FluoZin3} \leftrightarrows \text{Zn-FluoZin3 (excitation 492 nm, emission 518 nm)} \quad (57)$$

$$Zn_7\text{-MT} + \text{FluoZin-3} \rightarrow \text{No reaction} \quad (58)$$

5 µM FluoZin-3 solution in 20 mM Tris buffer (pH 7.4) showed a background fluorescence of about 2000 units at 518 nm. When reacted with 1.54 µM free Zn^{2+}, a rapid three-fold enhancement of fluorescent at 518 nm was observed (**Figure 30 B**). However, the reaction of 5 µM FluoZin-3 with purchased metallothionein containing 5 µM Zn^{2+} generated only about 2000 fluorescence units (**Figure 30 C**), equal that of background fluorescence in Tris buffer, at 518 nm, suggesting that the purchased metallothionein contained little or no free zinc. The lack of any slow step in the gain of fluorescence also was consistent with the lack of reactivity of MT-bound Zn^{2+} with FluoZin-3. The presence of free zinc in the purchased metallothionein was checked by another way. Metallothionein solution containing 5 µM Zn^{2+} was filtered using 3K molecular weight cut-off filter and the resulting filtrate was then reacted with 5 µM FluoZin-3. The reaction

produced only background fluorescence at 518 nm (**Figure 30 D**), further confirming that the purchased metallothionein did not contain any free zinc.

A.

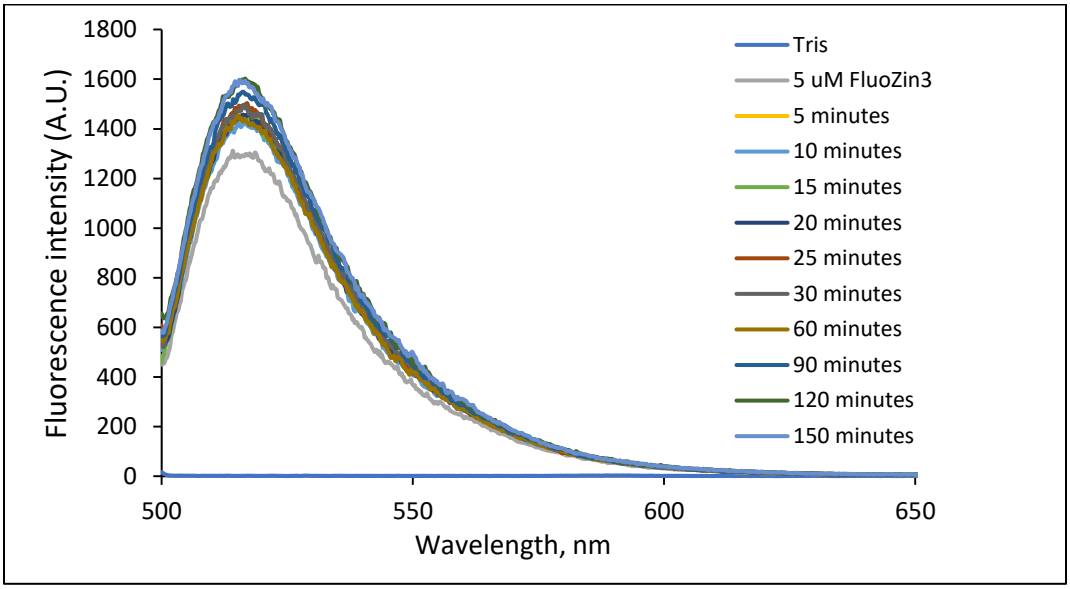
Fluorescence intensity (A.U.)
1800
1600
1400
1200
1000
800
600
400
200
0
500
550
600
650
Wavelength, nm
Tris
5 uM FluoZin3
5 minutes
10 minutes
15 minutes
20 minutes
25 minutes
30 minutes
60 minutes
90 minutes
120 minutes
150 minutes

B.

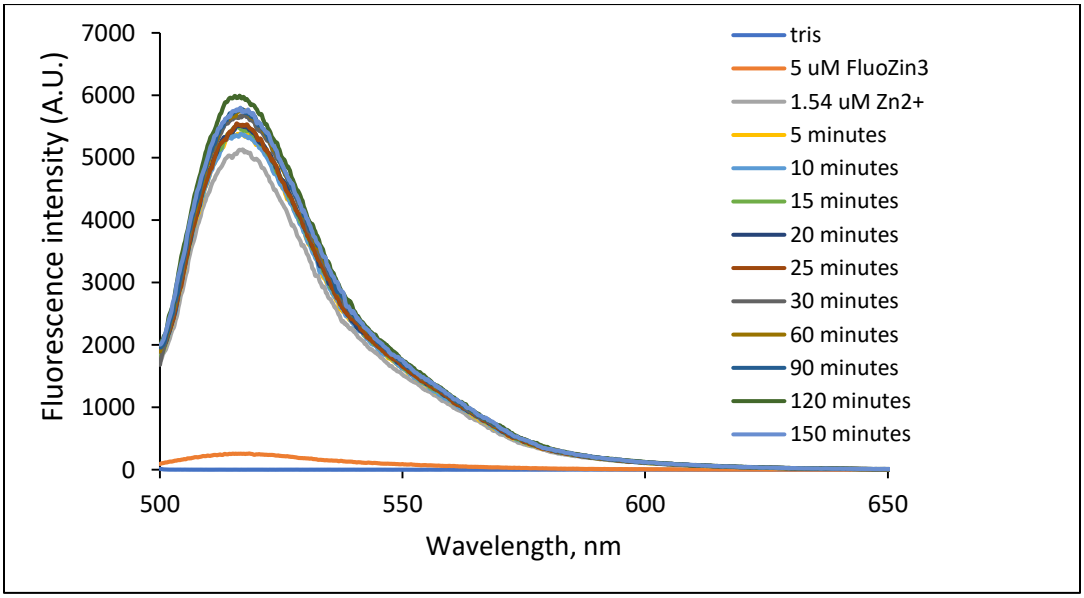
Fluorescence intensity (A.U.)
7000
6000
5000
4000
3000
2000
1000
0
500
550
600
650
Wavelength, nm
tris
5 uM FluoZin3
1.54 uM Zn2+
5 minutes
10 minutes
15 minutes
20 minutes
25 minutes
30 minutes
60 minutes
90 minutes
120 minutes
150 minutes

C.

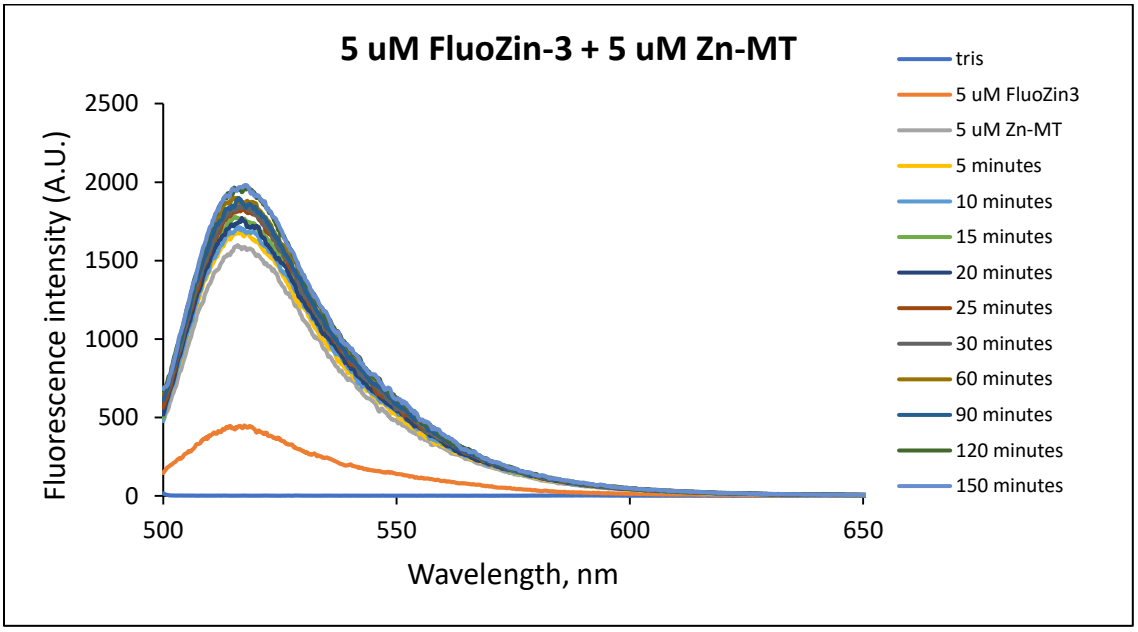
5 uM FluoZin-3 + 5 uM Zn-MT
Fluorescence intensity (A.U.)
2500
2000
1500
1000
500
0
500
550
600
650
Wavelength, nm
tris
5 uM FluoZin3
5 uM Zn-MT
5 minutes
10 minutes
15 minutes
20 minutes
25 minutes
30 minutes
60 minutes
90 minutes
120 minutes
150 minutes

D.

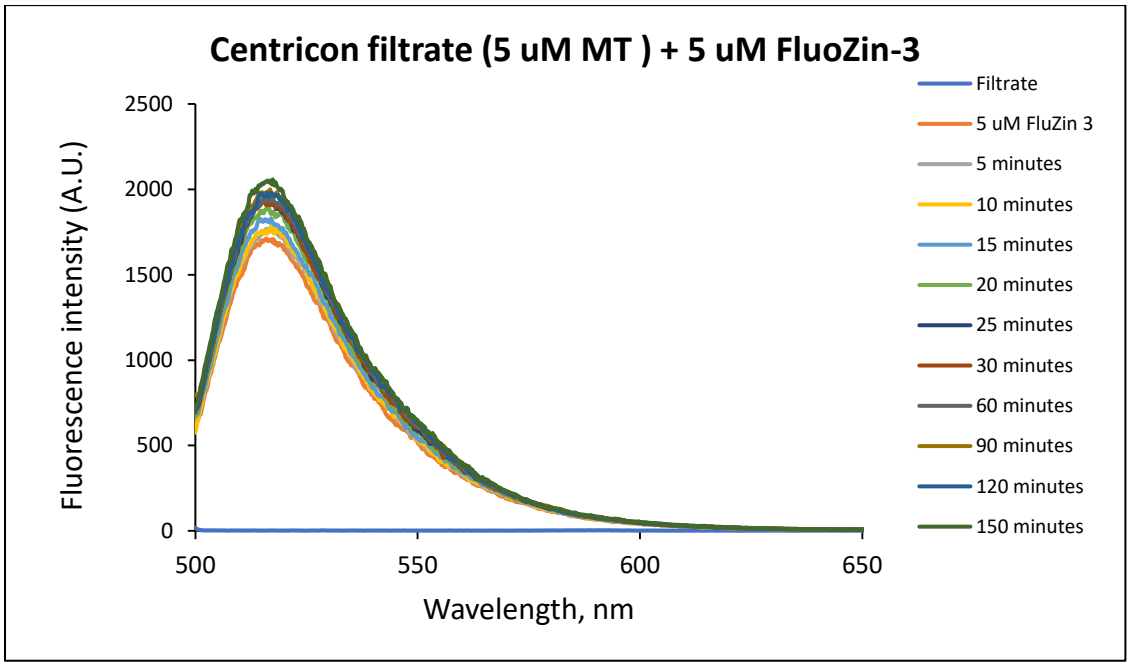
Centricon filtrate (5 uM MT) + 5 uM FluoZin-3
Fluorescence intensity (A.U.)
2500
2000
1500
1000
500
0
500
550
600
650
Wavelength, nm
Filtrate
5 uM FluZin 3
5 minutes
10 minutes
15 minutes
20 minutes
25 minutes
30 minutes
60 minutes
90 minutes
120 minutes
150 minutes

E.

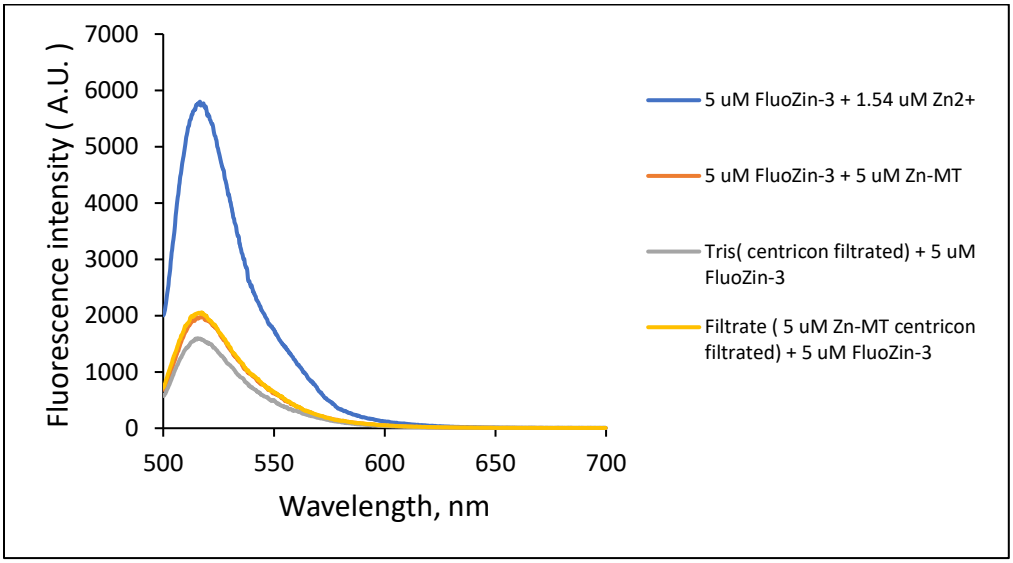

F.

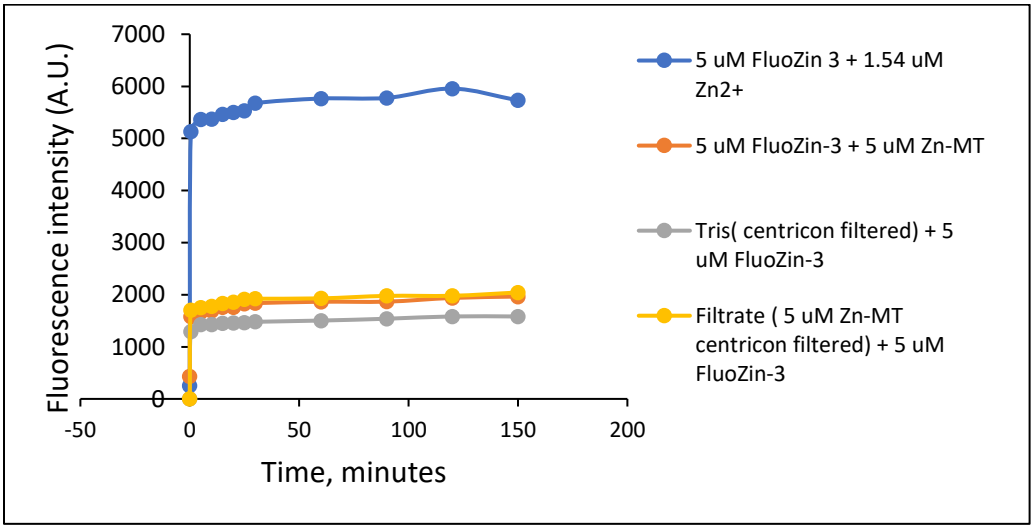

Figure 30. Reaction of FluoZin-3 with $ZnCl_2$ or Zn_7-MT. (A - C) 5 µM FluoZin-3 in (A) 20 mM Tris buffer (pH 7.4) was treated with (B) 1.54 µM $ZnCl_2$ or (C) Zn_7-MT containing 5 µM Zn^{2+}. Fluorescence spectra of the reaction mixtures (excitation 492 nm, emission 500 – 600 nm) was recorded with time. (D) Zn_7-MT (5 µM Zn^{2+}) in 20 mM Tris buffer (pH 7.4) was filtered using a 3K molecular weight cut-off filter, and the resulting filtrate was treated with 5 µM FluoZin-3 followed by the recording of fluorescence spectra at excitation 492 nm and emission 400 – 600 nm. (E) Comparison of spectra of the reactions. (F) Comparison of fluorescence change over time of the reactions of FluoZin-3 with $ZnCl_2$ and Zn_7-MT.

Next, zinc content of the purchased metallothionein was examined. A fully saturated Zn_7-metallothionein should have seven zinc ions and the ratio of zinc to sulfhydryl groups should be 1:2.86. Zinc content in metallothionein was quantified using inductively coupled plasma mass spectrometry and the sulfhydryl groups using DTNB (5,5'-dithiobis-(-nitrobenzoic acid) assay. Free sulfhydryl groups react with DTNB stoichiometrically, resulting in the cleavage of its disulfide bond and production of 5-thio-2-nitrobenzoic acid (TNB), which shows absorbance at 412 nm with an extinction coefficient of 13,600 $M^{-1}cm^{-1}$ [89]ahn. First, 3.7 µM purchased metallothionein was reacted with 1 mM DTNB to find out the time needed for the reaction to reach completion. The change of absorbance at 412 nm with time as in **figure 31** showed that in about 30 min, the reaction was complete. Therefore, to quantify the sulfhydryl groups of the purchased metallothionein, it was 10-fold serial diluted (75.7 µM, 7.57 µM and 0.75 µM) and incubated with 1 mM DTNB for 30 min followed by reading absorbance at 412 nm. Using the extinction coefficient of 13,600 $M^{-1}cm^{-1}$, the concentration of sulfhydryl groups was calculated. The ratio of zinc to sulfhydryl groups in the purchased metallothionein was measured to be 1:3.1, suggesting that metallothionein was fully saturated with seven zinc, Zn_7-metallothionein.

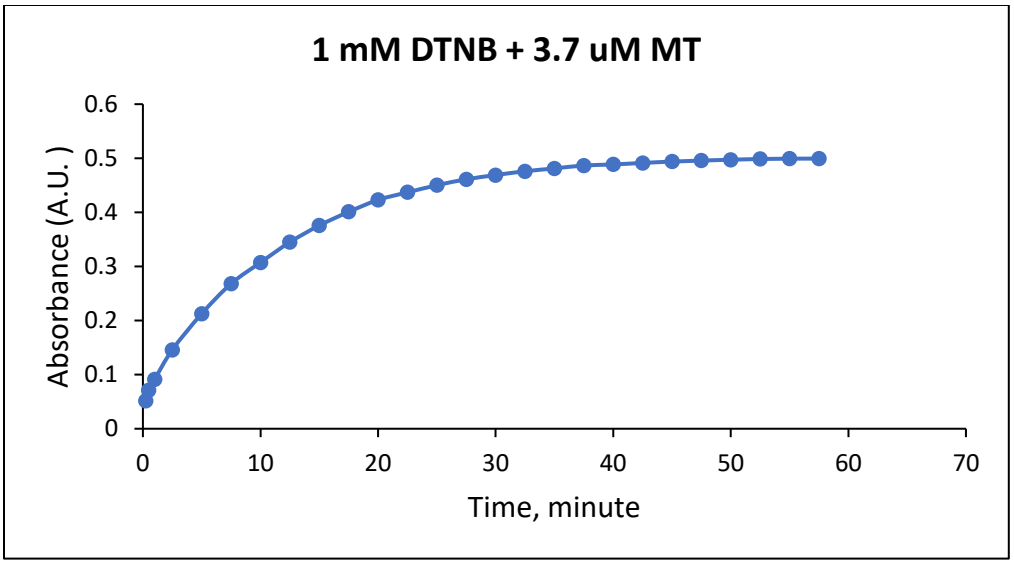

Figure 31. Quantification of sulfhydryl groups in metallothionein by DTNB assay. 3.7 µM metallothionein in 20 mM Tris buffer (pH 7.4) was reacted with 1 mM DTNB. The reaction progress was monitored by recording the absorbance at 412 nm.

3.3.2 Metallothionein-mediated reconstitution of Zn-CA

In order to investigate if metallothionein can help reconstitute zinc carbonic anhydrase from apo-carbonic anhydrase, Zn_7-metallothionein (Zn_7-MT) containing 1 µM Zn^{2+} was reacted with 1 µM apo-CA in the presence of 1.6 µM dansyl amide (DA). The gradual increase of fluorescence at 460 nm indicated the formation of DA-Zn-CA ternary complex (**Figure 32 A**), meaning that zinc was transferred from Zn_7-MT to apo-CA and thus Zn-CA was reconstituted. However, like proteome, metallothionein-mediated reconstitution of Zn-CA occurs at a slow rate.

$$Zn_7\text{-MT} + \text{apo-CA} \leftrightarrows Zn_6\text{-MT} + \text{Zn-CA} \quad (59)$$

Interestingly, the introduction of proteome containing 4 µM native Zn^{2+} further slowed down the rate of reconstitution of Zn-CA (**Figure 32 B** and **C**). When the reaction was carried out with denatured, unfolded apo-CA, similar slow reconstitution of Zn-CA was observed (**Figure 32 D**). The sluggish rate of the observed reactions might be due to the possibility that there existed an equilibrium between proteome and Zn_7-MT, resulting in the slow transfer of zinc to apo-CA.

$$Zn_7\text{-MT} + \text{Proteome-SH} \leftrightarrows Zn_6\text{-MT} + \text{Proteome-S}\bullet\text{Zn} \quad (60)$$

$$\text{Proteome-S}\bullet\text{Zn} + \text{apo-CA} \leftrightarrows \text{Proteome-SH} + \text{Zn-CA} \quad (61)$$

Alternatively, proteome may form ternary complex with Zn_7-MT as an intermediate during reaction X and, thus, slow down the transfer of zinc from metallothionein to apo-CA.

$$\text{Proteome-SH} + Zn_7\text{-MT} \leftrightarrows \text{Proteome-S}\bullet Zn_7\text{-MT} \quad (62)$$

$$\text{Proteome-S}\bullet Zn_7\text{-MT} + \text{apo-CA} \leftrightarrows \text{Proteome-SH} + Zn_6\text{-MT} + \text{Zn-CA} \quad (63)$$

A.

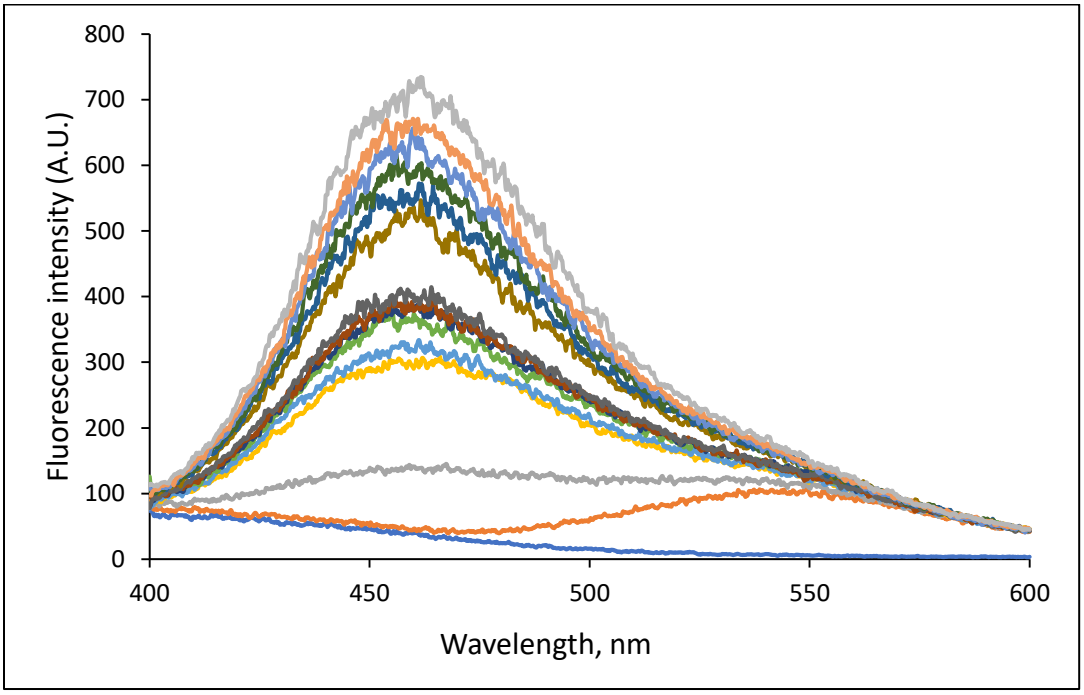
800
700
600
500
400
300
200
100
0
Fluorescence intensity (A.U.)
400
450
500
550
600
Wavelength, nm

B.

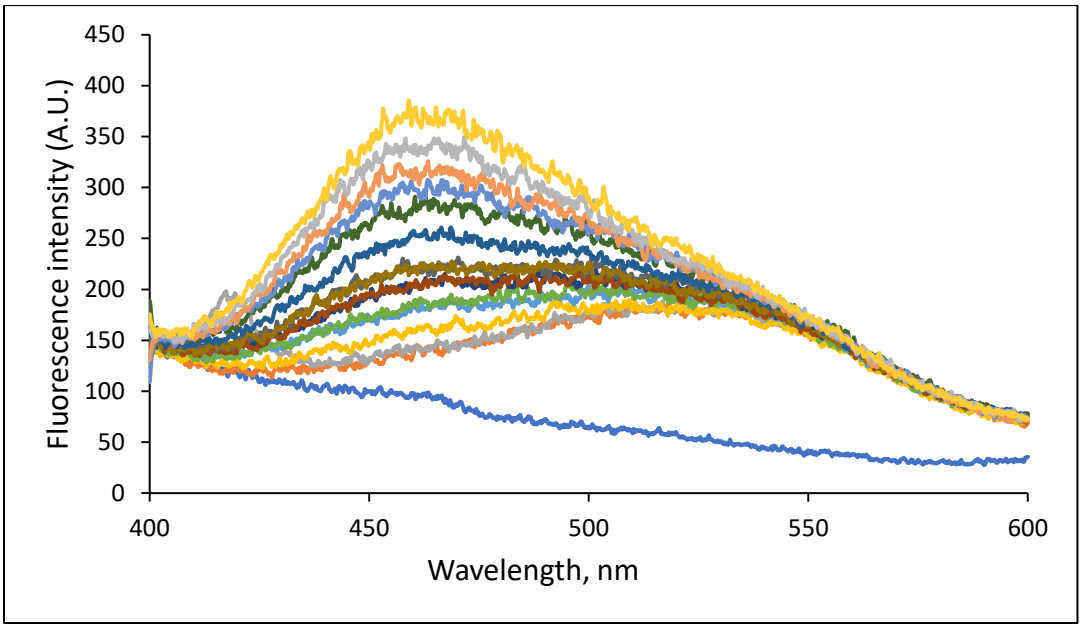
450
400
350
300
250
200
150
100
50
0
Fluorescence intensity (A.U.)
400
450
500
550
600
Wavelength, nm

C.

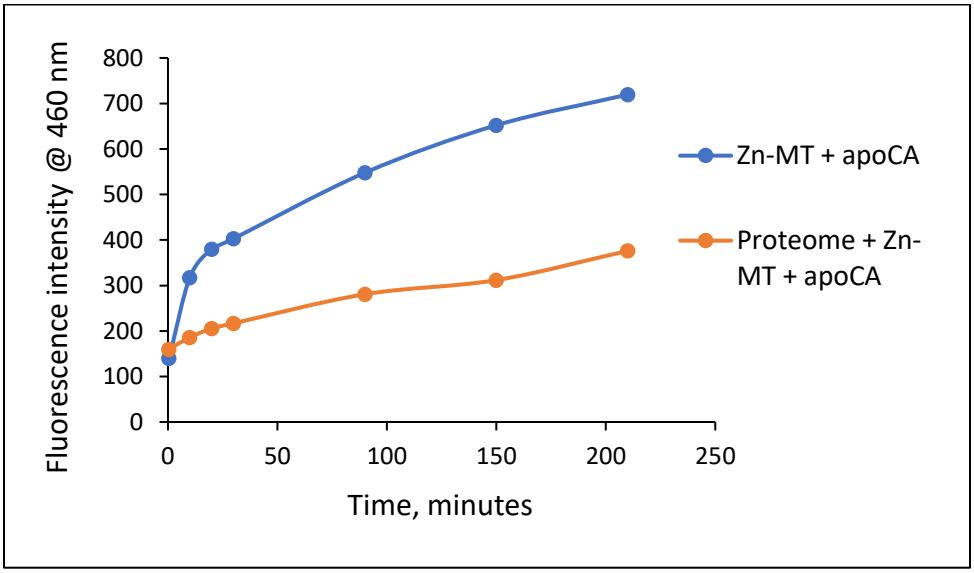

D.

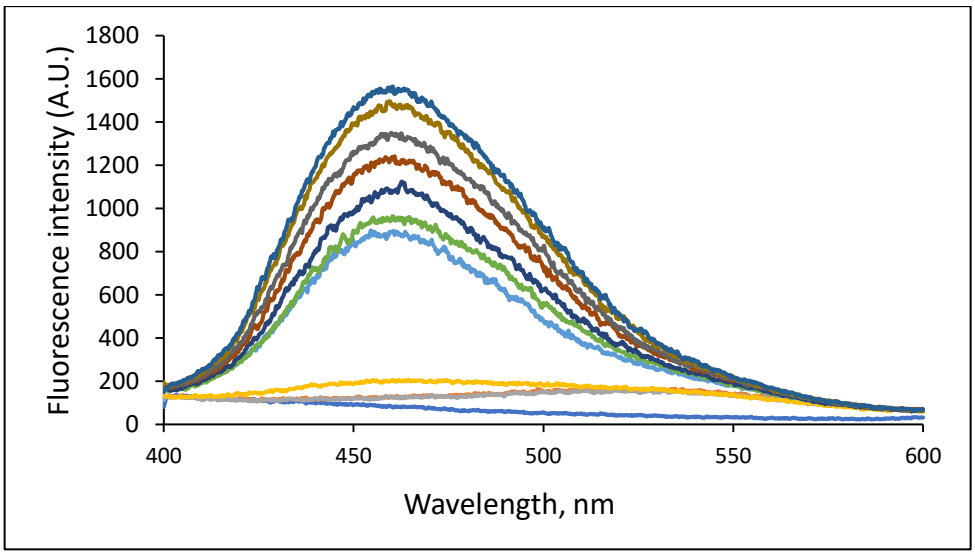

Figure 32. Metallothionein-mediated reconstitution of Zn-CA. (A) Zn_7-MT containing 1 µM Zn^{2+} in 20 mM Tris buffer (pH 7.4) was reacted with 1 µM native apo-CA in the absence (control) or presence of proteome containing 4 µM native Zn^{2+}. The reconstitution of Zn-CA was monitored with 1.6 µM dansyl amide. Fluorescence spectra of the reactions were recorded at excitation 320 nm and emission 400 – 600 nm. (B) Zn_7-MT containing 7 µM Zn^{2+} in 20 mM Tris buffer (pH 7.4) was reacted with 1 µM denatured apo-CA in presence of proteome containing 12.5 µM native Zn^{2+} and 1.6 µM dansyl amide. (C) Comparison of the rate of metallothionein-mediated Zn-CA reconstitution in the absence or presence of proteome. (D) Metallothionein-mediated reconstitution of Zn-CA from denatured apo-CA in the presence of proteome.

We tested the zinc transfer equilibrium between proteome and Zn_7-metallothionein may account for the depression of the rate of reaction of Zn_7-MT with apo-CA illustrated in **Figure 33**. For this purpose, Proteome containing 7.5 µM native Zn^{2+} was treated with 500 µM N-ethyl maleimide (NEM) for 1 hour to block the proteomic sulfhydryl groups and thus, its high affinity, zinc binding sites. Next, the resulting reaction mixture was filtered using a 3K molecular weight cut-off filter in order to remove the residual NEM. The NEM-treated and filtered proteome was then reacted with Zn_7-MT and apo-CA. Interestingly, a significant increase in the rate of Zn-CA reconstitution was observed (**Figure 33**), confirming that the proteomic thiolate sites inhibit the rate of ligand substitution between Zn_7-MT and apo-CA. According to our hypothesis, following the treatment with NEM, proteomic sulfhydryl groups were abolished and therefore the equilibrium between Proteome and Zn_7-MT was lost, resulting in direct transfer of zinc from Zn_7-MT to apo-CA and the rate enhancement of Zn-CA reconstitution.

$$\text{Proteome-SH} + \text{NEM} \leftrightarrows \text{Proteome-S-NEM} \qquad (64)$$

This experiment did not distinguish whether the role of Proteome-SH was to fully acquire Zn^{2+} from Zn_7-MT, altering the pathway of trafficking of Zn^{2+} to apo-CA or whether it had formed a ternary adduct with Zn_7-MT, Proteome-S-Zn_7-MT that reduced the rate of direct transfer of Zn^{2+} from Zn_7-MT to apo-CA.

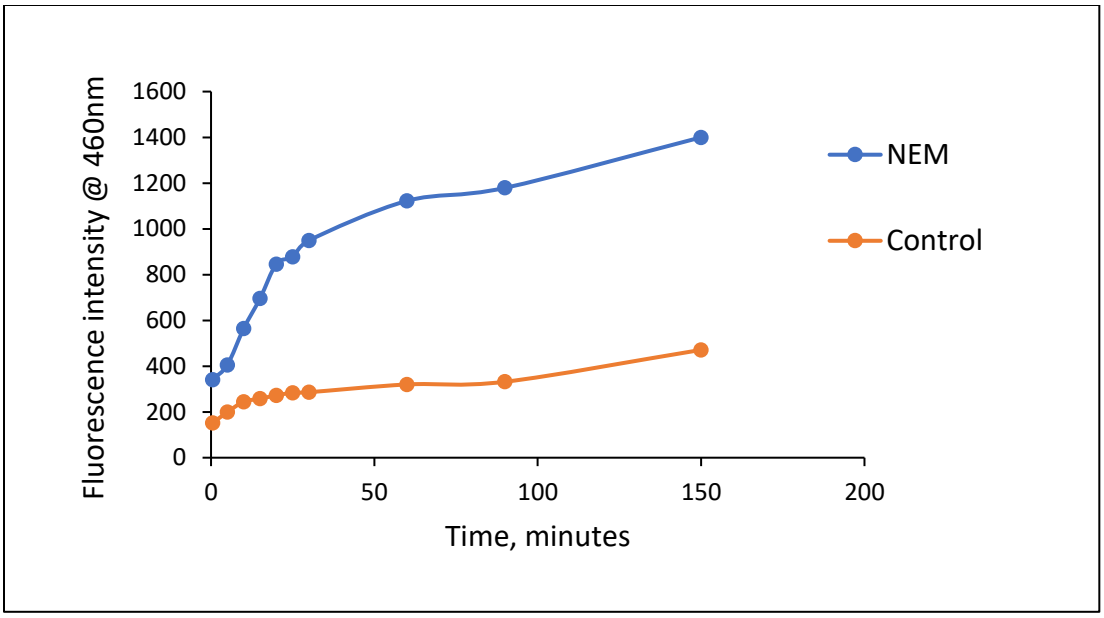

Figure 33. Reaction of Zn_7-MT with apo-CA in the presence of NEM-treated Proteome. Proteome containing 7.5 µM Zn^{2+} was treated with 500 µM NEM for 1 hour, and subsequently, filtered using a 3K molecular weight cut-off filter to remove the unreacted NEM. Filtered proteome was then reacted with Zn_7-MT containing 1 µM Zn^{2+} and 1 µM apo-CA. The reaction was monitored in the presence of 1.6 µM dansyl amide. As the control, the reaction was done with Proteome without NEM treatment. Fluorescence spectra of both reactions were recorded at excitation 320 nm and emission 400 – 600 nm.

3.3.3 In vitro distribution of Zn^{2+} between proteome and metallothionein

To explore if there existed any equilibrium between proteome and Zn-metallothionein, isolated proteome containing 40 µM native Zn^{2+} was incubated for an hour with Zn_7-MT having 50 µM Zn^{2+}. Subsequently, the reaction mixture was fractionated using size exclusion chromatography and each fraction was quantified for zinc content. As the control, untreated Proteome having 40 µM native Zn^{2+} or Zn_7-metallothionein containing 50 µM Zn^{2+} was fractionated with Sephadex G-75 and the zinc content in each fraction was measured. In the case of control Proteome, almost all zinc was found to be associated with high molecular weight Proteomic fractions (fraction 10-20). Likewise, following fractionation of control metallothionein, all of its Zn^{2+} was recovered from the corresponding metallothionein fractions (fraction 25-35). By contrast, a significant redistribution of zinc occurred between Proteome and metallothionein following their mixing (**Figure 34 and Table 1**). The total zinc content in Proteome fractions (47.1±3.9 µM) was found about 10 µM more than that in control proteome fractions (40 µM). Consistently, metallothionein fractions had about 10 µM less Zn^{2+} (reduced to 39.3±5.5 µM from 50 µM) after incubation with Proteome. This rearrangement of proteomic and metallothionein zinc clearly indicated that there existed an equilibrium between proteome and Zn_7-MT, which can be explained by either ligand substitution (reaction 60 above) or ternary complex formation (reaction 62 above).

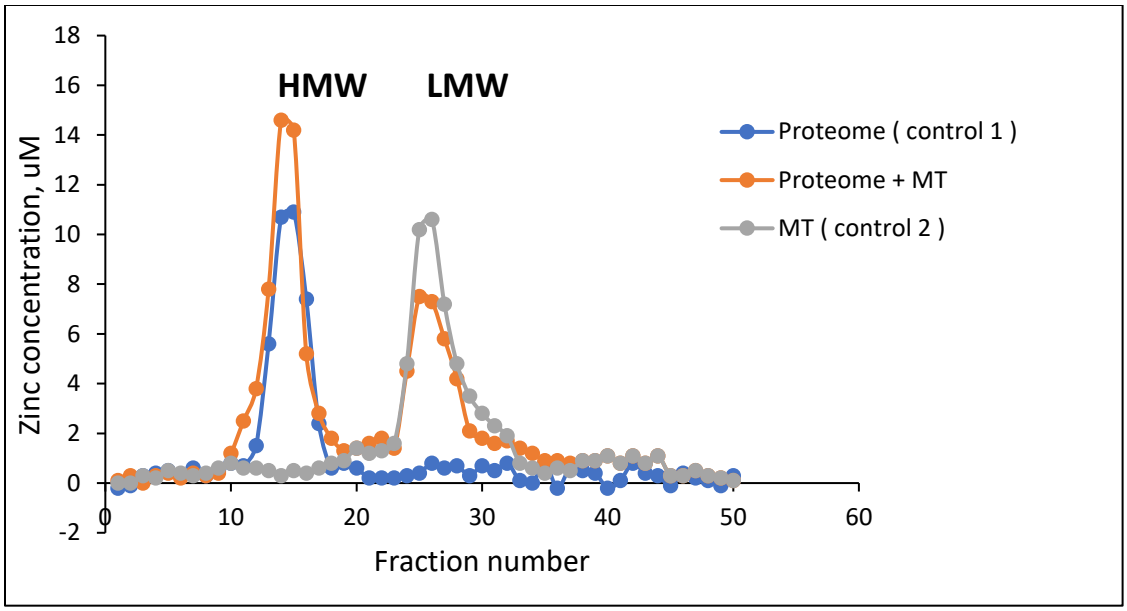

Figure 34. Isolated Proteome (40 uM Zn^{2+}) from LLC-PK1 cells was reacted with Zn_7-MT (50 uM Zn^{2+}) for 30 min. The reaction mixture was then loaded onto a Sephadex G-75 column and eluted with 20 mM degassed Tris buffer (pH 7.4). As controls, Proteome or metallothionein was loaded and eluted with Tris buffer. The zinc content in each fraction was measured by flame AAS.

Table 1. Zinc redistribution between Proteome and metallothionein following the incubation of proteome containing 40.4 µM native Zn^{2+} with Zn_7-MT (50 µM Zn^{2+}). The results are based on three runs and show the average ± standard deviation.

	$[Zn^{2+}]$, µM		HMW $[Zn^{2+}]$, µM	LMW $[Zn^{2+}]$, µM
Control : proteome	**40.4**		**38.3 ± 0.9**	
Control : MT	**50**			**49.5± 0.2**
Proteome + MT	**40.4**	**50**	**47.1± 3.9**	**39.3± 5.5**

3.4 Role of glutathione (GSH) in cellular zinc trafficking

We have already seen that proteomic sulfhydryl groups have a critical involvement in proteome-mediated zinc trafficking (Section **3.2.8** and **Figure 24**), presumably, other cellular components containing sulfhydryl groups have important roles in cellular zinc trafficking, as well. Consequently, we have investigated if glutathione (GSH) plays any part in the landscape of cellular zinc trafficking.

Glutathione is a small molecule and a tripeptide having one sulfhydryl group. In cells, it has a key antioxidant function that involves its thiol group and, thus prevents cellular damage caused by reactive oxygen species [103]. It also forms S-conjugates with reactive metabolites of xenobiotics [104]. One of the notable features of glutathione is its presence in cells at relatively high concentration, namely, 1-10 mM [85]. In addition, it has a moderate zinc binding affinity ($K_d \sim 10^{-4.2}$ M at pH 7) [105], that supports the hypothesis that glutathione plays an important role in overall zinc trafficking. This chapter focuses on this hypothesis and particularly on (i) the impact of glutathione on proteome- and/or metallothionein-mediated reconstitution of Zn-CA from apo-CA and (II) the possibility that GSH is a central player in cellular zinc trafficking.

3.4.1. Reconstitution of Zn-CA in the presence of glutathione

To examine if glutathione affects the rate of Zn-CA reconstitution, 1 µM apo-CA was reacted with increasing concentration of Zn^{2+} in the presence of 1 mM glutathione (GSH). In the absence of GSH, i.e., in control experiment, the rate of Zn-CA reconstitution from the reaction of 1 µM apo-CA and 1 µM Zn^{2+} was rapid as expected (**Figure 35**). However, the introduction of 1 mM GSH noticeably slowed down Zn-CA reconstitution even when a larger concentration of Zn^{2+} (2.5 µM) was used (**Figure 35**), implying that glutathione mediates zinc transfer to apo-CA and thus slows down the formation of Zn-CA (reaction 65**)** because ligand substitution must take place between apo-CA and zinc bound to GSH (reaction 66) instead of zinc associated with water (reaction Y).

$$GSH + Zn^{2+} \leftrightarrows GS\text{-}Zn \qquad (64)$$

$$GS\text{-}Zn + \text{apo-CA} \leftrightarrows GSH + \text{Zn-CA (slow)} \qquad (65)$$

With increasing concentration of Zn^{2+}, the rate of Zn-CA formation was enhanced, as expected.

A.

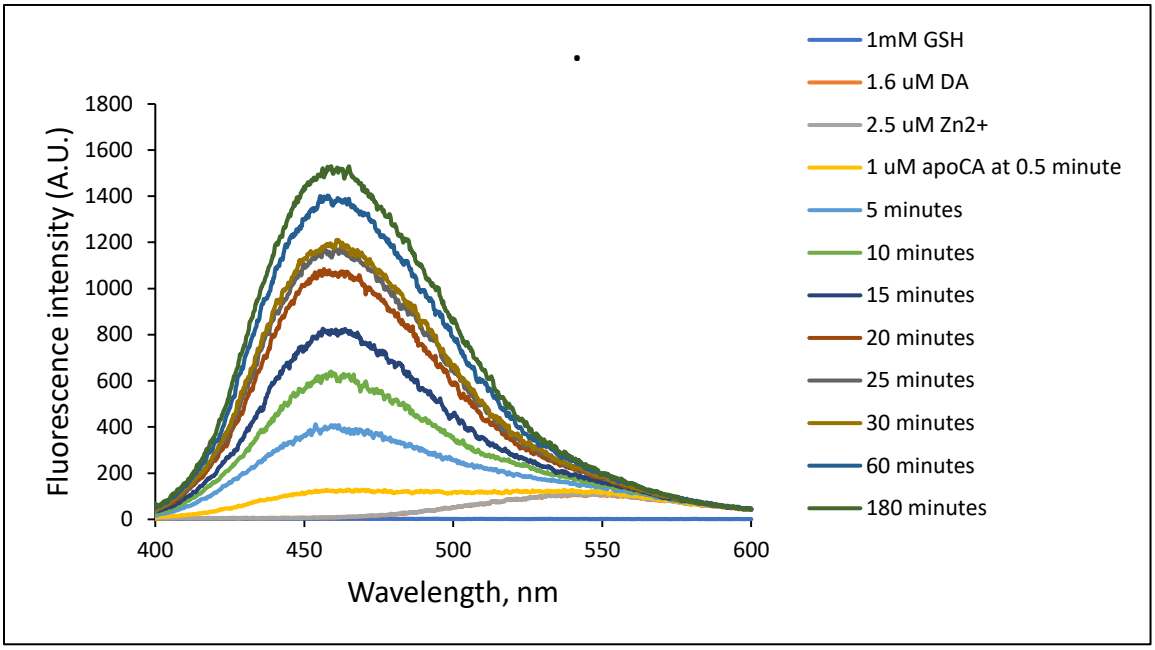
Fluorescence intensity (A.U.)
1800
1600
1400
1200
1000
800
600
400
200
0
400
450
500
550
600
Wavelength, nm
1mM GSH
1.6 uM DA
2.5 uM Zn2+
1 uM apoCA at 0.5 minute
5 minutes
10 minutes
15 minutes
20 minutes
25 minutes
30 minutes
60 minutes
180 minutes

B.

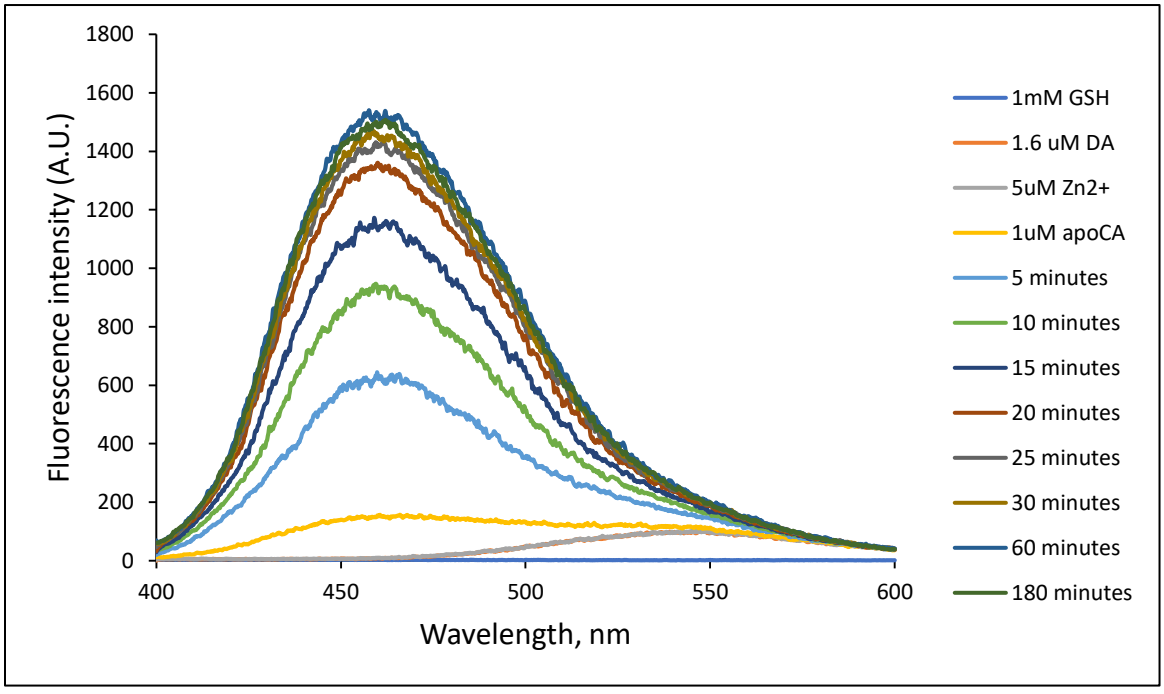
Fluorescence intensity (A.U.)
1800
1600
1400
1200
1000
800
600
400
200
0
400
450
500
550
600
Wavelength, nm
1mM GSH
1.6 uM DA
5uM Zn2+
1uM apoCA
5 minutes
10 minutes
15 minutes
20 minutes
25 minutes
30 minutes
60 minutes
180 minutes

C.

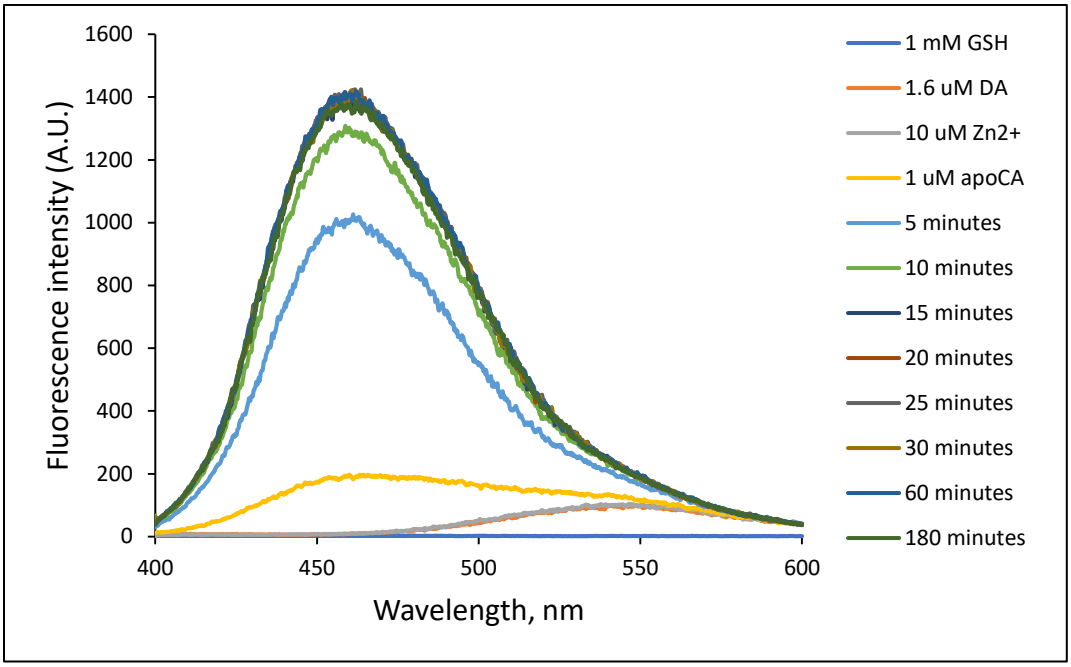
Fluorescence intensity (A.U.)
1600
1400
1200
1000
800
600
400
200
0
400
450
500
550
600
Wavelength, nm
1 mM GSH
1.6 uM DA
10 uM Zn2+
1 uM apoCA
5 minutes
10 minutes
15 minutes
20 minutes
25 minutes
30 minutes
60 minutes
180 minutes

D.

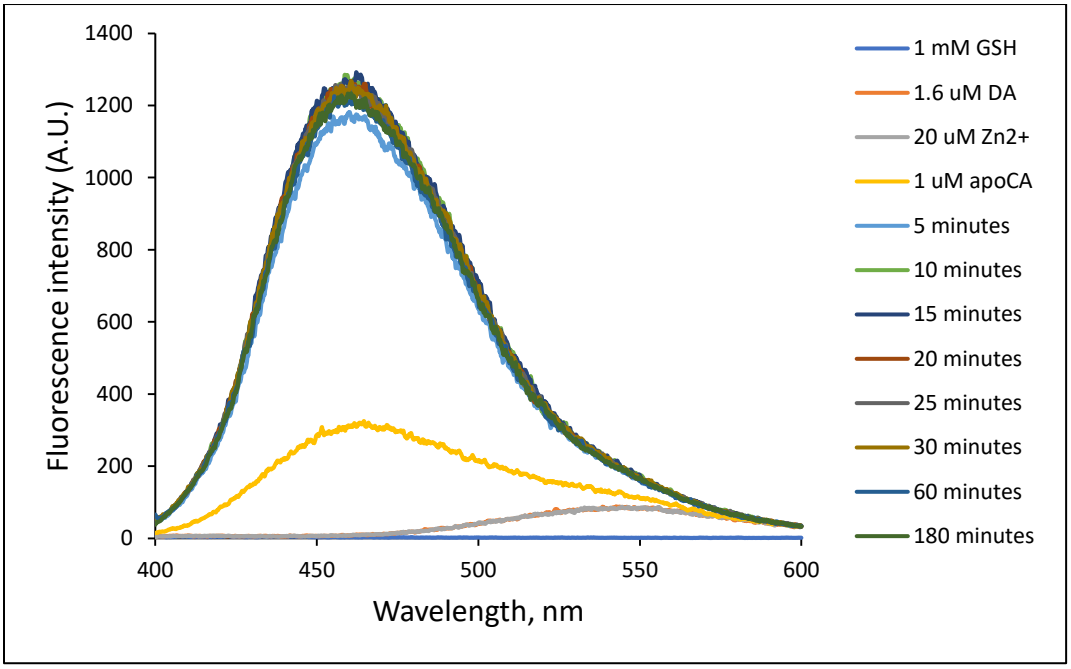
Fluorescence intensity (A.U.)
1400
1200
1000
800
600
400
200
0
400
450
500
550
600
Wavelength, nm
1 mM GSH
1.6 uM DA
20 uM Zn2+
1 uM apoCA
5 minutes
10 minutes
15 minutes
20 minutes
25 minutes
30 minutes
60 minutes
180 minutes

E.

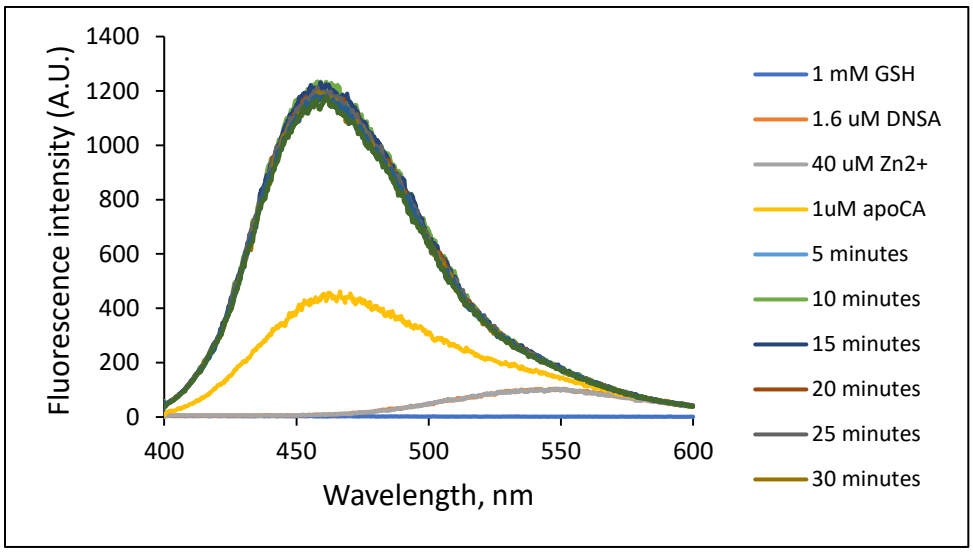

F.

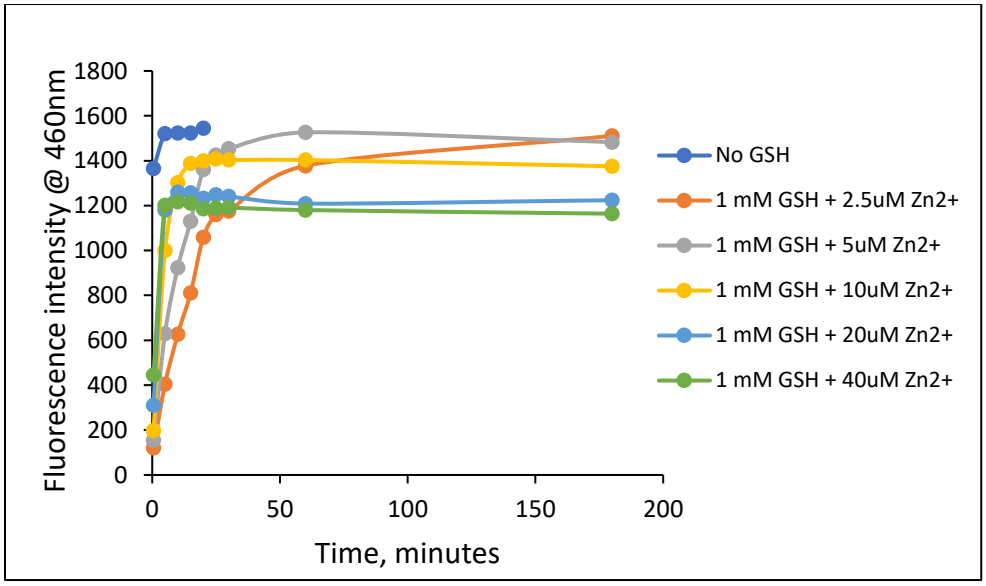

Figure 35. Reconstitution of Zn-CA in the presence of glutathione. (A – E) 1 µM apo-CA was reacted with (A) 2.5 µM, (B) 5 µM, (C) 10 µM, (D) 20 µM and (E) 40 µM Zn^{2+} in the presence of 1 mM GSH. The reactions were monitored in the presence of dansyl amide. Fluorescence spectra were recorded at excitation wavelength 320 nm and emission wavelength 400 – 600 nm. (F) Change of fluorescence at 460 nm during the reactions with time.

3.4.2. Effect of glutathione on proteome-mediated reconstitution of Zn-CA

The presence of proteome was previously found to significantly decrease the rate of Zn-CA reconstitution (section **3.2.6** and **figure 22**). Here, we investigated if glutathione could modify the rate of proteome-mediated reconstitution of Zn-CA. The experiments were based on the hypothesis that the presence of GSH may set up an equilibrium between Proteome•Zn and Zn-SG, providing a kinetic pathway through Zn-SG that speeds up the metal transfer apo-CA.

To test the effect, 1 µM apo-CA was reacted with 2 µM Zn^{2+} in the presence Proteome (5.6 µM native Zn^{2+}) and 1 mM glutathione. As a control experiment, the reaction was repeated without glutathione. As anticipated, the control reaction resulted in a slow reconstitution of Zn-CA (**Figure 36 A** and **C**).

$$\text{Proteome-SH} + Zn^{2+} \leftrightarrows \text{Proteome-S•Zn} + H^{+} \quad (67)$$

$$\text{Proteome-S•Zn} + \text{apo-CA} + H^{+} \leftrightarrows \text{Proteome-SH} + \text{Zn-CA} \quad \text{(slow)} \quad (68)$$

Interestingly, the introduction of 1 mM glutathione to the reaction significantly enhanced the rate of Zn-CA (**Figure 36 B** and **C**), suggesting an alternative and faster route of proteome-mediated zinc transfer to apo-CA in the presence of glutathione. Probably, as hypothesized above, there exists a zinc transfer equilibrium between Proteome and glutathione, and eventually, glutathione facilitates the transfer of zinc to apo-CA to reconstitute Zn-CA.

$$\text{Proteome-S•Zn} + \text{GSH} \leftrightarrows \text{Proteome-S•Zn-SG} + H^{+} \quad (69)$$

$$\text{Proteome-S•Zn-SG} + H^{+} \leftrightarrows \text{Proteome-SH} + \text{Zn-SG} \quad (70)$$

$$\text{Zn-SG} + \text{apo-CA} + H^{+} \leftrightarrows \text{Zn-CA} + \text{GSH} \quad \text{(fast)} \quad (71)$$

A.

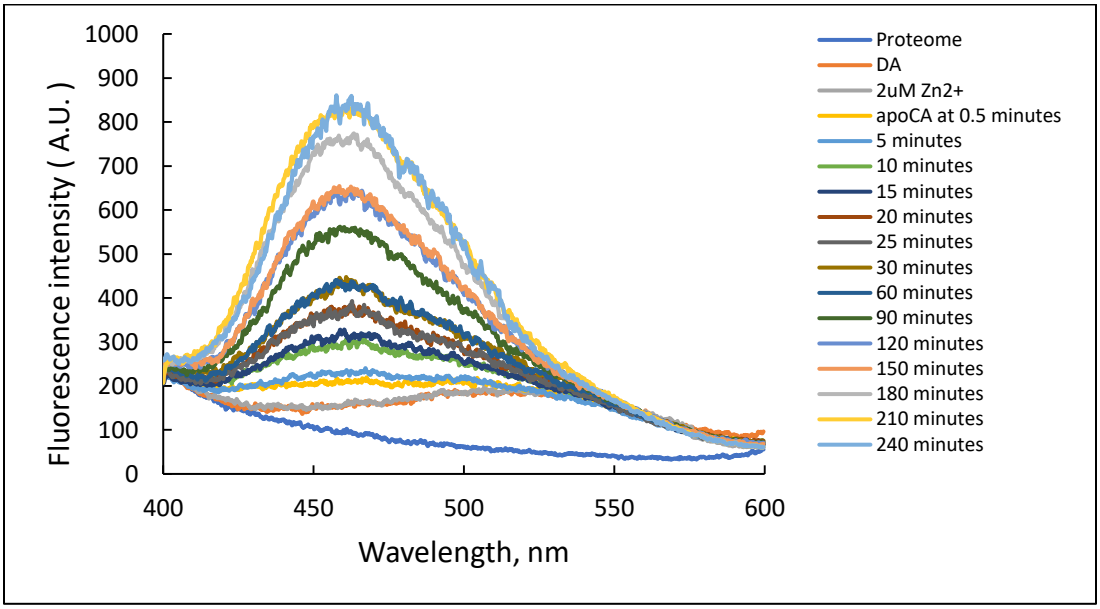
Fluorescence intensity (A.U.)
1000
900
800
700
600
500
400
300
200
100
0
400
450
500
550
600
Wavelength, nm
Proteome
DA
2uM Zn2+
apoCA at 0.5 minutes
5 minutes
10 minutes
15 minutes
20 minutes
25 minutes
30 minutes
60 minutes
90 minutes
120 minutes
150 minutes
180 minutes
210 minutes
240 minutes

B.

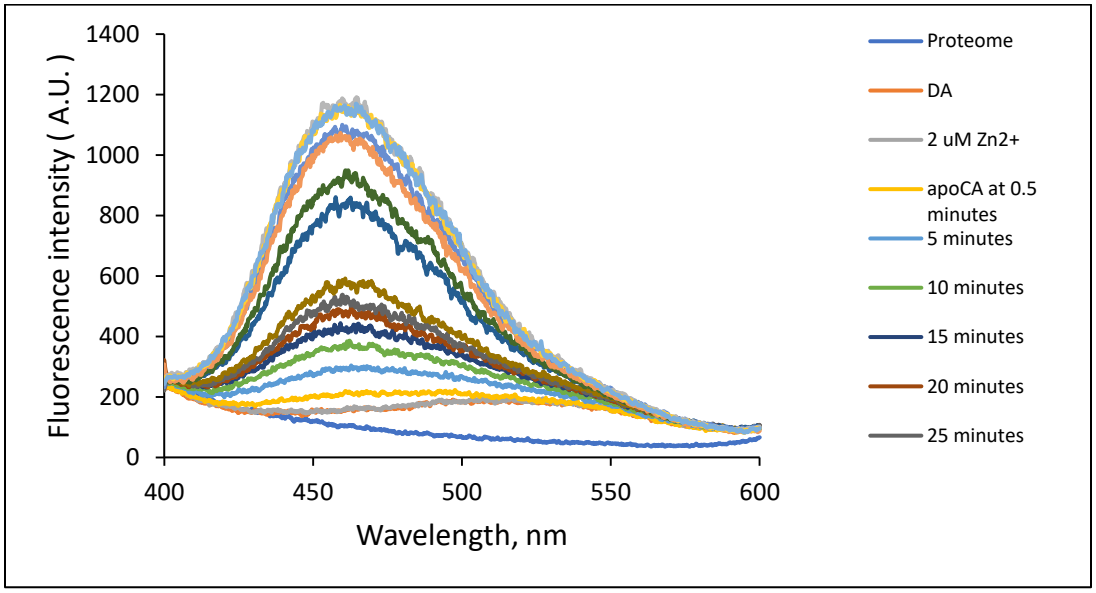
Fluorescence intensity (A.U.)
1400
1200
1000
800
600
400
200
0
400
450
500
550
600
Wavelength, nm
Proteome
DA
2 uM Zn2+
apoCA at 0.5 minutes
5 minutes
10 minutes
15 minutes
20 minutes
25 minutes

C.

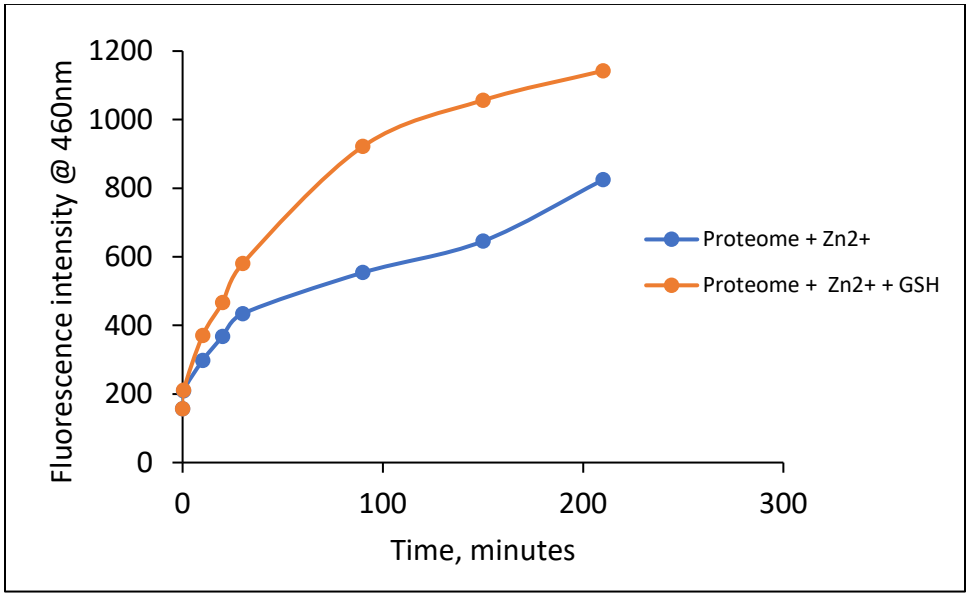

Figure 36. Effect of glutathione on proteome-mediated reconstitution of Zn-CA. (A and B) 1 µM apo-CA was reacted with 2 µM Zn^{2+} and Proteome containing 5.6 µM native Zn^{2+} in the absence (A) or presence of 1 mM GSH (B). The reaction was monitored using dansyl amide (DA). Fluorescence spectra were recorded using excitation wavelength 320 nm and emission wavelength 400 – 600 nm. (C) Change of fluorescence at 460 nm of both reactions with time.

The effect of glutathione on Proteome-mediated Zn-CA reconstitution was tested another way. Cell lysate was collected from $2x10^8$ LLC-PK_1 cells and filtered using a Centricon 3K molecular weight cut-off filter to separate the high molecular weight (HMW) and low molecular weight (LMW) fractions. Since LLC-PK_1 cells contain undetectable amount of metallothionein under basal condition, the isolated high molecular weight (HMW) fraction contains only high molecular weight soluble proteins. By contrast, the low molecular weight (LMW) fraction is a collection of all small molecules of cells, including glutathione. Subsequently, the HMW fraction was split into three aliquots. Each aliquot contained 8.8 µM native Zn^{2+}. One aliquot of HMW fraction was reacted with 1 µM apo-CA and 1 µM exogenous Zn^{2+}. As expected, a slow rate of Zn-CA was observed in the presence of high molecular weight proteome fractions (**Figure 37 A** and **D**). Another aliquot of HMW fraction was reacted the same way, except that the LMW fraction was added to reaction mixture. A dramatic increase in rate was observed in the LMW-treated reaction (**Figure 37 B** and **D**), indicating that cellular small molecules, including glutathione, played a significant part in cellular zinc trafficking to generate native Zn-proteins. The third aliquot of HMW fraction was reacted with 1 µM apo-CA and 1 µM exogenous Zn^{2+} in the presence of 1 mM exogenous glutathione. Interestingly, in this case, an identical increase of reaction rate as in the second case was observed (**Figure 37 C** and **D**), confirming that glutathione present in LMW fraction was implicated in the rate enhancement in the second reaction.

A.

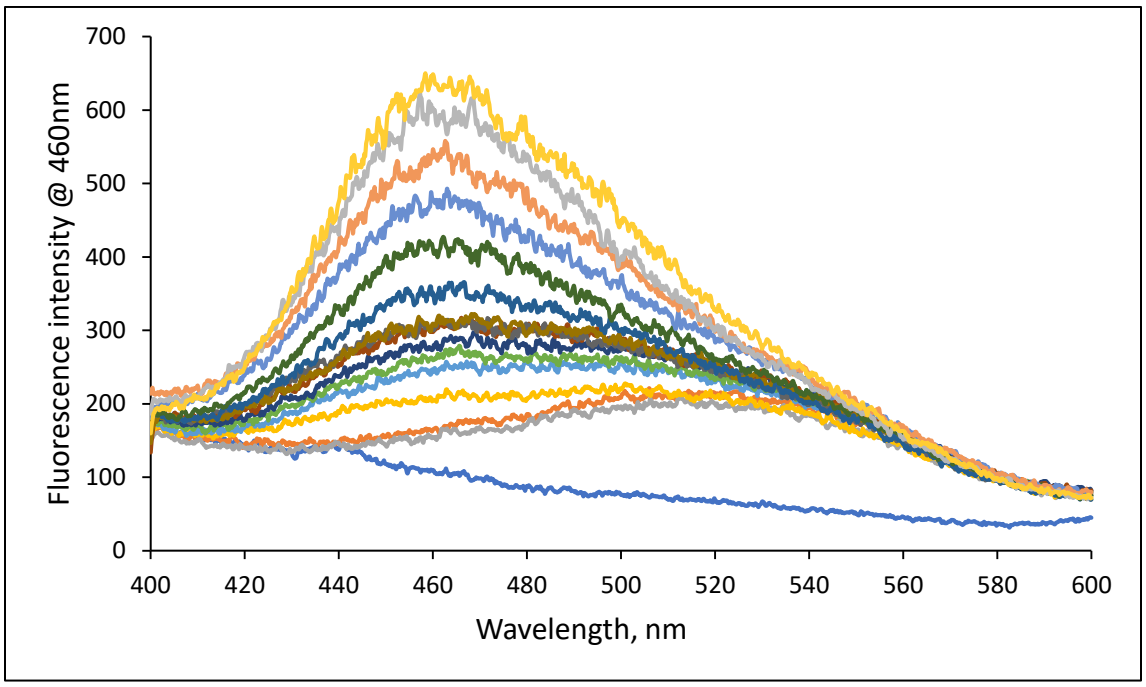
Fluorescence intensity @ 460nm
700
600
500
400
300
200
100
0
400
420
440
460
480
500
520
540
560
580
600
Wavelength, nm

B.

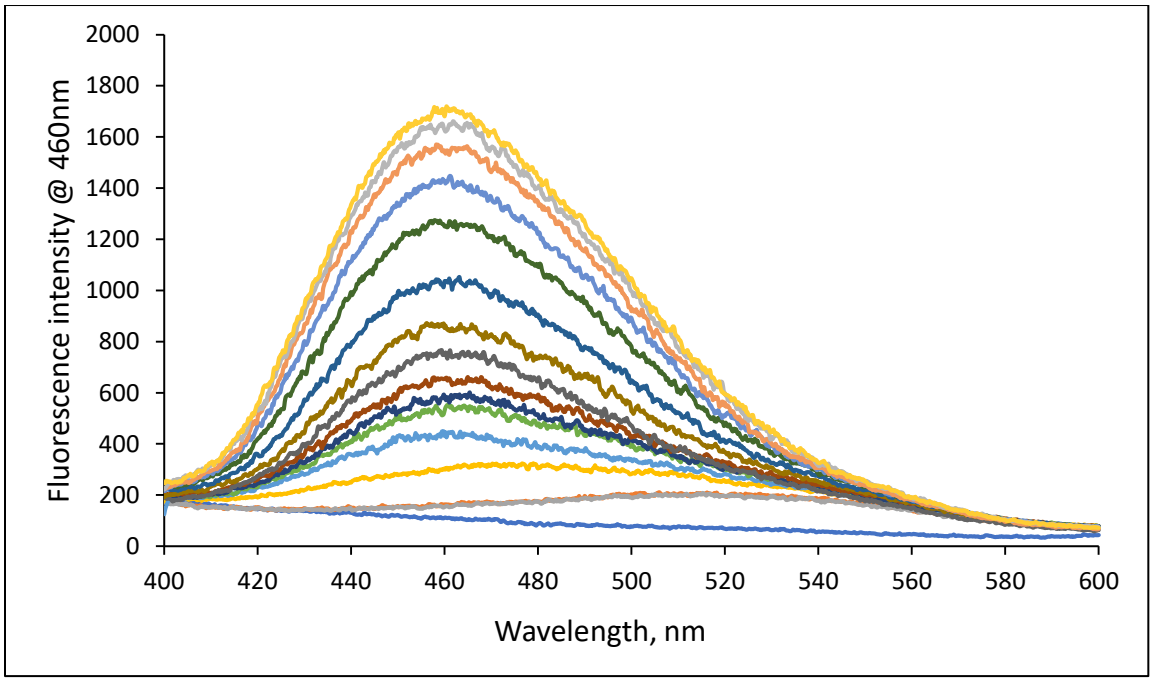
Fluorescence intensity @ 460nm
2000
1800
1600
1400
1200
1000
800
600
400
200
0
400
420
440
460
480
500
520
540
560
580
600
Wavelength, nm

C.

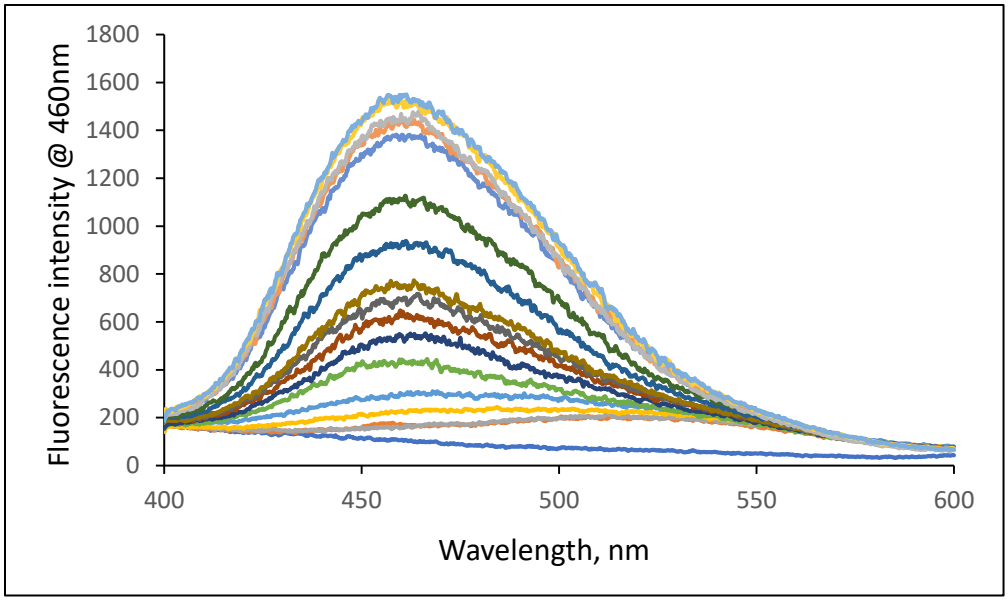

D.

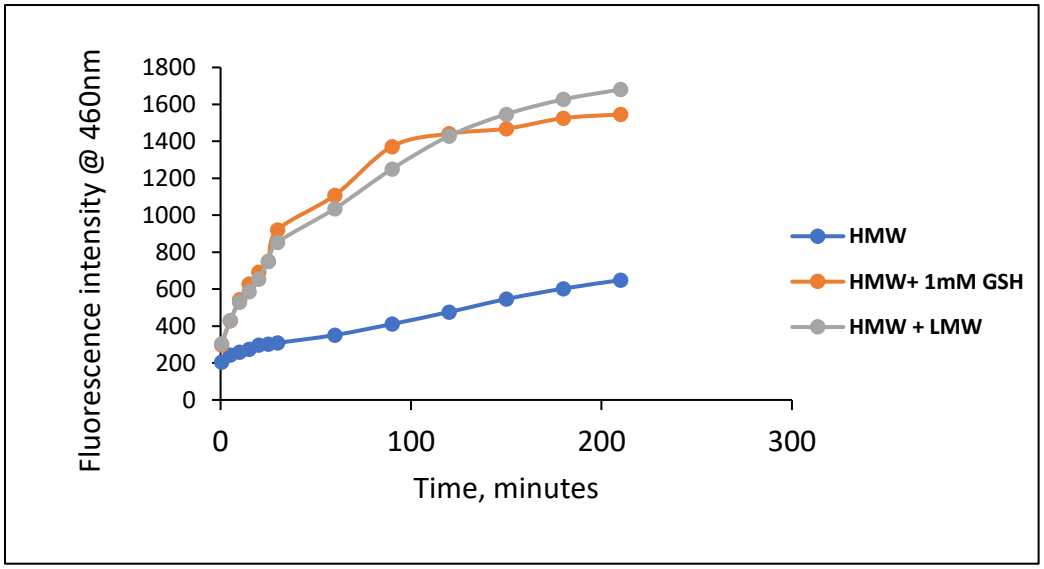

Figure 37. Zn-CA reconstitution in the presence of high molecular weight (HMW) and low molecular weight (LMW) fractions. (A – C) 1 µM apo-CA was reacted with 1 µM exogenous Zn^{2+} in the presence of (A) high molecular weight (HMW) fraction isolated from LLC-PK1 cells, or (B) HMW and LMW fractions, or (C) HMW fraction and 1 mM exogenous GSH. The reaction progress was followed using dansyl amide (DA). Fluorescence spectra were recorded using excitation wavelength 320 nm and emission wavelength 400 – 600 nm. (D) Change of fluorescence at 460 nm of the reactions with time.

3.4.3 Effect of glutathione on Zn-CA reconstitution in presence of proteome and Zn_7-MT

Having found that glutathione facilitated proteome-mediated reconstitution of Zn-CA, next we probed its effect on Zn-CA regeneration in presence of both proteome and Zn_7-metallothionein. The rate and extent of reaction of Zn_7-MT with apo-CA was reduced by the addition of 1 mM GSH, like in the presence of Proteome. But the impact of GSH was different when Proteome was part of the reaction.

1 µM apo-CA was reacted with 2 µM Zn_7-MT and proteome containing 5.6 µM native Zn^{2+} followed by the addition of 1 mM GSH. The control experiment did not include any glutathione. As seen before, the control experiment yielded the slow regeneration of Zn-CA in the presence of both proteome and metallothionein (**Figure 38 A** and **C**). This slow reaction can be explained by referring to the previous analysis of the reaction of Zn_7-MT with apo-CA in the presence of Proteome which suggested two possible mechanisms by which Proteome could retard the reconstitution reaction.

Possibility 1.

$$Zn_7\text{-MT} + \text{Proteome-SH} \leftrightarrows Zn_6\text{-MT} + \text{Proteome-S}\bullet\text{Zn} + H^+ \quad (72)$$

$$\text{Proteome-S}\bullet\text{Zn} + \text{apo-CA} + H^+ \leftrightarrows \text{Proteome-SH} + \text{Zn-CA (slow)} \quad (73)$$

In this scheme, the Proteome competes for Zn^{2+} bound to MT and then reacts with apo-CA, like Zn-MT. If Proteome-S•Zn reacts slower with apo-CA than Zn_7-MT, the observed reaction rate will decrease.

Possibility 2.

$$\text{Proteome-SH} + Zn_7\text{-MT} \leftrightarrows \text{Proteome-S}\bullet Zn_7\text{-MT} + H^+ \quad (74)$$

$$Zn_7\text{-MT} + \text{apo-CA} \leftrightarrows Zn_6\text{-MT} + \text{Zn-CA} \ \text{(slow)} \quad (75)$$

According to this mechanism, the plausible intermediate in reaction 74 above, Proteome-S•Zn_7-MT, becomes a quantitatively important product in the equilibrium of reaction 76:

$$Zn_7\text{-MT} + \text{Proteome-SH} \leftrightarrows \text{Proteome-S}\bullet Zn_7\text{-MT} \leftrightarrows Zn_6\text{-MT} + \text{Proteome-S}\bullet\text{Zn} + H^+ \quad (76)$$

It is then hypothesized that it is unreactive or relatively unreactive with apo-CA.

Surprisingly, in the presence of 1 mM glutathione, a large increase in the rate of Zn-CA reconstitution was observed (**Figure 38 B** and **C**), indicating a possible faster route of zinc transfer to apo-CA that involved glutathione. This mechanism might include the formation of a ternary complex, Proteome-S•Zn7-MT, which then reacts with GSH and produces a new ternary complex, GS•Zn_7-MT. Eventually, zinc is transferred in a faster rate from the newly formed adduct to apo-CA to regenerate Zn-CA.

$$\text{Proteome-SH} + Zn_7\text{-MT} \leftrightarrows \text{Proteome-S}\bullet Zn_7\text{-MT} \quad (77)$$

$$\text{Proteome-S}\bullet Zn_7\text{-MT} + \text{GSH} \leftrightarrows \text{Proteome-SH} + \text{GS}\bullet Zn_7\text{-MT} \quad (78)$$

$$\text{GS}\bullet Zn_7\text{-MT} + n(\text{apo-CA}) \leftrightarrows n(\text{Zn-CA}) + Zn_{7-n}\text{-MT} + \text{GSH} \ \text{(fast)} \quad (79)$$

A.

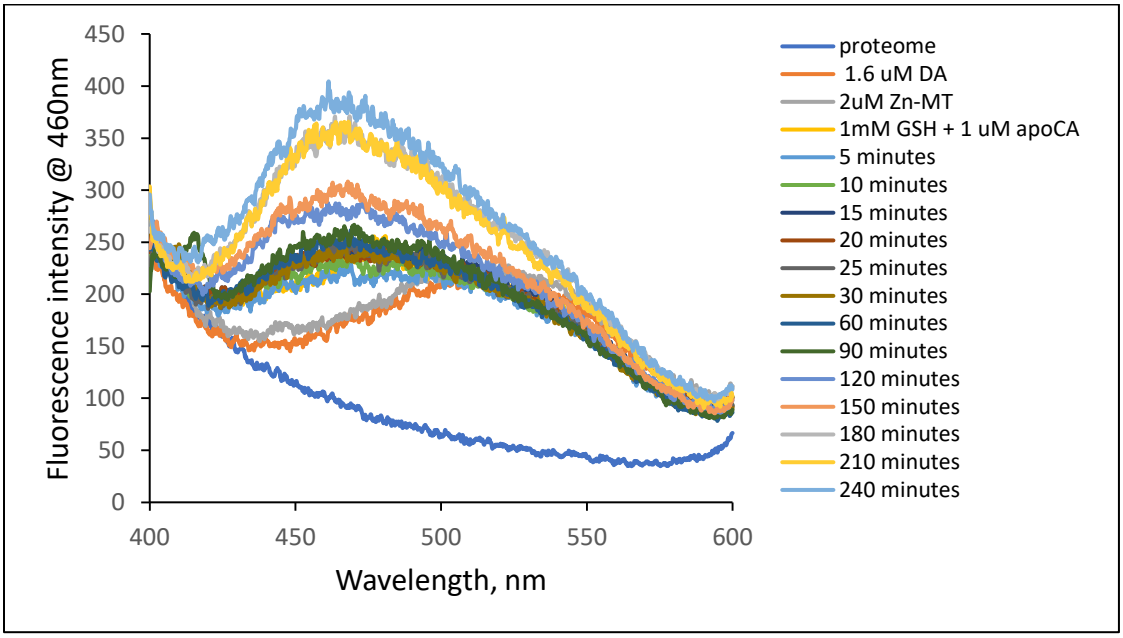
Fluorescence intensity @ 460nm
450
400
350
300
250
200
150
100
50
0
400
450
500
550
600
Wavelength, nm
proteome
1.6 uM DA
2uM Zn-MT
1mM GSH + 1 uM apoCA
5 minutes
10 minutes
15 minutes
20 minutes
25 minutes
30 minutes
60 minutes
90 minutes
120 minutes
150 minutes
180 minutes
210 minutes
240 minutes

B.

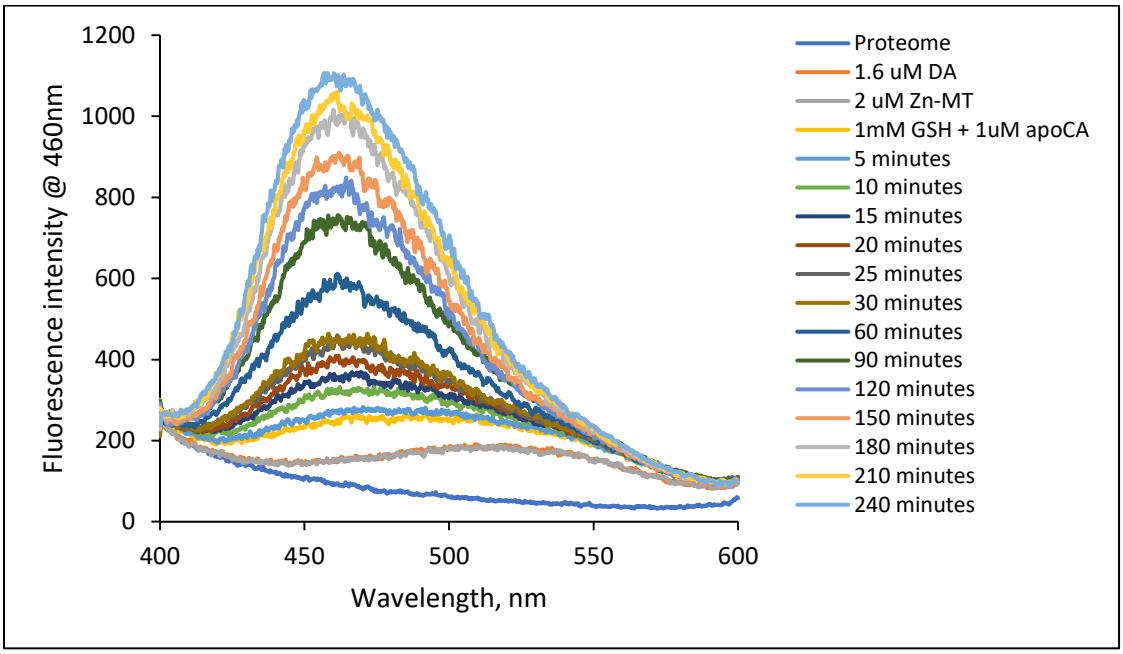
Fluorescence intensity @ 460nm
1200
1000
800
600
400
200
0
400
450
500
550
600
Wavelength, nm
Proteome
1.6 uM DA
2 uM Zn-MT
1mM GSH + 1uM apoCA
5 minutes
10 minutes
15 minutes
20 minutes
25 minutes
30 minutes
60 minutes
90 minutes
120 minutes
150 minutes
180 minutes
210 minutes
240 minutes

C.

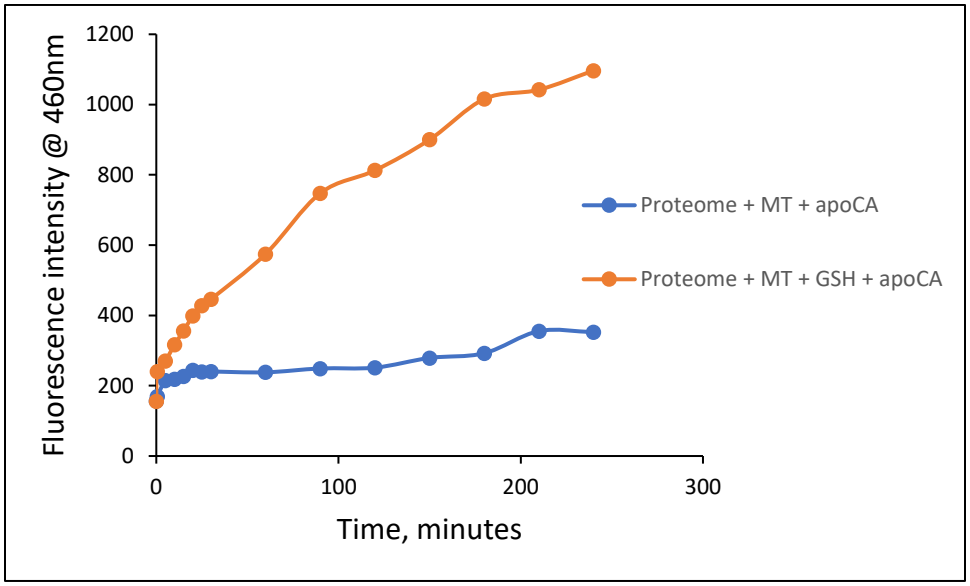

Figure 38. Effect of glutathione on Zn-CA reconstitution in the presence of both proteome and Zn_7-MT. (A and B) 1 µM apo-CA was reacted with 2 µM Zn_7-MT and proteome containing 5.6 µM native Zn^{2+} in the absence (A) or presence of 1 mM GSH (B). The reaction was monitored using dansyl amide (DA). Fluorescence spectra were recorded using excitation wavelength 320 nm and emission wavelength 400 – 600 nm. (C) Change of fluorescence at 460 nm of both reactions with time.

A previous study by Brouwer et al demonstrated that GSH forms an adduct with Zn_7-MT [106]. On the basis of molecular modeling, they suggested that GSH associates specifically with one of the crevices in the α-domain of Zn_7-MT. In so doing, it may compete with Proteome-SH for binding to the α-domain Zn_4S_{11} cluster, preventing the formation of Proteome-S-Zn_7-MT. If this mechanism is correct, GS-Zn_7-MT retains its reactivity toward apo-CA.

3.4.4 Effect of inhibition of cellular glutathione synthesis on zinc trafficking

We have demonstrated that glutathione enhanced the rate of formation of Zn-CA from apo-CA in the presence of either Proteome•Zn or Proteome plus Zn_7-MT. Thus, we have explored the effect of glutathione synthesis on cellular zinc trafficking. To inhibit cellular glutathione synthesis, LLC-PK_1 cells were treated with buthionine sulfoximine (BSO) for 24 hours. BSO inhibits gamma-glutamylcysteine synthetase, the enzyme necessary to catalyze the first step of glutathione synthesis, and thus greatly reduces the cellular level of glutathione over this time period [107]. First, the toxicity of BSO to LLC-PK_1 cells was examined by staining BSO-treated and untreated cells with trypan blue dye. According to **Figure 39**, even at a concentration as high as 200 μM of BSO, the cell viability was found to be greater than 90%. Therefore, to study the impact of BSO on cellular zinc trafficking by inhibiting glutathione synthesis, LLC-PK_1 cells were treated with 100 μM BSO for 24 hours. The efficiency of BSO in inhibiting glutathione synthesis in LLC-PK_1 cells was also tested. Following the treatment of $2x10^8$ LLC-PK_1 cells with 100 μM BSO (cell viability ≥, cell 90%, **Figure 39**), supernatant was collected and filtered to separate the high molecular weight (HMW) and low molecular weight (LMW) fractions. Using the DTNB assay, the sulfhydryl content in both fractions was quantified. As a control, the similar procedure was done with $2x10^8$ LLC-PK_1 cells untreated with BSO. According to DTNB assay, 8 nmol/10^7 cells of sulfhydryl groups found in high molecular weight (HMW) fraction of BSO treated cells, as well as 8 nmol/10^7 cells in that of control cells, meaning that BSO treatment did not have any noticeable effect on proteomic sulfhydryl groups (**Figure 40**)**.** However, a dramatic change was observed in low molecular weight (LMW) fractions. The LMW fraction of untreated cells contained 29 nmol/10^7 cells of sulfhydryl content. By contrast, only 0.4 nmol/10^7 cells was

detected in that of BSO-treated cells. That is, the low molecular weight sulfhydryl content was almost completely abolished following BSO treatment. This result confirmed the effectiveness of BSO in reducing the cellular level of glutathione.

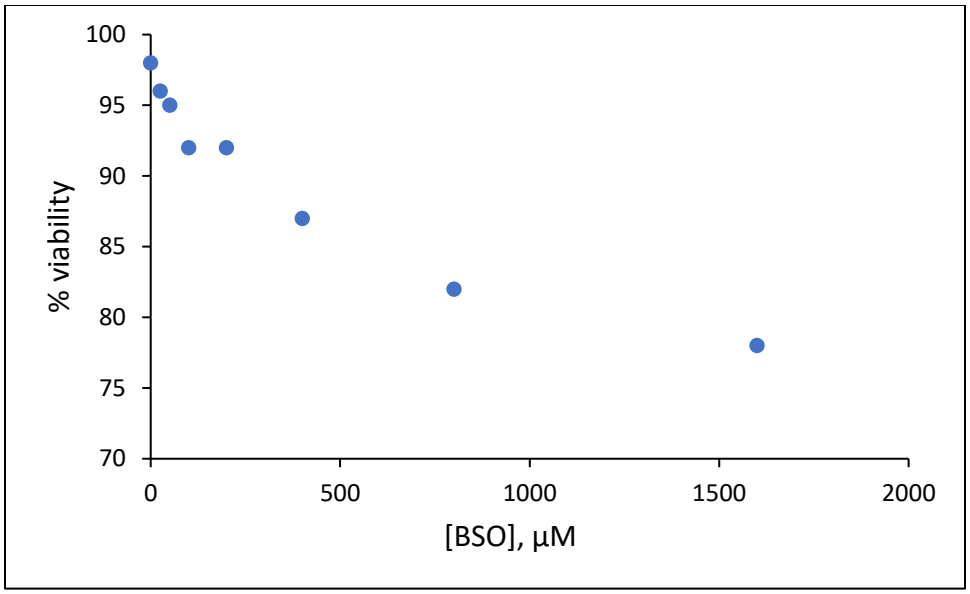

Figure 39. Toxicity of buthionine sulfoximine (BSO) to LLC-PK1 cells. 1 x 10^7 LLC-PK1 cells were treated with various concentration of BSO dissolved in culture medium for 24 hours. Subsequently, cells were released by trypsin-EDTA treatment and resuspended in DPBS. The cell suspension was then stained with trypan blue at 1:1 ratio. Number of live and dead cells were counted using a hemacytometer.

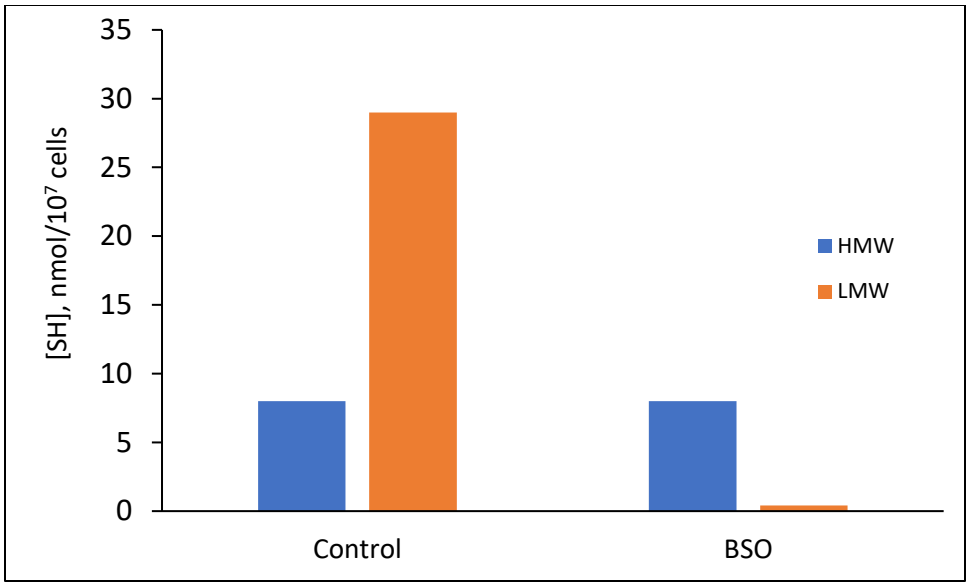

Figure 40. Comparison of sulfhydryl content in BSO-treated and control cells. 2 x 10^8 LLC-PK_1 cells were treated with 100 µM BSO for 24 hours. Afterwards, cells were washed and cell supernatant was collected via sonication and centrifugation. Cell lysate was then filtered using a Centricon 3K molecular weight cut-off filter separate high molecular weight (HMW) and low molecular weight (LMW) fractions. The sulfhydryl content in each fraction was quantified using DTNB assay.

We then investigated if the reduction of glutathione level by BSO treatment had any effect on the cellular zinc status. To test this, both BSO treated and untreated (control) 2 x 10^7 LLC-PK_1 cells were reacted with 20 µM TSQ, a fluorescent zinc sensor that (i) reacts with Zn^{2+} to form $Zn(TSQ)_2$ with an emission wavelength maximum of 492 nm and (II) can also form ternary adducts with proteomic Zn^{2+} characterized by a wavelength maximum of 470-475 nm [76-78]. In the case of control cells, as anticipated, a slow increase of fluorescence at 470 nm was observed (**Figure 41 A**), indicative of the formation of ternary complex of TSQ and native Zn-proteins, TSQ-Zn-protein.

$$\text{Zn-Proteome} + \text{TSQ} \leftrightarrows \text{TSQ-Zn-Proteome} \quad \text{(slow)}$$

It has been previously reported that TSQ reacts slowly with about 25% of native Zn-proteins and generates TSQ-Zn-protein ternary complex with a signature fluorescence spectrum centered at 470 nm [76-78]. Surprisingly, the reaction of BSO-treated cells and TSQ produced a much faster and greater fluorescence enhancement with an emission maximum of 470 nm (**Figure 41 B**). This remarkable 2.7x increase of fluorescence relative to the same number of control cells suggested that BSO treated cells appeared to contained a significant amount of adventitiously bound proteomic zinc, Proteome-S•Zn, with which TSQ reacted to form proteome-S•Zn-TSQ ternary complex and resulted in a faster increase of fluorescence at 470 nm.

$$\text{Proteome-S•Zn} + \text{TSQ} \leftrightarrows \text{Proteome-S•Zn-TSQ} \quad \text{(fast)}$$

The apparent generation of proteome-S•Zn following inhibition of glutathione synthesis by BSO treatment suggested that under basal cellular conditions, some cellular zinc binds to

glutathione in the steady state of zinc trafficking and, thus, is involved in mediating the trafficking of Zn^{2+} to apo-Zn protein binding sites. As glutathione level in cell drops, the GSH dependent pathway is blocked (**Figure 41**):

$$Zn^{2+}_{\text{outside cell}} \rightarrow Zn^{2+}_{\text{inside cell}} \rightarrow \text{Proteome•Zn} \rightarrow Zn(SG)_{n+} \rightarrow \text{Zn-Protein} \quad (80)$$

As a consequence, Zn^{2+} begins to accumulate in the Proteome, bound to proteomic non-specific sites. Overall, this finding strongly supported the novel hypothesis that glutathione plays a critical role in cellular zinc trafficking leading to the formation of native Zn-proteins. Since cells were still able to divide and acquire their required set of Zn-proteins for cell proliferation even in the almost complete absence of GSH, we hypothesized that the apparent elevation in Proteome•Zn supported its capacity to directly supply Zn^{2+} to apo-Zn proteins.

A.

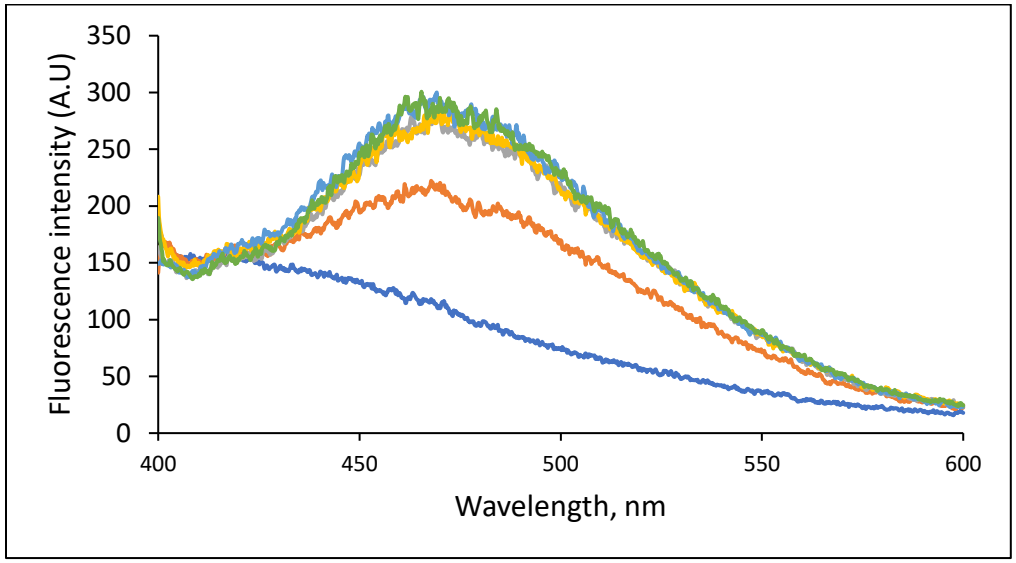
Fluorescence intensity (A.U)
350
300
250
200
150
100
50
0
400
450
500
550
600
Wavelength, nm

B.

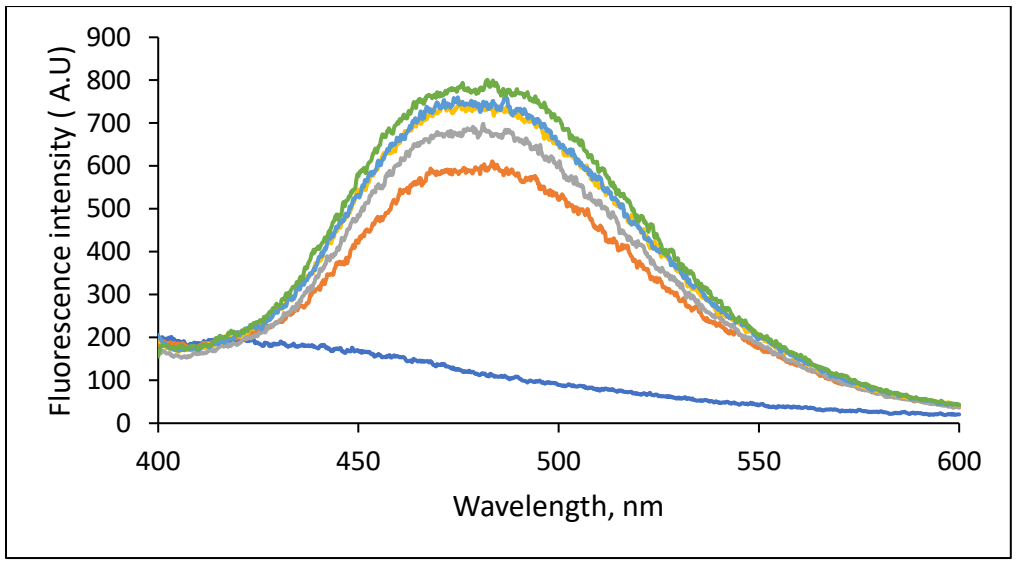
Fluorescence intensity (A.U)
900
800
700
600
500
400
300
200
100
0
400
450
500
550
600
Wavelength, nm

C.

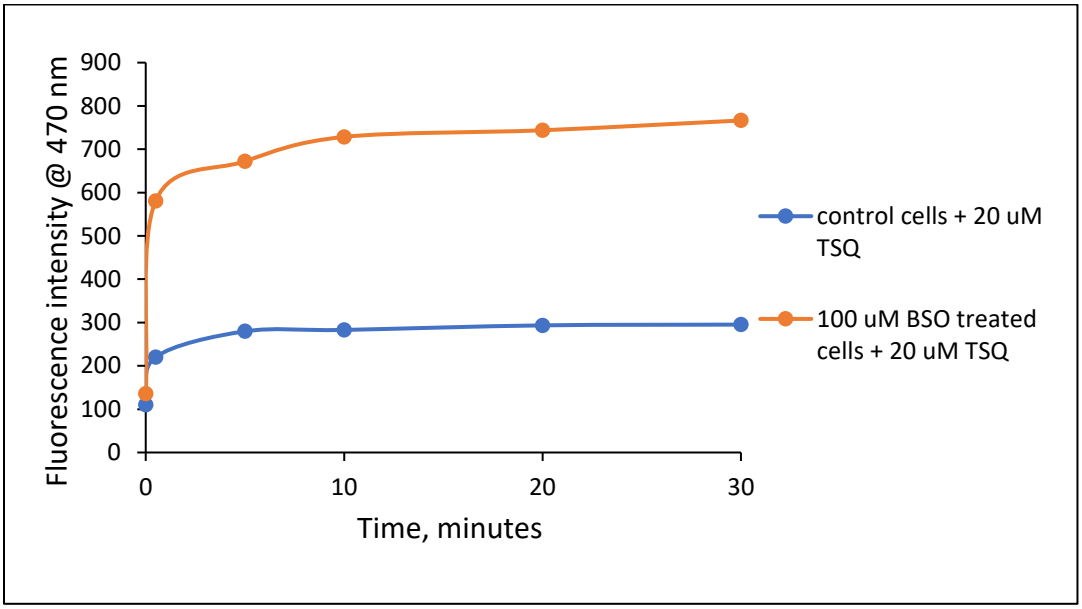

Figure 41. Reaction of BSO-treated cells with TSQ. (A) Control experiment: $2x10^7$ LLC-PK_1 cells resuspended in DPBS were reacted with 20 µM TSQ for 30 min. Fluorescence spectra were recorded using excitation wavelength 370 nm and emission wavelength 400 – 600 nm. (B) $2x10^7$ LLC-PK_1 cells were treated with 100 µM BSO for 24 hours. Thereafter, cells resuspended in DPBS were treated with 20 µM TSQ for 30 min. (C) Change of fluorescence at 470 nm with time for both reactions.

The reaction of isolated Proteome from BSO-treated cells with TSQ showed a similar faster enhancement of fluorescence in comparison with control Proteome, as was observed in the study of the reaction of TSQ with whole cells (**Figure 42**). The result of isolated proteome experiment further supported the hypothesis that glutathione-bound zinc plays an important role in cellular zinc trafficking, and thus inhibition of its synthesis in cells by BSO resulted in the non-specific binding of zinc to proteome.

A.

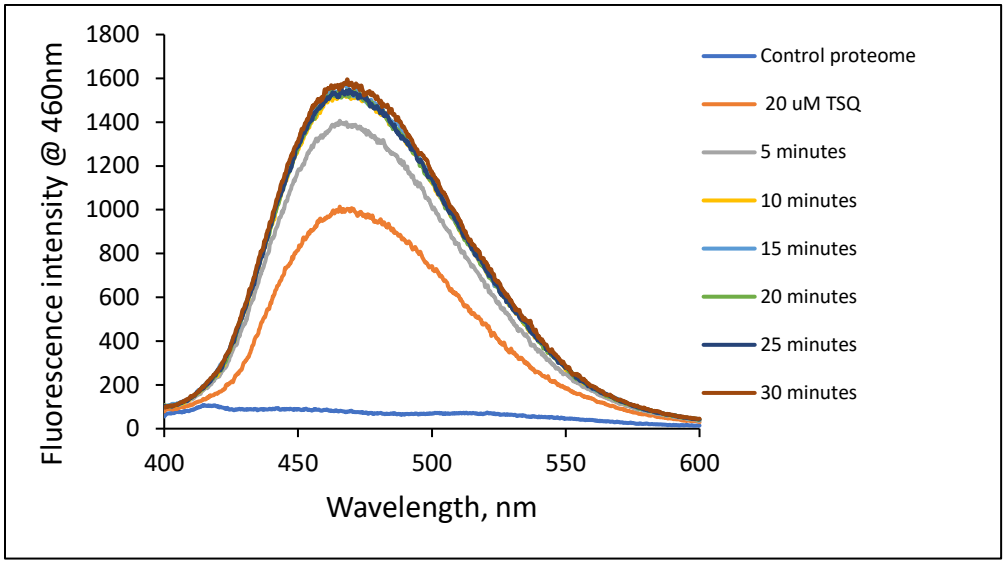
Fluorescence intensity @ 460nm
1800
1600
1400
1200
1000
800
600
400
200
0
400
450
500
550
600
Wavelength, nm
Control proteome
20 uM TSQ
5 minutes
10 minutes
15 minutes
20 minutes
25 minutes
30 minutes

B.

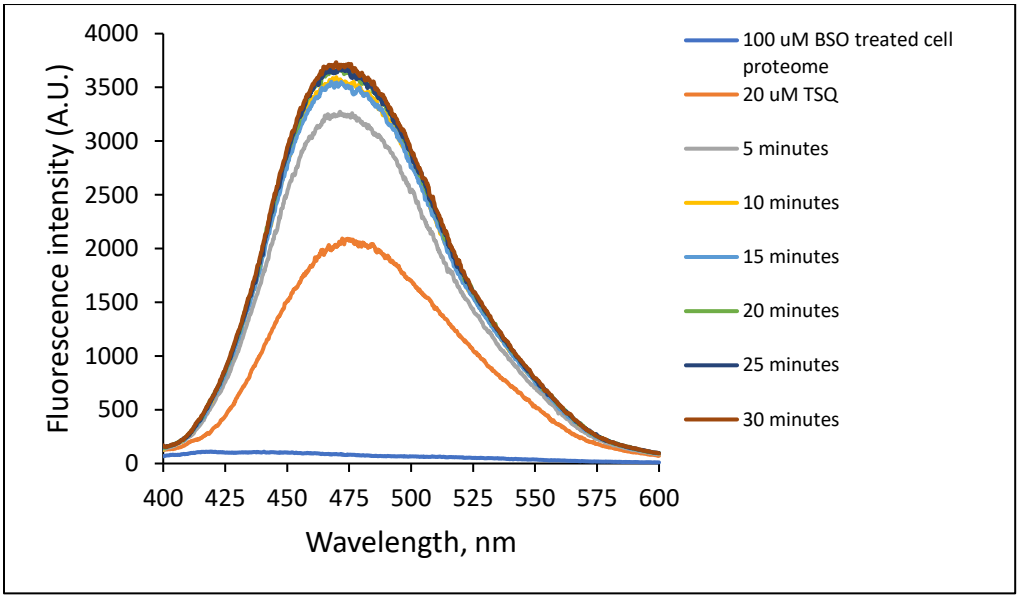
Fluorescence intensity (A.U.)
4000
3500
3000
2500
2000
1500
1000
500
0
400
425
450
475
500
525
550
575
600
Wavelength, nm
100 uM BSO treated cell proteome
20 uM TSQ
5 minutes
10 minutes
15 minutes
20 minutes
25 minutes
30 minutes

C.

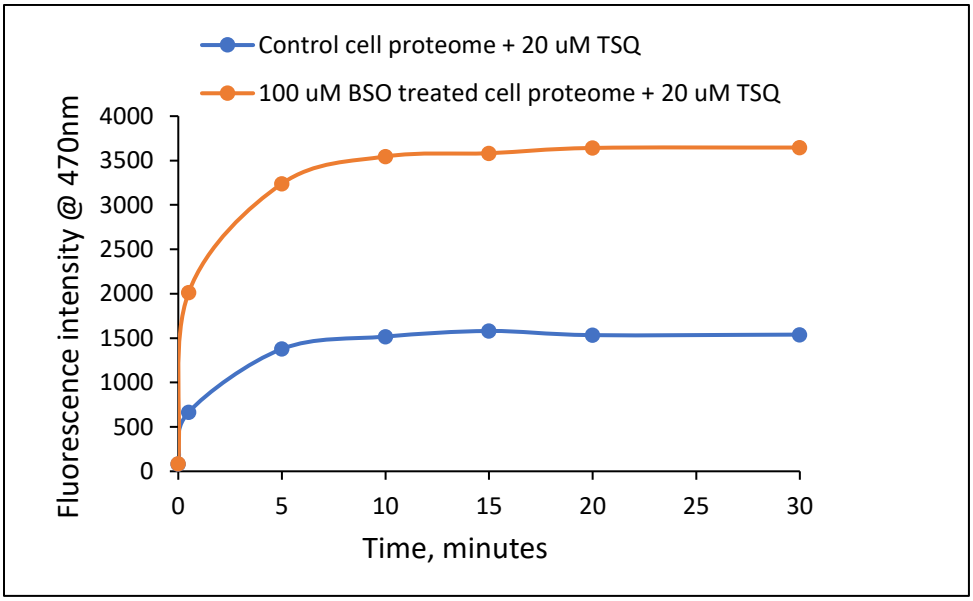

Figure 42. Reaction of TSQ with proteome isolated from BSO-treated cells. (A and B) Isolated proteome from untreated LLC-PK1 cells (A) or treated with 100 µM BSO for 24 hours (B) was reacted with 20 µM TSQ for 30 min. Fluorescence spectra were recorded using excitation wavelength 370 nm and emission wavelength 400 – 600 nm. (C) Change of fluorescence at 470 nm with time for both reactions.

The amount and distribution of zinc in BSO-treated and control cells were determined by Sephadex G-75 chromatography. Over the course of 24 h both sets of cells grew at nearly the same rate, approximately doubling their numbers (1.9x and 1.8x respectively). When the cell supernatant collected from $2x10^8$ LLC-PK_1 cells previously treated with 100 µM BSO was fractionated using Sephadex G-75 chromatography, a significant increase in proteome zinc was observed, as compared with that from same number of control cells (**Figure 43**). This is consistent with the fluorescence enhancement observed in the reaction of TSQ with BSO-treated cells. Overall, BSO-treated cells contained 2.1x of the total zinc measured in control cells. On the basis of the concentration of proteomic Zn in the control cells (58 nmol/10^8 cells), the ratio of Proteome•Zn to Zn-Proteome was 2.3. For comparison, in earlier experiments, 1 µM Zn^{2+} was added to Proteome containing 3-6 µM Zn^{2+}, resulting in a ratio of Proteome•Zn to Zn-Proteome in the range of 0.16 – 0.33. Thus, the cellular experiment has resulted in a concentration of Proteome•Zn that is ca. 10 times that of the *in vitro* experiments.

Only 1.7 nmol/10^7 cells was required for native Zn-protein synthesis during cell proliferation (control cells). Therefore, the BSO-exposed cells had obtained 1.9 nmol/10^7 cells of additional zinc from the extracellular medium in the form of Proteome•Zn. As well, a noticeable pool of metallothionein zinc was present in BSO-treated cells, implying that the inhibition of glutathione synthesis and the consequent increase in intracellular Zn^{2+} has induced the upregulation of metallothionein synthesis. Hypothetically, preventing glutathione synthesis has **upregulated** the cell membrane ZIP transporter that shuttles extra zinc into cytosol causing both the appearance of Zn-MT and the huge increase in Proteome•Zn.

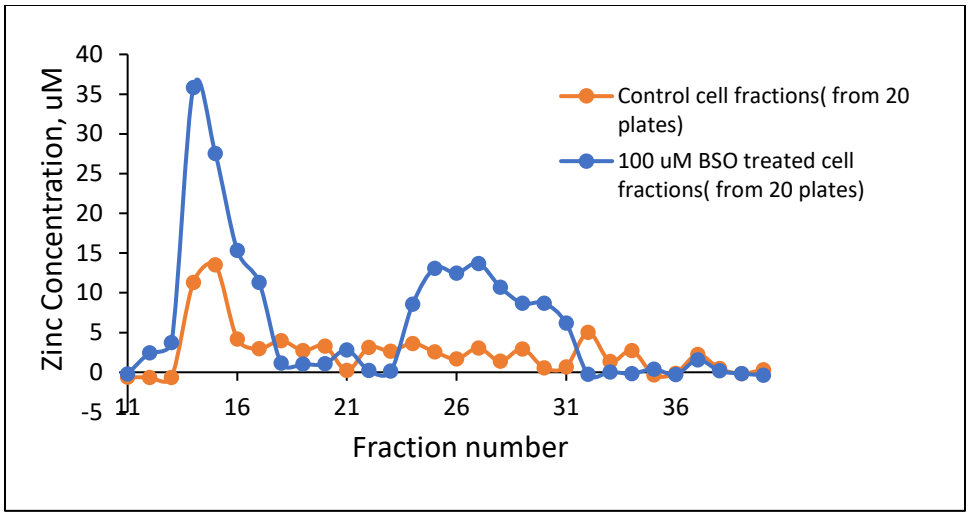

Figure 43. Sephadex G-75 gel filtration chromatography of lysate from BSO-treated cells. $2x10^8$ LLC-PK_1 cells were treated with 100 µM BSO for 24 hours. Cells were then washed, sonicated and centrifuged to collect the lysate, which was then loaded onto a Sephadex G-75 column and eluted with 20 mM degassed Tris buffer, pH 7.4. The collected fractions were analyzed for zinc content using ICP-MS. A control experiment was done with cells without any treatment with BSO.

3.4.5 Effect of BSO on Proteome-mediated reconstitution of Zn-CA

The effect of glutathione depletion by BSO on the reconstitution of Zn-CA from apo-CA was investigated using Proteome•Zn from BSO-treated cells as the source of Zn^{2+}. First, control proteome isolated from untreated LLC-PK_1 cells was reacted with 1 µM apo-CA in the presence of 1.6 µM dansyl amide. Since the control proteome contained only native Zn^{2+} and no added Zn^{2+}, no detectable reconstitution of Zn-CA was observed, as expected. Even in the presence of 1 mM glutathione (GSH), control proteome did not support any reconstitution of Zn-CA, suggesting that no adventitiously bound proteomic zinc is available for glutathione to mediate its transfer to apo-CA and reconstitute Zn-CA.

$$\text{Zn-proteins + apo-CA} \rightarrow \text{No reaction} \quad (81)$$

$$\text{Zn-proteins + apo-CA + GSH} \rightarrow \text{No reaction} \quad (82)$$

In contrast, when the reaction was carried out in presence of proteome collected from BSO-treated cells, a rapid increase of fluorescence at 460 nm was observed, indicating reconstitution of Zn-CA (**Figure 44**). Interestingly, the addition of GSH further enhanced the rate of reconstitution, consistent with experiments with the reactivity of exogenously added proteomic Zn^{2+} with apo-CA.

This result completed the confirmation of our hypothesis that reduction of cellular glutathione level caused adventitious zinc binding to the Proteome that was available for/reactive with the reconstitution of apo-Zn proteins such as apo-CA. According to the results, the loss of GSH content interrupted the steady-state trafficking pathway of Zn^{2+} that is present in cells containing normal, mM concentrations of GSH. Because BSO-treated cells were still competent

to divide and, in the process, acquire their requisite amount of Zn^{2+} for the new synthesis of Zn-proteins from the extracellular medium, we hypothesized that the much elevated concentrations of Proteome•Zn and Zn-MT that exist in these cells become the proximate sources of Zn^{2+} for Zn-Protein constitution (reaction 83):

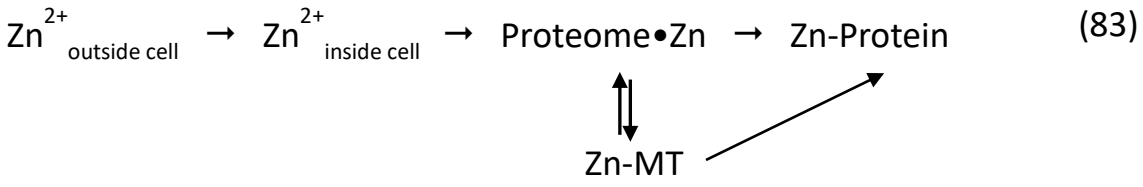

(83)

A.

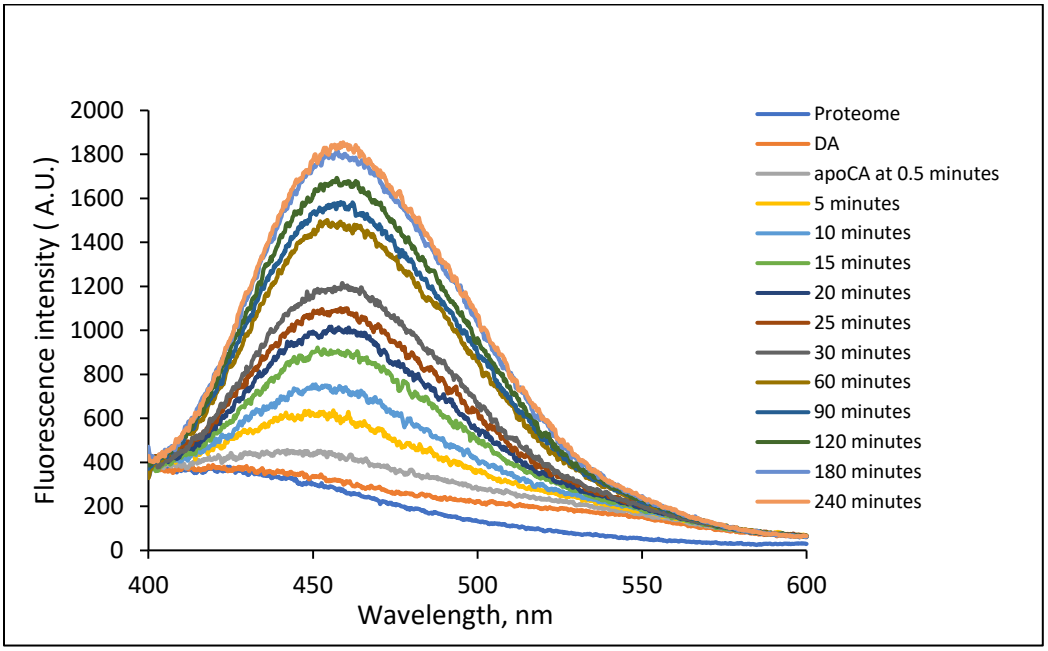
Fluorescence intensity (A.U.)
2000
1800
1600
1400
1200
1000
800
600
400
200
0
400
450
500
550
600
Wavelength, nm
Proteome
DA
apoCA at 0.5 minutes
5 minutes
10 minutes
15 minutes
20 minutes
25 minutes
30 minutes
60 minutes
90 minutes
120 minutes
180 minutes
240 minutes

B.

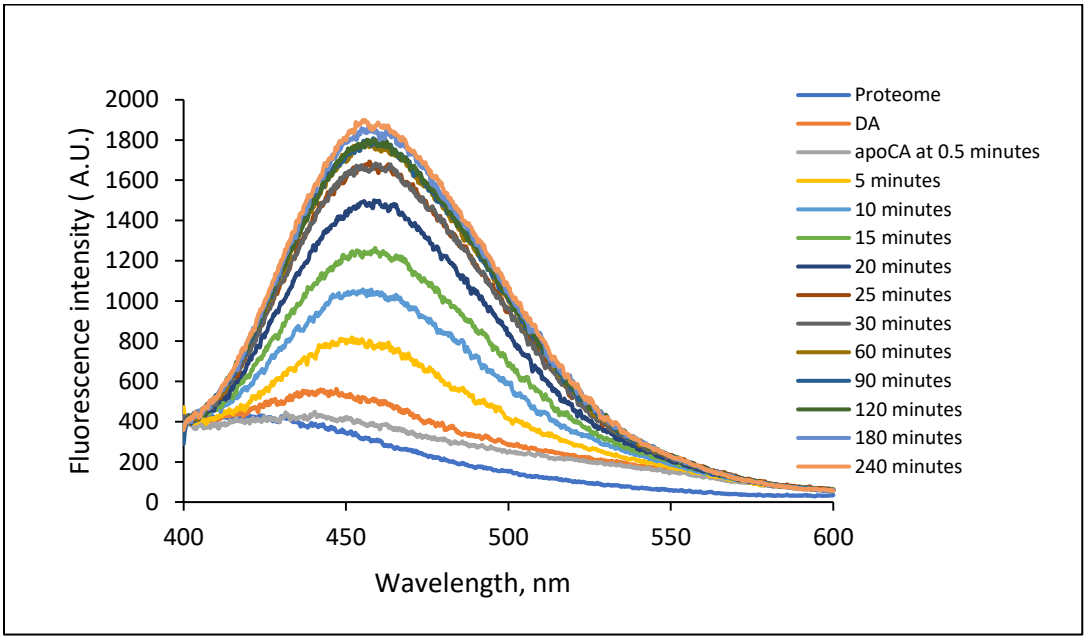
Fluorescence intensity (A.U.)
2000
1800
1600
1400
1200
1000
800
600
400
200
0
400
450
500
550
600
Wavelength, nm
Proteome
DA
apoCA at 0.5 minutes
5 minutes
10 minutes
15 minutes
20 minutes
25 minutes
30 minutes
60 minutes
90 minutes
120 minutes
180 minutes
240 minutes

C.

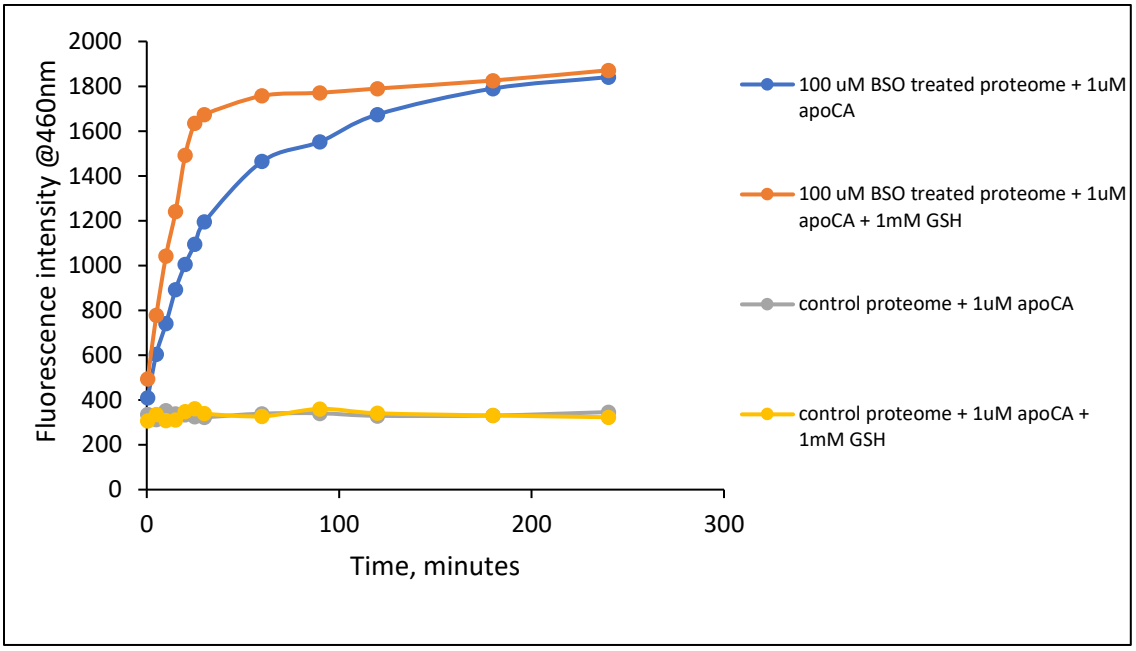

Figure 44. Effect of glutathione inhibition on proteome-mediated Zn-CA reconstitution. (A) Proteome isolated from 100 µM BSO treated cells was reacted with 1 µM apo-CA in the presence of 1.6 µM dansyl amide. Fluorescence spectra were recorded at excitation wavelength 320 nm and emission wavelength 400 – 600 nm. (B) Reaction (A) was repeated in the presence of 1 mM added glutathione. (C) Change of fluorescence at 460 nm for the reactions with control and BSO-treated proteome in absence or presence of 1 mM added glutathione.

4. Discussion

Zinc is the second most abundant transition metal in living organisms [8]. A eukaryotic cell contains 100 – 500 mM zinc [9, 10]. Most of the cellular zinc is bound to thousands of proteins, in which it functions as either a structural or a catalytic cofactor [4, 14-16]. Of the proteins in which zinc acts a structural cofactor, zinc finger transcription factors are common. These zinc binding proteins bind promotor regions of DNA and aid the initiation of DNA transcription. As a catalytic cofactor, zinc constitutes the active site of a number of important enzymes, e.g., carbonic anhydrase, alcohol dehydrogenase, alkaline phosphatase, etc. Apart from structural and catalytic functions, according to various reports, zinc can also act as a secondary messenger and thus has a signaling function [53-57]. Due to these numerous important functions of zinc, its proper balance in cells needs to be maintained. Both deficiency and excess of zinc can cause many biological disorders. Deficiency is related to developmental defects, growth inhibition, loss of immune function. However, despite having critical roles in many biological processes, zinc trafficking and signaling mechanisms are still poorly understood. In general, zinc trafficking refers to the pathway of uptake of zinc into cytosol through the plasma membrane and its subsequent transport to apo-proteins to make native Zn-proteins. Alternately, trafficking refers to the molecular mechanisms by which labile zinc becomes available to act as a signaling chemical in various processes. Some studies have concluded that metallothionein acts a thermodynamic sink for the incoming flux of zinc, which, in turn, transfers zinc to apo-proteins for the generation of native Zn-proteins [15, 31, 37, 38, 45]. However, the evidence of metallothionein role in zinc trafficking remains meager. The fact that zinc trafficking remains intact in MT-null cells demonstrates that metallothionein is not required for functional zinc

trafficking [52]. Therefore, a detailed understanding of cellular chemistry of zinc is needed to understand the cellular zinc trafficking and signaling mechanisms, which encourages researchers to study the interaction of zinc with cellular components.

Maret et al examined the interaction of zinc with cellular proteome in the presence of a colorimetric zinc sensor, Zincon, which displays a red-shift of absorption maximum from 490 nm to 620 nm upon binding zinc (**Figure 6**) [9]. They discovered that the cellular Proteome has a zinc buffering capacity, meaning that proteome has numerous adventitious zinc binding sites that can bind zinc in equilibrium fashion. In their study, a titration of the Proteome with Zn^{2+} in the presence of ZI demonstrated the Proteome's buffering capacity. When extra zinc was added to the Proteome in the presence of ZI, Zn-ZI failed to form in the initial part of the titration as indicated by the initial absence of 620 nm absorbance (**Figure 5**). Beyond the initial zinc buffering region of Proteome, a gradual increase of absorbance was observed with the addition of more zinc (**Figure 5**), which was interpreted by Maret group as the formation of the Zn-ZI complex. However, they did not provide any explanation for the fact the slope of titration curve reflecting the increase of absorbance in presence of Proteome was very different from that in the absence of Proteome (**Figure 5**). We hypothesized that the Proteome contains two kinds of adventitious zinc binding sites relative to Zincon higher affinity and lower affinity zinc binding sites. The high affinity sites relative to Zincon form the buffering region and outcompete Zincon for the added zinc. We hypothesized that, the low affinity binding sites form ternary complexes, Proteome•Zn-ZI, with zinc and Zincon. Therefore, the increase of absorbance following the saturation of Proteome's zinc buffering region was not due to the formation of Zn-ZI complex, but for proteome•Zn-ZI ternary complex.

To test the hypothesis that Proteome's relatively low affinity, non-specific zinc binding sites form ternary complexes with added zinc and Zincon showing the linear increase of absorbance, we repeated the titration experiment done by Maret's research group. As we titrated proteome isolated from LLC-PK_1 cells with extra zinc in the presence of ZI, we observed a similar zinc buffering region, in which no change of ZI absorbance appeared (≤10 μM added zinc), indicating Proteome's relatively high affinity, adventitious zinc binding sites outcompeted Zincon for the initially added zinc (**Figure 7**). Like Maret's research group, we also found a gradual increase of absorbance, as more zinc was added following the saturation of the Proteome's buffering zone, and the slope of the titration curve was significantly different from control titration curve, i.e., titration of ZI with zinc in absence of Proteome. Additionally, the amount of zinc needed to complete the titration in the presence of Proteome was much higher than that for control titration, clearly indicating that there existed a competition between Proteome's relatively low affinity zinc binding sites and ZI for the added zinc. Also, the final absorbance reached after the titration was only about 40% of that observed in the titration of the same concentration of ZI with Zn^{2+} in the absence of Proteome. Most surprisingly, the increase of absorbance beyond the buffering region proteome was accompanied by absorption maximum of 640 nm. Since Zn-ZI complex shows absorbance at 620 nm, the absorption maximum of 640 nm clearly suggested that the absorbing species is not Zn-ZI complex. Interestingly, as the final reaction mixture of titration experiment was filtered using 3K molecular weight cut-off filter, almost all of the absorbance and zinc were located in the retentate fraction (**Figure 8**). Furthermore, the absorption spectra of the retentate fraction was centered at 640 nm, and much of this 640 nm absorbance was abolished when reacted with TPEN, (N,N,N',N'-tetrakis(2-pyridinylmethyl)-1,2-

ethanediamine), a strong zinc chelator. Together, these findings were consistent with the hypothesis that proteome's relatively low affinity zinc binding sites make ternary complexes, proteome•Zn-ZI, with zinc and ZI, characterized by the absorption maximum of 640 nm.

$$\text{Proteome} + Zn^{2+} \leftrightarrows \text{Proteome•Zn} \quad \text{(higher and lower affinity binding buffering region)} \tag{84}$$

$$\text{Proteome•Zn} + \text{ZI} \leftrightarrows \text{Proteome•Zn-ZI} \quad \text{(lower affinity binding sites, 640 nm absorbance)} \tag{85}$$

When the final reaction mixture of titration experiment was reacted with TSQ, the 640 nm absorbance declined (**Figure 9**). A fluorescent sensor, TSQ forms ternary complexes with both native Zn-proteins (TSQ-Zn-proteins) and adventitiously bound zinc to proteome (proteome•Zn-ZI) (ref). Therefore, the decline of 640 nm absorbance following the introduction of TSQ to the reaction mixture, was consistent with the hypothesis that TSQ replaced ZI from proteome•Zn-ZI ternary complex and generated proteome•Zn-TSQ ternary complex.

$$\text{Proteome•Zn-ZI} + \text{TSQ} \leftrightarrows \text{Proteome•Zn-TSQ} + \text{ZI} \tag{86}$$

However, this reaction and, indeed, all of the findings might be consistent with a reaction in which Zn-ZI reacted with the Proteome at sites other than ones that can bind Zn^{2+} through non-specific interactions between ZI and proteomic side chains and backbone.

$$\text{Proteome} + Zn^{2+} + \text{ZI} \leftrightarrows \text{Proteome•ZI-Zn} \tag{87}$$

The details of the reaction of TPEN with the product of the titration help to distinguish the nature of its structure. TPEN binds Zn^{2+} with a conditional stability constant at pH 7.4 that is

about 10 orders of magnitude larger than that of ZI. Yet, according to **Figure 8**, the exchange of Zn^{2+} between ZI and TPEN was not stoichiometric. In fact, a large excess of TPEN was needed to complete the reaction. This result suggested that Zn-ZI was not bound to Proteome, primarily as a Proteome•ZI adduct which would likely leave Zn^{2+} in ZI-Zn sterically open for reaction with TPEN:

$$\text{Proteome•ZI-Zn + TPEN} \leftrightarrows \text{Zn-TPEN + Proteome + ZI} \quad (88)$$

Instead, in a ternary complex mediated by Zn^{2+}, Proteome•Zn-ZI, the zinc ion may be sterically buried and kinetically hindered in its reaction with TPEN:

$$\text{Proteome•Zn-ZI + TPEN} \leftrightarrows \text{Zn-TPEN + Proteome + ZI} \quad (89)$$

We considered the possibility that the appearance of the 640 nm absorbance spectral maximum during the titration of ZI with zinc in the presence of Proteome was due to the nature of proteomic environment in which Zn-ZI was located, but not because of ternary complex formation. **Figure 13** shows the spectra of Zn-ZI in a range of solvents with different dielectric constants**.** Although solvents markedly perturbed the spectrum of Zn-ZI, none of them resembled the simple red-shift seen in the reaction with Proteome (**Figure 13**). This finding further strengthened the hypothesis that ZI forms ternary complex, proteome•Zn-ZI, with zinc bound to relatively lower affinity adventitious sites of proteome.

Pre-treatment of proteome with N-ethylmaleimide (NEM), a sulfhydryl binding reagent, significantly reduced its high affinity, zinc buffering capacity (**Figure 14**). A similar finding was made in studies that employed the fluorescent zinc probe, Newport Green [85]. This

experiment demonstrated that proteomic sulfhydryl groups are centrally involved in generating its high affinity, zinc buffering capacity.

$$\text{Proteome-(SH)}_n + Zn^{2+} \leftrightarrows \text{Proteome-S}_n\bullet Zn + nH^+ \quad (90)$$

Presumably, when bound to these sites, Zn^{2+} is coordinated with thiolate and perhaps some other ligands such that it is unavailable to form ternary complexes with ZI.

Having shown that the Proteome has many relatively lower affinity, non-specific zinc binding sites that can form ternary complexes with added zinc and Zincon, we used bovine serum albumin (BSA) as a model protein that binds Zn^{2+} with a moderate stability constant at pH 7.4 and whether ZI reacts with BSA and Zn^{2+} similarly to its reaction with Proteome and Zn^{2+}. BSA has been reported to contain a number potential zinc binding sites including a primary one that in involved in the transport of plasma Zn^{2+}, and therefore, we hypothesized that BSA will form ternary complex with ZI and added zinc via its potential zinc binding sites [100]. As anticipated, titration of ZI with zinc in the presence of BSA resulted in the increase of absorbance with an absorption maximum of 640 nm. In addition, as the final reaction mixture was filtered using a 3K molecular weight cut-off filter, most of the 640 nm absorbance and zinc were located in the retentate fraction (**Figure 10**). Taken together, these results indicated that like proteome, the model protein, BSA, formed ternary complexes with added zinc and ZI.

To summarize the findings from Zincon study, Proteome has many adventitious zinc binding sites that are implicated in binding more zinc than needed for native Zn-proteins synthesis, primarily via sulfhydryl groups. Relative to the zinc binding affinity of Zincon, these proteomic adventitious zinc binding sites can be classified into two groups higher affinity and lower affinity

sites. The higher affinity proteomic sites, which contain sulfhydryl ligands, outcompete Zincon for the added zinc, while the low affinity sites form ternary complexes, Proteome-S•Zn-ZI.

The zinc binding constants of native Zn-proteins have been reported in the range of $10^9 – 10^{12}$ M^{-1}, while Proteome's high affinity, non-specific zinc binding constants were calculated to be on the order of 10^{10} M^{-1} [11, 12]. The presence of such high affinity, non-specific sites for Zn^{2+} in the cell suggests that free Zn^{2+} concentration must be very small and probably not significant in mechanisms of cellular zinc trafficking. Therefore, we hypothesized that these high affinity, adventitious zinc binding sites of Proteome play a critical role in the intracellular trafficking of zinc and zinc signaling. Namely, following transport of zinc across the plasma membrane, zinc first binds to various adventitious sites within the Proteome and then is transferred to the various apo-zinc proteins to generate native Zn-proteins. Thus, Proteome acts as an intermediate in cellular zinc trafficking and signaling.

$$\text{Proteome-SH} + Zn^{2+} \leftrightarrows \text{Proteome-S•Zn} + H^{+} \quad (91)$$

$$\text{Proteome-S•Zn} + \text{apo-Proteins} \leftrightarrows \text{Proteome-SH} + \text{Zn-Proteins} \quad (92)$$

To test the hypothesis, LLC-PK_1 cells were treated with excess zinc and the distribution of excess zinc among the cellular components was examined. The result of the experiment showed that only 1% of the added zinc made its way into cytosol, of which 73% was captured by the induced metallothionein, Zn_7-MT and 26% was bound to high molecular weight Proteome (**Figure 15**). When the Proteome isolated from these cells was reacted with zinc fluorescent sensor, TSQ, a rapid enhancement of fluorescence centered at 470 nm was detected (**Figure 17).** This indicated that the excess zinc is adventitiously associated with proteome, denoted as

Proteome•Zn**.** As reported, TSQ reacts slowly with 15-20% native Zn-Proteins to form ternary complex, TSQ-Zn-Proteins, with slow increase of 470 nm fluorescence [76-78]. In contrast, TSQ exhibits a rapid increase of fluorescence with the same emission maximum when it reacts with zinc adventitiously bound to the Proteome, Proteome•Zn (reaction 93).

$$\text{Proteome•Zn} + \text{TSQ} \leftrightarrows \text{Proteome•Zn-TSQ} \qquad (93)$$

Another possibility of the form of extra zinc associated with Proteome was the ternary complex, Proteome-S-Zn_7-MT, between proteome and Zn_7-MT. However, since Zn_7-MT does not display any reactivity with TSQ, the above-mentioned TSQ reaction that produced rapid fluorescence enhancement at 470 nm ruled out this possibility. Together, these results supported our hypothesis that following cellular uptake, zinc binds to various adventitious sites of Proteome as Proteome•Zn, as well as to the induced metallothionein, Zn_7-MT.

Next, we examined if Proteome-bound zinc can be transferred to precursor apo-proteins to make native Zn-Proteins. For this study, we chose Zn-carbonic anhydrase (Zn-CA) as a model Zn-protein because of its known structure (**Figure 18**), zinc stability constant ($10^{11.4}$ at pH 7) and availability, and probed if Proteome can transfer its non-specifically bound zinc to apo-carbonic anhydrase (apo-CA) and regenerate Zn-CA (Reaction 33) [29]. As a marker of Zn-CA reconstitution, we employed dansyl amide (DA), which shows no reactivity with either free zinc or apo-CA, but makes a ternary complex with Zn-CA and exhibits fluorescence enhancement, along with a blue shift from 540 nm to 460 nm (Reaction 94) [93].

$$\text{Zn-CA} + \text{DA} \leftrightarrows \text{DA-Zn-CA} \qquad (94)$$

The reconstitution of Zn-CA from the reaction of apo-CA and free zinc was found to be relatively fast (**Figure 19**). A stoichiometric reaction between apo-CA and free zinc was completed in 5 – 10 minutes.

Proteome-mediated reconstitution of Zn-CA was tested by reacting pre-formed Proteome•Zn and apo-CA under conditions in which Zn^{2+} was bound only to high affinity proteomic sites. The gradual increase of 460 nm fluorescence indicated that zinc was transferred from proteome to apo-CA and, thus, that Zn-CA was reconstituted (**Figure 22**). However, the rate of Proteome-mediated Zn-CA reconstitution was slow. While in the absence of Proteome, 100% reconstitution occurred in few minutes, it required several hours only for 50% reconstitution to happen in presence of Proteome (**Figure 22**). Clearly, binding of zinc to Proteome slowed down the rate of reaction. This was attributed to two factors: first Zn^{2+} was firmly bound with ligands other than water that had to be exchanged with the imidazole ligands of apo-CA during the reaction. Second, the proteomic zinc binding sites presented significant steric hindrance to apo-CA during it reaction with Proteome•Zn. The latter factor would be significant if the overall reaction were second order, first order in Proteome•Zn and first order in apo-CA. Higher Proteome concentration at constant Zn^{2+} concentration further slowed down the kinetics of the reaction (**Figure 23**), which was understandable, because increased Proteome concentration presented a higher number of high affinity adventitious zinc binding sites and, as a consequence, made zinc less available for apo-CA. By contrast, pre-incubation of proteome with N-ethylmaleimide (NEM), a sulfhydryl binding reagent, caused a large increase in rate of proteome-mediated Zn-CA reconstitution (**Figure 24**), further confirming that high affinity, proteomic sites primarily bind zinc via sulfhydryl groups. As a result of blocking of sulfhydryl

groups, zinc probably became bound to weaker ligands, e.g., imidazole and carboxylate groups, favoring the formation of Zn-CA.

In order to further understand the possible cause of slow and incomplete reconstitution of Zn-CA by Zn^{2+} in presence of the Proteome, we considered the possibility that perhaps under native, cellular condition, zinc binds to unfolded apo-$CA_{Denatured}$ (apo-CA_D) to generate folded, native Zn-CA. For our *in-vitro* experiments, apo-CA_{Native} (apo-CA_N) was used in the absence of denaturants. It adopts the folded structure of Zn-CA (ref). As such, apo-CA_D may be more favorable thermodynamically for the reconstitution of Zn-CA if folding is coupled to zinc binding:

$$\text{apo-CA}_D \leftrightarrows \text{apo-CA}_N \quad \text{(energetically favorable)} \tag{95}$$

$$\text{apo-CA}_N + Zn^{2+} \leftrightarrows \text{Zn-CA}_N \quad \text{(energetically favorable)} \tag{96}$$

$$\text{apo-CA}_D + Zn^{2+} \leftrightarrows \text{Zn-CA}_N \tag{97}$$

Similarly, the pre-folded apo-CA may also add a steric factor to the reconstitution process that slows down the kinetics of the reaction. That is, since apo-CA_N adopts the native conformation of Zn-CA, the ligand binding site for Zn^{2+} is also pre-formed and inflexible. Considering the multiple, intermediate ligand substitution steps that must be involved during the complex ligand substitution of three imidazole ligands from apo-CA_N for several ligands that bind Zn^{2+} in Proteome•Zn. However, when the proteome-assisted Zn-CA regeneration was conducted with denatured, unfolded apo-CA, the rate of the reaction was, in fact, even slower than that with pre-folded apo-CA (**Figure 28**). Also, the extent of Zn-CA reformation from denatured apo-CA

was only 50% of native apo-CA. We were unclear as to how to interpret these results without further experimentation and decided to focus on the reactions with apo-CA_N.

The basic reaction was repeated with systemic variation in Proteome concentration. As seen in **Figure 23**, increasing the Proteome concentration decreased the extent of reaction of Proteome•Zn with apo-CA. Using the overall reaction,

$$\text{Proteome•Zn + apo-CA} \leftrightarrows \text{Zn-CA + Proteome} \qquad (K_{eq}) \qquad (98)$$

the conditional log stability constant at pH 7.4 of Zn-CA (11.4), and the total concentrations of high affinity binding sites for Zn^{2+} within the Proteome (1.5x the concentration of Zn-proteins), we first calculated K_{eq} for each reaction and then secondarily $K_{Proteome•Zn}$ from the equation, $K_{eq} = K_{Zn\text{-}CA}/K_{Proteome•Zn}$. A value of 10.5 ± 0.3 was obtained, which is in good agreement with the value of 10.2 obtained from a previous study (unpublished data).

Next, we investigated the kinetics of the reaction. A pseudo-first order rate study was done using large excess of apo-CA relative of Proteome•Zn, According to **Figure 29**, the rate of Proteome-mediated Zn-CA reformation reaction was calculated to be strictly second order, indicating that the reaction is a straight-forward ligand substitution between Proteome•Zn and apo-CA, with no first-order rate limiting step, such as dissociation of Zn^{2+} from proteomic sites. The bimolecular character of the reaction supports the view that the slow and partial reconstitution of Zn-CA in the presence of Proteome•Zn results from the large steric hindrance that occurs when two macromolecules must get into proper steric proximity to exchange ligands.

Having observed the slow and incomplete Proteome-assisted reformation of Zn-CA, we hypothesized that besides high molecular weight proteome, other cellular components, such as metallothionein (Zn_7-MT) and glutathione (GSH), etc. are involved in Proteome-mediated zinc trafficking to make native Zn-Proteins. When fully saturated, each metallothionein molecule has seven zinc ions bound to two thiolate clusters with stability constants of $10^{10\text{-}11}$ [37, 38]. By contrast, glutathione does not have large binding constant, but it exists in cells at relatively high concentrations [85]. Due to these facts, it was hypothesized that their involvement in cellular zinc trafficking possibly makes the formation of Zn-Proteins mediated by proteome kinetically faster. To examine this hypothesis, the impact of metallothionein and glutathione on the kinetics of Proteome-mediated Zn-CA regeneration was studied.

As was observed in Proteome-mediated reaction, the transfer of zinc from Zn_7-MT to apo-CA was slow (**Figure 32**). Interestingly, the presence of Proteome further slowed down the reaction between Zn_7-MT and apo-CA (**Figure 32**). The reaction with denatured apo-CA produced similar slow reconstitution. A zinc transfer equilibrium (Reaction 60) or ternary adduct formation (Reaction 62) between Proteome via its sulfhydryl ligands and Zn_7-MT might account for the slow reaction of apo-CA and Zn_7-MT in the presence of Proteome. To examine the putative equilibrium between Proteomic sulfhydryl ligands and Zn_7-MT, the reaction of apo-CA and Zn_7-MT was repeated in the presence Proteome which was pre-treated with N-ethylmaleimide (NEM). Pre-treatment of Proteome with NEM resulted in a dramatic increase in the rate of Zn-CA reconstitution (**Figure 33**), confirming the interaction between Proteomic thiolate ligands and Zn_7-MT, that might explain their negative effect on the reaction rate. To further probe the equilibrium, Proteome and Zn_7-MT were incubated and the re-distribution of zinc was

quantified. Following incubation, a significant transfer of zinc from metallothionein to Proteome was observed (**Figure 34** and **Table 1**). When the Proteome fraction was separated from the metallothionein fraction using a 10K molecular weight cut-off filter and subsequently reacted with TSQ, a rapid fluorescence enhancement at 470 nm was exhibited, confirming that excess zinc associated with Proteome and transferred from Zn_7-MT was adventitiously bound as Proteome-S•Zn, but not in the form of ternary adduct, Proteome-S•Zn_7-MT, because TSQ does not show any reactivity with metallothionein-bound zinc. These results clearly indicated that metallothionein potentially plays an important role in zinc trafficking and in the synthesis of native Zn-proteins by transferring its bound zinc to pre-cursor apo-Proteins via the formation of Proteome•Zn.

Next, we investigated if glutathione has any impact on proteome- and/or metallothionein-mediated Zn-CA reformation, and if it plays a central role in cellular zinc trafficking. As mentioned earlier, glutathione has a moderate zinc binding affinity with stability constant of 10^{4-5} [85]. However, cells maintain a relatively high concentration of glutathione, namely 1 – 10 mM, under basal condition, that primarily acts as an anti-oxidant via its thiol group and thus protects cells from damage caused by reactive oxygen species and reactive metabolites of xenobiotics [104 - 106].

The presence of 1 mM glutathione (GSH) slowed down the reaction of apo-CA and Zn^{2+} to regenerate Zn-CA, implying that glutathione mediated the transfer of zinc to apo-CA (Reactions 65 and 66). Surprisingly, glutathione caused an increase of the Proteome-mediated Zn-CA reconstitution rate (**Figure 36**). Apparently, an equilibrium had been established between Proteome-S•Zn and GSH, which resulted the generation of GS-Zn (Reactions 69-70). Finally, zinc

from GS-Zn was transferred to apo-CA in a faster rate, instead of a slow transfer from Proteome-S•Zn (Reaction 71). In addition, when the low molecular weight (LMW) fraction isolated from the cell lysate of LLC-PK_1 cells under basal condition was added to the high molecular weight (HMW) Proteome fraction of the same lysate, a dramatic enhancement of Zn-CA reconstitution, relative to that in the presence of HMW fraction only, was observed (**Figure 37**). This result further confirmed that glutathione, present in the LMW fraction, caused the rate enhancement of Proteome-mediated Zn-CA regeneration. A similar rate enhancement was exhibited when 1 mM exogenous glutathione was added to the same HMW Proteome fraction (**Figure 37**). These results further supported the role of glutathione in Proteome-mediated Zn-CA reformation.

Glutathione facilitated metallothionein-mediated Zn-CA reconstitution (**Figure 38**), suggesting the formation of an intermediate, GS-Zn_7-MT, (Reaction 77-79) that may have increased the rate of transfer of zinc from Zn_7-MT to apo-CA. Glutathione further enhanced the kinetics of Zn-CA regeneration when both Proteome and Zn_7-MT were present in the reaction (**Figure 38**). The greater rate enhancement implied that glutathione prevented adduct formation between Zn_7-MT and Proteome, and instead, formed a complex, GS-Zn_7-MT, that eventually transferred zinc to apo-CA at a faster rate. The formation of GS-Zn_7-MT, resulting from the association of GSH with one of the crevices in the α-domain of Zn_7-MT has been reported in a previous study [107].

Having shown that glutathione has a significant impact on *in vitro* zinc trafficking in the presence of Proteome and/or metallothionein, we then studied the effect of inhibition of cellular glutathione synthesis on zinc trafficking *in vivo*. To inhibit glutathione synthesis, LLC-PK_1 cells were treated with buthionine sulfoximine (BSO), a small molecule that inhibits the

necessary enzyme, gamma-glutamylcysteine synthetase, from catalyzing the first step of cellular glutathione synthesis and thereby diminishes the cellular level of glutathione [108]. Treatment of LLC-PK_1 cells with 100 µM BSO for 24 hours did not affect the proteomic sulfhydryl content, but almost completely abolished the low molecular weight sulfhydryl content, including glutathione while having only a marginal impact on cell viability.

When BSO-treated cells were reacted with TSQ, a rapid increase of 470-475 nm fluorescence was observed, as opposed to untreated cells, which exhibited a much slower and smaller increase of 470-475 nm fluorescence (**Figure 41**). TSQ has been reported to generate ternary adducts, TSQ-Zn-Proteins, with native Zn-Proteins accompanied by a slow increase of 470-475 nm fluorescence [76-78]. It forms ternary complexes, Proteome•Zn-TSQ with non-specifically bound proteomic zinc, Proteome•Zn, but with a rapid increase of fluorescence at 470-475 nm [33]. Therefore, the experiment with BSO-treated cells indicated that the treatment caused a greater accumulation of cellular zinc adventitiously bound to Proteome as Proteome•Zn, which would have otherwise remained bound to cellular glutathione under basal conditions. The apparent accumulation of Proteome•Zn following inhibition of glutathione synthesis implied that under basal condition, a significant fraction of cellular labile zinc is bound by glutathione, which mediates steady state zinc trafficking by transferring its bound zinc to pre-cursor apo-Proteins to generate native Zn-Proteins. When GSH was depleted, much larger concentrations of labile Zn^{2+} accumulated in the Proteome as Proteome•Zn and some Zn-MT (**Figure 43**). These larger concentrations were then hypothesized to become kinetically and thermodynamically competent to supply Zn^{2+} for the constitution of Zn-proteins from apo-protein precursors.

Similar fluorescence enhancement was observed when Proteome isolated from BSO-treated cells was reacted with TSQ, relative to control Proteome (**Figure 42**). This experiment further supported the conclusion that non-specifically bound proteomic zinc, Proteome•Zn had been generated following glutathione inhibition. That cells proliferated normally even after inhibition of glutathione synthesis indicated that the accumulated Proteome•Zn served as one of the major sources of zinc for the synthesis of native Zn-Proteins.

As determined by Sephadex G-75 chromatography, Proteome collected from BSO-treated cells contained a much larger zinc content, compared with non-treated control cell Proteome, supporting the results of the TSQ reactions with cells and isolated Proteome. In total, BSO-treated cells contained as much as 2.1 times of zinc content of the same number of untreated cells. Along with the increase in proteomic zinc, BSO treatment induced a sizeable pool of metallothionein zinc as well, inferring that the increase of cellular zinc following glutathione synthesis inhibition, apparently, upregulated metallothionein expression. Seemingly, preventing glutathione synthesis caused an upregulation of cellular ZIP transporter activity that in turn resulted in a greater uptake of extracellular zinc, leading to induced metallothionein synthesis and the increase of proteomic zinc as Proteome•Zn.

As expected, the reaction of apo-CA with Proteome isolated from BSO-treated cells resulted in a dramatic increase in rate and extent of Zn-CA reconstitution, relative to control cell Proteome (**Figure 44**), confirming the presence of the much higher zinc content associated with BSO-treated Proteome as in the form of Proteome•Zn. The addition of 1 mM glutathione to BSO-

treated Proteome did not change the extent of the reaction, which had gone to completion, but further enhanced the rate of reaction significantly (**Figure 45**).

This experiment further supported our hypothesis that glutathione plays a crucial role in cellular zinc trafficking to produce native Zn-Proteins. However, the fact that cells survived and proliferated normally in the face of a greatly reduced concentration of cellular glutathione indicated that the increased amount of non-specifically bound proteomic zinc as Proteome•Zn and metallothionein zinc (Zn_7-MT) could also serve as primary sources of zinc to make native Zn-Proteins and satisfy the need of proliferative cells for Zn-Proteins.

In summary, according to the experiments described in this thesis, the mechanism of cellular zinc trafficking leading to the formation of native Zn-Proteins does not involve the straight-forward transfer of zinc from one particular cellular component or chaperone to apo-Proteins. Instead, trafficking occurs through a complex interconnected pathway that primarily includes proteomic non-specific zinc binding sites, metallothionein and glutathione, and thus can be depicted by the following schematic diagram.

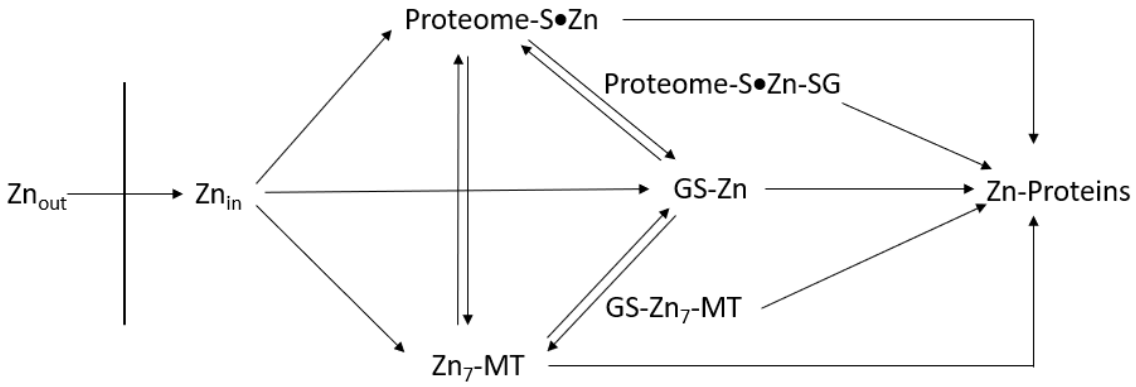

5. REFERENCES

[1] Que, E. L., Domaille, D. W., and Chang, C. J. (2008) Metals in neurobiology: probing their chemistry and biology with molecular imaging, Chemical Reviews 108, 1517-1549.

[2] Carter, K. P., Young, A. M., and Palmer, A. E. (2014) Fluorescent sensors for measuring metal ions in living systems, Chemical reviews 114, 4564-4601.

[3] Bertini, I.; Sigel, A.; Sigel, H. Handbook on Metalloproteins; Marcel Dekker: New York, 2001; pp 1-1800.

[4] Andreini, C., Banci, L., Bertini, I., and Rosato, A. (2006) Counting the zinc-proteins encoded in the human genome, Journal of proteome research 5, 196-201.

[5] Changela, A.; Chen, K.; Xue, Y.; Holshen, J.; Outten, C. E.; O'Halloran, T. V.; Mondragon, A. Science (2003), Molecular basis of metal-ion selectivity and zeptomolar sensitivity by CueR, Science, 301, 1383-1387.

[6] Finney, L. A.; O'Halloran, T. V. Science (2003) Transition metal speciation in the cell: insights from the chemistry of metal ion receptors, Science, 300, 931-936.

[7] Bertinato, J.; L'Abbe, M. R. J. Biol. Chem. (2003) Copper modulates the degradation of copper chaperone for Cu,Zn superoxide dismutase by the 26 S proteosome , Journal of biological chemistry, 278, 35071-35078.

[8] Outten, C. E., and O'Halloran, T. V. (2001) Femtomolar sensitivity of metalloregulatory proteins controlling zinc homeostasis, Science 292, 2488-2492.

[9] Krężel, A., and Maret, W. (2006) Zinc-buffering capacity of a eukaryotic cell at physiological pZn, Journal of Biological Inorganic Chemistry 11, 1049-1062.

[10] Eide, D. J. (2006) Zinc transporters and the cellular trafficking of zinc, Biochimica et Biophysica Acta (BBA)-Molecular Cell Research 1763, 711-722.

[11] Maret, W. and Li, Y. Coordination dynamics of zinc in proteins. Chem. Rev. 2009, 109, 4682–4707.

[12] Kochanczyk, T., Drozd, A. and Krezel, A. Relationship between the architecture of zinc coordination and zinc binding affinity in proteins—Insights into zinc regulation. Metallomics2015,7,244–257.

[13] Vinkenborg, J. L., Nicolson, T. J., Bellomo, E. A., Koay, M. S., Rutter, G. A., and Merkx, M. (2009) Genetically encoded FRET sensors to monitor intracellular Zn2+ homeostasis, Nature methods 6, 737-740.

[14] Andreini, C., Banci, L., Bertini, I. and Rosato, A. (2006) Zinc through the three domains of life, Journal of proteome research 5, 3173.

[15] Maret, W. and Li, Y. (2009) Coordination dynamics of zinc in proteins, Chemical reviews 109, 4682–4707.

[16] Sousa, S. F., Lopes, A. B., Fernandes, P. A. and Ramos, M. J. (2009), The Zinc proteome: a tale of stability and functionality, Dalton Transactions 14, 7946.

[17] Andreini, C., Bertini, I. and Rosato, A. (2009), Metalloproteomes: A Bioinformatic Approach, Account of chemical research 42, 1471.

[18] Christianson, D. W. and Cox, J. D. (1999) Catalysis by metal-activated hydroxide in zinc and manganese metalloenzymes, Annual review of Biochemistry 68, 33-57.

[19] McCall, K. A., Huang, C. C. and Fierke, C. A. (2000) Function and mechanism of zinc metalloenzymes, Journal of nutrition 130, 1437S-46S.

[20] Masuoka, J., Hegenauer, J., Van Dyke, B.R. and Saltman, P. (1993) Intrinsic stoichiometric equilibrium constants for the binding of zinc(II) and copper(II) to the high affinity site of serum albumin, Journal of biological Chemistry 268, 21533.

[21] Jeong, J. and Eide, D. J. (2013) The SLC39 family of zinc transporters, Molecular aspects of medicine 34, 612.

[22] Fukada T. and Kambe, T. (2011) Molecular and genetic features of zinc transporters in physiology and pathogenesis, Metallomics 3, 662.

[23] Huang, L. and Tepaamorndech, S. (2013) The SLC30 family of zinc transporters - a review of current understanding of their biological and pathophysiological roles, Mol. Asp. Med. 34, 548.

[24] Bin, B. H., Fukada, T.,Hosaka, T., Yamasaki, S., Ohashi, W.,Hojyo, S.,Miyai, T.,Nishida, K., Yokoyama, S. and Hirano, T. (2011) Biochemical characterization of human ZIP13 protein: a homo-dimerized zinc transporter involved in the spondylocheiro dysplastic Ehlers-Danlos syndrome, Journal of biological Chemistry 286, 40255.

[25] Lu, M. and Fu, D. (2007), Bifunctional Magnetic Silica Nanoparticles for Highly Efficient Human Stem Cell Labeling, Science 317, 1746.

[26] Liu, M., Chai, J. and Fu, D. (2009) Structural basis for autoregulation of the zinc transporter YiiP, Nature Structural and Molecular Biology 16, 1063.

[27] Ohana, E., Hoch, E., Keasar, C., Kambe, T., Yifrach, O., Hershfinkel, M. and Sekler, I.(2009) Identification of the Zn2+ binding site and mode of operation of a mammalian Zn^{2+} transporter, Journal of biological Chemistry 284, 17677.

[28] Nevitt, T., Ohrvik, H. and Thiele, D.J. (2012) Charting the travels of copper in eukaryotes from yeast to mammals, Biochimica et Biophysica Acta 1823, 1580–1593.

[29] Nowakowski, A., Karim, M., Petering, D. (2015) Zinc proteomics, In Encyclopedia of Inorganic and Bioinorganic Chemistry; Scott, 1-10.

[30] Colvin, R.A., Holmes, W. R., Fontaine, C.P. and Maret, W. (2010) Cytosolic zinc buffering and muffling: their role in intracellular zinc homeostasis, Metallomics 2, 306-17.

[31] Mahim, A. and Petering, D. (2017) Proteomic high affinity zinc trafficking: Where does metallothionein fit in?, International Journal of Molecular Sciences 18, 1289.

[32] Petering, D.H.; Kothinti, R.; Meeusen, J.; Rana, U. (2010) Cellular inorganic chemistry concepts and examples. In Cellular and Molecular Biology of Metals; Zalups, R.K., Koropatnick, J., Eds.; CRC Press, Taylor and Francis Group: Boca Raton, FL, USA Chapter 1, 1–35.

[33] Karim, M.R. and Petering, D.H. (2016) Detection of Zn^{2+} release in nitric oxide treated cells and proteome: Dependence on fluorescent sensor and proteomic sulfhydryl groups. Metallomics 9, 391–401.

[34] Robbins, A.H., McRee, D.E., Williamson, M., Collett, S.A., Xuong, N.H., Furey, W.F., Wang, B.C., Stout, C.D. (1991) Refined crystal structure of Cd, Zn metallothionein at 2.0 A resolution, Journal of molecular biology 221, 1269–1293.

[35] Petering, D.H., Krezoski, S., Tabatabai, N.M. (2009) Metallothionein toxicology: Metal ion trafficking and Cellular protection. In Metallothioneins and Related Chelators: Metal Ions in Life Sciences; Sigel, A., Sigel, H., Sigel, R.O., Eds.; RSC Publishing: Cambridge Volume 5, 353–397.

[36] Otvos, J. D. and Armitage, I. M. (1980) Structure of the metal clusters in rabbit liver metallothionein, Proceedings of the national academy of sciences of United States of America 77, 7094.

[37] Namdarghanbari, M.A., Meeusen, J., Bachowski, G., Giebel, N., Johnson, J. and D. H. Petering (2010) Reaction of the zinc sensor FluoZin-3 with Zn(7)-metallothionein: Inquiry into the existence of a proposed weak binding site, Journal of inorganic biochemistry 104, 224.

[38] Pinter, T.B. and Stillman, M.J. (2014) The zinc balance: competitive zinc metalation of carbonic anhydrase and metallothionein 1A, Biochemistry 53, 6276.

[39] Petering, D. H., Zhu, J., Krezoski, S., Meeusen, J., Kiekenbush, C., Krull, S., Specher, T. and Dughish, M. (2006) Apo-metallothionein emerging as a major player in the cellular activities of metallothionein, Experimental biology and medicine (Maywood) 231, 1528.

[40] Yang, Y., Maret, W. and Vallee, B. L. (2001) Differential fluorescence labeling of cysteinyl clusters uncovers high tissue levels of thionein, Proceedings of the national academy of sciences of United States of America 98, 5556.

[41] Oh, S.H., Deagen, J.T., Whanger, P.D. and Weswig, P.H. (1978) Biological Function of Metallothionein. V. Its induction in rats by various stresses. Am. J. Physiol. 234, E282–E285.

[42] Petering, D.H., Loftsgaarden, J., Schneider, J., Fowler, B. (1984) Metabolism of cadmium, zinc and copper in the rat kidney: The role of metallothionein and other binding sites, Environmental health perspectives 54, 73–81.

[43] Andrews, G. K., Lee, D. K., Ravindra, R., Lichtlen,P., Sirito,M., Sawadogo,M. and Schaffner, W. (2001) The transcription factors MTF-1 and USF1 cooperate to regulate mouse metallothionein-I expression in response to the essential metal zinc in visceral endoderm cells during early development, European Molecular Biology Organization 20, 1114–1122.

[44] Pedersen, M.Ø., Larsen, A., Stoltenberg, M. and Penkowa, M. (2009) The Role of metallothionein in oncogenesis and cancer prognosis. Progress in Histochemistry and Cytochemistry 44, 29–64.

[45] Kochanczyk, A., Drozd, A. and Krezel, A. (2015) Relationship between the architecture of zinc coordination and zinc binding affinity in proteins – insights into zinc regulation. Metallomics, 7, 244 – 257.

[46] Quesada, A.R., Byrnes, R.W., Krezoski, S.O. and Petering, D.H. (1996) Direct reaction of H_2O_2 with sulfhydryl groups in HL-60 cells: Zinc-metallothionein and other sites. Archives of Biochemistry and Biophysics, 334, 241–250.

[47] Lazo, J.S., Kuo, S.M., Woo, E.S. and Pitt, B.R. (1998) The protein thiol metallothionein as an antioxidant and protectant against antineoplastic drugs. Chemico-Biological Interacteractions, 111, 255–262.

[48] Ejnik, J., Robinson, J., Zhu, J.; Försterling, H., Shaw, C.F. and Petering, D.H. (2002) Folding pathway of Apo-metallothionein induced by Zn^{2+}, Cd^{2+} and Co^{2+}. Journal of Inorganic Biochemistry, 88, 144–152.

[49] Zhu, J., Meeusen, J., Krezoski, S. and Petering, D.H. (2010) Reactivity of Zn-, Cd-, and Apo-metallothionein with nitric oxide compounds: In vitro and cellular comparison. Chemical Research in Toxicology, 23, 422–431.

[50] Ruttkay-Nedecky, B., Nejdl, L., Gumulec, J., Zitka, O., Masarik, M., Eckschlager, T., Stiborova, M., Adam, V. and Kizek, R. (2013) The role of metallothionein in oxidative stress. International Journal of Molecular Sciences 14, 6044–6066.

[51] Maret, W. (2011) Redox biochemistry of mammalian metallothioneins. Journal of Biological Inorganic Chemistry 16, 1079–1086.

[52] Michalska, A.E. and Choo, K.H.A. (1993) Targeting and Germ-line transmission of a null mutation at the metallothionein I and II loci in mouse. Proc. Natl. Acad. Sci. USA, 90, 8088–8092

[53] Paoletti, P., Vergnano, A., Barbour, B., and Casado, M. (2009) Zinc at glutamatergic synapses, Neuroscience 158, 126-136.

[54] Li, H., Cao, R., Wasserloos, K. J., Bernal, P., Liu, Z. Q., Pitt, B. R., and St Croix, C. M. (2010) Nitric oxide and zinc homeostasis in pulmonary endothelium, Annals of the New York Academy of Sciences 1203, 73-78.

[55] Frederickson, C. J., and Bush, A. I. (2001) Synaptically released zinc: physiological functions and pathological effects, Biometals 14, 353-366.

[56] Budde, T., Minta, A., White, J. A., and Kay, A. (1997) Imaging free zinc in synaptic terminals in live hippocampal slices, Neuroscience 79, 347-358.

[57] Kay, A. R., and Tóth, K. (2008) Is zinc a neuromodulator?, Science signaling 1, re3.

[58] Andrews, G. K. (2001) Cellular zinc sensors: MTF-1 regulation of gene expression, In Zinc Biochemistry, Physiology, and Homeostasis, Springer, 37-51.

[59] Petering, D. H., Zhu, J., Krezoski, S., Meeusen, J., Kiekenbush, C., Krull, S., Specher, T., and Dughish, M. (2006) Apo-metallothionein emerging as a major player in the cellular activities of metallothionein, Experimental Biology and Medicine 231, 1528-1534.

[60] Zhang, B., Georgiev, O., Hagmann, M., Günes, Ç., Cramer, M., Faller, P., Vasák, M., and Schaffner, W. (2003) Activity of metal-responsive transcription factor 1 by toxic heavy metals and H2O2 in vitro is modulated by metallothionein, Molecular and cellular biology 23, 8471-8485.

[61] Laity, J. H., and Andrews, G. K. (2007) Understanding the mechanisms of zinc-sensing by metal-response element binding transcription factor-1 (MTF-1), Archives of biochemistry and biophysics 463, 201-210.

[62] Langmade, S. J., Ravindra, R., Daniels, P. J., and Andrews, G. K. (2000) The transcription factor MTF-1 mediates metal regulation of the mouse ZnT1 gene, Journal of Biological Chemistry 275, 34803-34809.

[63] Günther, V., Lindert, U., and Schaffner, W. (2012) The taste of heavy metals: gene regulation by MTF-1, Biochimica et Biophysica Acta (BBA)-Molecular Cell Research 1823, 1416-1425.

[64] Bozym, R. A., Chimienti, F., Giblin, L. J., Gross, G. W., Korichneva, I., Li, Y., Libert, S., Maret, W., Parviz, M., and Frederickson, C. J. (2010) Free zinc ions outside a narrow concentration range are toxic to a variety of cells in vitro, Experimental Biology and Medicine 235, 741-750.

[65] Pluth, M. D., Tomat, E., and Lippard, S. J. (2011) Biochemistry of mobile zinc and nitric oxide revealed by fluorescent sensors, Annual review of biochemistry 80, 333.

[66] Domaille, D. W., Que, E. L., and Chang, C. J. (2008) Synthetic fluorescent sensors for studying the cell biology of metals, Nature chemical biology 4, 168-175.

[67] Jiang, P., and Guo, Z. (2004) Fluorescent detection of zinc in biological systems: recent development on the design of chemosensors and biosensors, Coordination Chemistry Reviews 248, 205-229.

[68] Frederickson, C. J., Kasarskis, E., Ringo, D., and Frederickson, R. (1987) A quinoline fluorescence method for visualizing and assaying the histochemically reactive zinc (bouton zinc) in the brain, Journal of neuroscience methods 20, 91-103.

[69] Haase, H., and Beyersmann, D. (2002) Intracellular zinc distribution and transport in C6 rat glioma cells, Biochemical and biophysical research communications 296, 923-928.

[70] Kaltenberg, J., Plum, L. M., Ober-Blöbaum, J. L., Hönscheid, A., Rink, L., and Haase, H. (2010) Zinc signals promote IL-2-dependent proliferation of T cells, European journal of immunology 40, 1496-1503.

[71] Truong-Tran, A. Q., Ruffin, R. E., and Zalewski, P. D. (2000) Visualization of labile zinc and its role in apoptosis of primary airway epithelial cells and cell lines, American Journal of Physiology-Lung Cellular and Molecular Physiology 279, 1172-1183.

[72] Zalewski, P. D., Forbes, I. J., and Betts, W. (1993) Correlation of apoptosis with change in intracellular labile Zn (II) using zinquin [(2-methyl-8-p-toluenesulphonamido-6quinolyloxy) acetic acid], a new specific fluorescent probe for Zn (II), Biochemical Journal 296, 403-408.

[73] Zalewski, P. D., Millard, S. H., Forbes, I. J., Kapaniris, O., Slavotinek, A., Betts, W. H., Ward, A. D., Lincoln, S. F., and Mahadevan, I. (1994) Video image analysis of labile zinc in viable

pancreatic islet cells using a specific fluorescent probe for zinc, Journal of Histochemistry & Cytochemistry 42, 877-884.

[74] Haase, H., and Beyersmann, D. (1999) Uptake and intracellular distribution of labile and total Zn (II) in C6 rat glioma cells investigated with fluorescent probes and atomic absorption, Biometals 12, 247-254.

[75] Thompson, R. B. (2005) Studying zinc biology with fluorescence: ain't we got fun?, Current opinion in chemical biology 9, 526-532.

[76] Meeusen, J. W., Tomasiewicz, H., Nowakowski, A., and Petering, D. H. (2011) TSQ (6methoxy-8-p-toluenesulfonamido-quinoline), a common fluorescent sensor for cellular zinc, images zinc proteins, Inorganic chemistry 50, 7563-7573.

[77] Nowakowski, A. B., Meeusen, J. W., Menden, H., Tomasiewicz, H., and Petering, D. H. (2015) Chemical–Biological Properties of Zinc Sensors TSQ and Zinquin: Formation of Sensor-Zn-Protein Adducts versus Zn (Sensor) 2 Complexes, Inorganic chemistry 54, 24, 11637-11647.

[78] Meeusen, J. W., Nowakowski, A., and Petering, D. H. (2012) Reaction of metal-binding ligands with the zinc proteome: zinc sensors and N, N, N', N'-tetrakis (2-pyridylmethyl) ethylenediamine, Inorganic chemistry 51, 3625-3632.

[79] Priel, T., Aricha-Tamir, B., and Sekler, I. (2007) Clioquinol attenuates zinc-dependent β-cell death and the onset of insulitis and hyperglycemia associated with experimental type I diabetes in mice, European journal of pharmacology 565, 232-239.

[80] Stork, C. J., and Li, Y. V. (2006) Measuring cell viability with membrane impermeable zinc fluorescent indicator, Journal of neuroscience methods 155, 180-186.

[81] Stork, C. J., and Li, Y. V. (2006) Intracellular zinc elevation measured with a “calcium specific” indicator during ischemia and reperfusion in rat hippocampus: a question on calcium overload, The Journal of neuroscience 26, 10430-10437.

[82] Lukowiak, B., Vandewalle, B., Riachy, R., Kerr–Conte, J., Gmyr, V., Belaich, S., Lefebvre, J., and Pattou, F. (2001) Identification and purification of functional human β-cells by a new specific zinc-fluorescent probe, Journal of Histochemistry & Cytochemistry 49, 519527.

[83] Stork, C. J., and Li, Y. V. (2010) Zinc release from thapsigargin/IP3-sensitive stores in cultured cortical neurons, Journal of molecular signaling 5, 5.

[84] Ohana, E., Hoch, E., Keasar, C., Kambe, T., Yifrach, O., Hershfinkel, M., and Sekler, I. (2009) Identification of the Zn2+ binding site and mode of operation of a mammalian Zn^{2+} transporter, Journal of Biological Chemistry 284, 17677-17686.

[85] Karim, M.R. and Petering, D.H. (2016) Newport green, a fluorescent sensor of weakly bound cellular Zn^{2+}: Competition with proteome for Zn^{2+}, Metallomics, 8, 201–210.

[86] Strober, W. (2001) Trypan blue exclusion test of cell viability, Current protocols in immunology, A3. B. 1-A3. B. 3.

[87] Avelar-Freitas, B., Almeida, V. G., Pinto, M. C. X., Mourão, F. A. G., Massensini, A. R., Martins-Filho, O. A., Rocha-Vieira, E., and Brito-Melo, G. (2014) Trypan blue exclusion assay by flow cytometry, Brazilian Journal of Medical and Biological Research 47, 307315.

[88] El-Sayed, I. H., Huang, X., and El-Sayed, M. A. (2006) Selective laser photo-thermal therapy of epithelial carcinoma using anti-EGFR antibody conjugated gold nanoparticles, Cancer letters 239, 129-135.

[89] Ellman, G., and Lysko, H. (1979) A precise method for the determination of whole blood and plasma sulfhydryl groups, Analytical biochemistry 93, 98-102.

[90] Hunt, J. B., Rhee, M. and Storm, C.B. (1977) A rapid and convenient preparation of apo-carbonic anhydrase, Analytical Biochemistry, 79, 1-2, 614-617.

[91] Wagner, F. W. (1988) Preparation of metal-free enzymes, Methods in Enzymology, 158, 21-32.

[92] Henkens, R. W. and Sturtevant, J. M. (1968) The kinetics of the binding of Zn(II) by apo-carbonic anhydrase, Journal of American Chemical Society, 90, 10, 2669-2676.

[93] Banarjee, A.L., Tobwala, S., Ganguly, B., Mallik, S. and Srivastava, D.K. (2005) Molecular basis for the origin of differential spectral and binding profiles of dansyl amide with human carbonic anhydrase I and II, Biochemistry, 44, 3673-3682.

[94] Wong, K. and Tanford, C. (1973) Denaturation of bovine carbonic anhydrase B by guanidine hydrochloride, The Journal of Biological Chemistry, 243, 24, 3313-3523.

[95] Croix, C. M. S., Wasserloos, K., Dineley, K., Reynolds, I., Levitan, E., and Pitt, B. (2002) Nitric oxide-induced changes in intracellular zinc homeostasis are mediated by metallothionein/thionein, American Journal of Physiology-Lung Cellular and Molecular Physiology 282, L185-L192.

[96] Pearce, L. L., Wasserloos, K., Croix, C. M. S., Gandley, R., Levitan, E. S., and Pitt, B. R. (2000) Metallothionein, nitric oxide and zinc homeostasis in vascular endothelial cells, The Journal of nutrition 130, 1467S-1470S.

[97] Kroncke, K.-D., Fehsel, K., Schmidt, T., Zenke, F. T., Dasting, I., Wesener, J. R., Bettermann, H., Breunig, K. D., and Kolbbachofen, V. (1994) Nitric oxide destroys zinc-sulfur clusters inducing zinc release from metallothionein and inhibition of the zinc finger-type yeast transcription activator LAC9, Biochemical and biophysical research communications 200, 1105-1110.

[98] Katakai, K., Liu, J., Nakajima, K., Keefer, L. K., and Waalkes, M. P. (2001) Nitric oxide induces metallothionein (MT) gene expression apparently by displacing zinc bound to MT, Toxicology letters 119, 103-108.

[99] Schwarz, M. A., Lazo, J. S., Yalowich, J. C., Allen, W. P., Whitmore, M., Bergonia, H. A., Tzeng, E., Billiar, T. R., Robbins, P. D., and Lancaster, J. R. (1995) Metallothionein protects against the cytotoxic and DNA-damaging effects of nitric oxide, Proceedings of the National Academy of Sciences 92, 4452-4456.

[100] Handing, K. B., Shabalin, I. G. and Minor, W. (2016) Circulatory zinc transport is controlled by distinct interdomain sites on mammalian albumins, Chemical Science, 7, 11, 6635-6648.

[101] Nowakowski, A. and Petering, D. (2012) Sensor specific imaging of proteomic zinc with Zinquin and TSQ after cellular exposure to N-ethylmaleimide, Metallomics, 4, 5, 448-456.

[102] Hakansson, K., Carlsson, M. and Svensson, L. A. (1992) Structure of native and apo carbonic anhydrase II and structure of some of its anion-ligand complexes, Journal of Molecular Biology 227, 1192-204.

[103] Pompella, A., Visvikis, A., Paolicchi, A., De Tata, V. and Casini, A. F. (2003). The changing faces of glutathione, a cellular protagonist". *Biochemical Pharmacology* 66, 1499–503.

[104] Hayes, J. D., Flanagan, J. U. and Jowsey, I. R. (2005). Glutathione transferases, Annual Review of Pharmacology and Toxicology 45, 51–88.

[105] Walsh, M.J. and Ahner, B. A. (2013) Determination of stability constants of Cu(I), Cu(II) and Zn(II) with thiols using fluorescent probes, Journal of Inorganic Biochemistry 128 , 112 —123.

[106] Brouwer, M., Hoexum-Brouwer, T. and Cashon, R. E. (1993) A putative glutathione-binding site in CdZn-metallothionein identified by equilibrium binding and molecular-modelling studies, Biochemical Journal, 194, 219-225.

[107] Tagde, A., Singh, H., Kang, M. H. and Reynolds, C. P. (2014) The glutathione synthesis inhibitor buthionine sulfoximine synergistically enhanced melphalan activity against preclinical models of multiple myeloma, Blood Cancer Journal 4, e229.

CURRICULUM VITAE

Afsana Alam Mahim

Experiences

Graduate Research Assistant | University of Wisconsin-Milwaukee | January 2013 – December 2019

- Designed and executed experiments to study the mechanism of cellular zinc trafficking
- Implemented various biochemical and enzymatic assays to probe the interaction of Dengue virus-2 helicase with natural ligands and small molecule inhibitors
- Gained expertise in bacterial culture, DNA cloning, gene expression and protein purification
- Became skilled in biochemical and analytical techniques, including fluorescence spectroscopy, PCR, fluorescence microscopy, gel electrophoresis, isothermal titration calorimetry, mammalian cell culture, ICP-MS, UV-visible spectrophotometry, flame atomic absorption spectrophotometry
- Mentored undergraduate researchers
- Wrote manuscripts for publication and presented research at international conferences
- Collaborated with external researchers

Graduate Researcher | University of Dhaka - Bangladesh | December 2007 – August 2009

- Established a method to analyze organochlorine pesticides in poultry meat
- Acquired skill in solvent extraction, rotary evaporation and GC-MS operation

Graduate Teaching Assistant | University of Wisconsin-Milwaukee | January 2013 – May 2016

- Taught chemistry discussion and laboratory classes for pre-medical and pre-nursing majors
- Proctored and graded quizzes and exams
- Mentored new teaching assistants

Skills & Training

Biology and Biochemistry: Mammalian and bacteria cell culture, molecular beacon assay, ATPase assay, thermal shift assay, live cell imaging, proteome extraction, gel filtration, SDS-PAGE, DNA cloning, PCR, gene expression, protein purification, affinity chromatography, isothermal titration calorimetry

Instrumentation: Fluorometer, UV-Vis spectrophotometer, isothermal titration calorimeter, plate reader, fluorescence microscopy, ICP-MS

Computer: Biochemical and analytical instrument softwares, Data analysis softwares (GraphPad Prism, Microsoft Excel)

Education

Ph.D. in (bio-inorganic) Chemistry | University of Wisconsin-Milwaukee, USA	2019
M.S. in (organic and analytical) Chemistry | University of Dhaka, Bangladesh	2009
B.S. in Chemistry | University of Dhaka, Bangladesh	2007

Selected Accomplishments

Publications:

• Proteomic High Affinity Zn^{2+} Trafficking: Where Does Metallothionein Fit in? (2017) International Journal of Molecular Science, 18(6), 1289.

• Organochlorine pesticide residues in poultry meat of Bangladesh. (2016) Croatian Journal of Food Science and Technology, 8(1), 30.

Awards:

• Chancellor's Fellowship Award | 2014 – 2016 | University of Wisconsin – Milwaukee • Teaching Assistant Mentor Award | 2015 | University of Wisconsin – Milwaukee • Graduate Student Travel Award | 2017 - 2018 | University of Wisconsin – Milwaukee • ACS Milwaukee Travel Award | 2019

Presentations:

• Probing proteomic zinc binding with Zincon. (2019) 256th American Chemical Society Meeting, Florida

• Understanding proteome dependent cellular zinc trafficking to form native Zn-proteins. (2018), 254th American Chemical Society Meeting, Washington D.C.

Volunteer Experiences

• Central Committee Member | Bangladesh Chemical and Biochemical Association in North America (BACABANA) | 2018 – present

• President | Bangladesh Students Association | University of Wisconsin – Milwaukee | 2017 - 2018

• Officer | Chemistry & Biochemistry Graduate Students Council | University of Wisconsin – Milwaukee | 2017 - 2019